IDENTIFYING THE MODE OF ACTION OF NOVEL ANTI-TUBERCULAR DRUGS

A THESIS SUBMITTED BY

Jonathan A. G. Cox

OF THE INSTITUTE OF MICROBIOLOGY AND INFECTION (IMI)

UNIVERSITY OF BIRMINGHAM[§]

IN COLLABORATION WITH GLAXOSMITHKLINE (GSK)

DISEASES IN THE DEVELOPING WORLD (DDW)[†]

A thesis submitted to the University of Birmingham for the degree of

DOCTOR OF PHILOSOPHY

UNDER THE SUPERVISION OF

Prof. G. S. Besra[§]

AND CO-SUPERVISION OF

Dr. Aproova Bhatt[§] and Dr. Lluis Ballell[†]

Institute of Microbiology and Infection (IMI)
School of Biosciences
University of Birmingham
August 2015

UNIVERSITY OF
BIRMINGHAM

University of Birmingham Research Archive

e-theses repository

This unpublished thesis/dissertation is copyright of the author and/or third parties. The intellectual property rights of the author or third parties in respect of this work are as defined by The Copyright Designs and Patents Act 1988 or as modified by any successor legislation.

Any use made of information contained in this thesis/dissertation must be in accordance with that legislation and must be properly acknowledged. Further distribution or reproduction in any format is prohibited without the permission of the copyright holder.

i. Abstract

The demand for novel antibiotics in the treatment of infections by *Mycobacterium tuberculosis* (*M. tb*), the causative agent of tuberculosis (TB) has reached new highs with the recent emergence of totally-drug resistant TB (TDR-TB). Efforts to develop antibiotics with revolutionary mechanisms of action, low minimal inhibitory concentrations (MICs) that will decrease the current drug burden and clear infection without compromising side effects has led to several collaborative efforts between pharmaceutical companies and academic institutions throughout the world. This interdisciplinary collaborative effort and advances in drug development technologies, such as high throughput phenotypic screening of compound libraries and whole genome sequencing (WGS) has accelerated the identification of new compounds (or hits) with potent anti-tubercular activity and delivered a variety of unique drug targets. These hits are also potent against drug-resistant strains of *M. tb*, and have significant efficacy *in vivo* models of TB infection. Bedaquiline (Sirturo™) is the first new specifically designed anti-TB drug to be approved by the Food and Drug Administration (FDA) for use against multi-drug resistant (MDR-TB) in 40 years. This considerable step forward marks the beginning of a paradigm shift in antibiotic development, signaling a new age of drug discovery. In this thesis, the modern age of TB drug discovery will be examined as well as the efforts made to further this field through the identification of novel hits with activity against *M. tb* and identifying their respective inhibitory mechanisms.

ii. Acknowledgements

"Discovery consists of seeing what everybody else has seen, and thinking what nobody has thought."

- Albert Szent-Gyorgyi

First and foremost I must thank my supervisor Prof. Gurdyal "Del" Besra for giving me the opportunity, support and guidance to complete this PhD. Without Del, none of this would have been possible. Most importantly, I will always remember our mantra, *"This time next year, Rodney, we'll be millionaires!"* I must also extend my eternal gratitude to Dr. Katherine Abrahams for her patience, teamwork and friendship, not to mention her support in the form of her superhuman abilities in the field of molecular genetics. Next, I thank the members of the Besra Group, GSK Tres Cantos and Cellzome who have helped me to complete this work (detailed below). Of course, all of the rest of the Besra Group have helped me at some point or another to a lesser or greater extent, and therefore I am very grateful to all. The cumulative knowledge they have imparted has helped me to produce my best scientific work to date in the form of this thesis, and for that I will be forever grateful. I would also like to thank Dr. Lluis Ballell for fulfilling the role of both co-supervisor and guidance counselor.

I am grateful to Dr. Katherine Abrahams (University of Birmingham), for providing the overexpresser constructs for Chapter 2 of this thesis, and the pVV16-*echA6* construct in Chapter 4 as well as her continued assistance throughout my PhD in countless aspects of this thesis. Dr. Sudagar Gurcha (University of Birmingham) for his assistance with the lipid labeling experiments in Chapter 3 and 4 of this thesis. Dr.

Vijayashankar Nataraj (University of Birmingham) for completing the bacterial two-hybrid experiment detailed in Chapter 4 of this thesis. Dr. Klaus Fütterer (University of Birmingham) for X-ray crystallography support in Chapter 4 of this thesis. Mr. Albel Singh (University of Birmingham) for preparing the EchA6 conditional mutant as detailed in Chapter 4 of this thesis as well as his technical support with this work. Dr. Nic Loman (University of Birmingham) for completing the genome sequencing of all resistant mutants detailed in this thesis. GSK (Tres Cantos, Madrid) and Dr. Giovanna Poce (Sapienza University of Rome) for providing the compounds used in this thesis. Cellzome (Heidelberg) for completing the chemoproteomic identification of EchA6 in Chapter 4. GSK (Tres Cantos, Madrid) for providing the *in vivo* data of the THPPs and performing the *in vivo* validation experiment (Chapter 4) and Dr. Laura Vela-Glez Del Peral GSK (Tres Cantos, Madrid) for assisting with the analysis of the results detailed in Chapter 5.

This work is dedicated to my parents, Vivienne and Michael, whose support and love has carried me through my toughest hours. They have taught me the most important lessons in life and made me who I am today. Finally, I would like to thank those of you who take the time to read this work. The only thing harder than writing a thesis is reading one. However, I believe the work I have presented here is both interesting and important. I hope you agree.

"Scientists have become the bearers of the torch of discovery in our quest for knowledge."

- Stephen Hawking

iii. Declaration

The work presented in this thesis has been carried out under the supervision of Prof. G. S. Besra and Dr. Aproova Bhatt of the School of Biosciences, University of Birmingham, UK, B15 2TT and Dr. Lluis Ballell of Diseases of the Developing World, GlaxoSmithKline, Tres Cantos, Madrid during the period of September 2011 until September 2015. The work in this thesis is original except where acknowledged by reference. The thesis resulted in several publications that may bear similarities to Chapters 1, 2, 4 and 5. These similar sections included in my thesis are my original work with no significant contributions to the text by the co-authors. No part of the work is being or has been submitted for a degree, diploma or any other qualification at any other University.



iv. Publications

Abrahams K*, **Cox J***, Spivey V, Loman N, Pallen M, Constantinidou C, Fernandez R, Alemparte C, Remuinan M, Barros D, Ballell L and Besra G (2012). Identification of Novel Imidazo[1,2-*a*]pyridine Inhibitors Targeting *M. tuberculosis* QcrB. *PLoS One* 7(12):e52951

Gurcha S, Veeraraghavan U, **Cox J,** Futterer K, Abrahams K, Bhatt A, Alderwick L, Reynolds R, Loman N, Alemparte C, Barros D, Lloyd A, Ballell L and Besra G (2014). Biochemical and structural characterization of mycobacterial aspartyl-tRNA synthetase AspS. *PLoS One* 9(11):e113568

Mugumbate G, Abrahams K, **Cox J**, Lelievre J, Barros D, Ballell L, Overington J and Besra G (2014). Mycobacterial Dihydrofolate Reductase Inhibitors Identified Using Chemogenomic Methods and *In Vitro* Validation. *PLoS One* 10(3):e0121492. doi:10.1371/journal.pone.0121492

Jankute M, **Cox J**, Harrison J and Besra G (2015). Assembly of the mycobacterial wall. *Annual Review of Microbiology* 69:405-23

Cox J, Abrahams K, Alemparte C, Ghidelli-Disse S, Rullas J, Angulo-Barturen I, Singh A, Gurcha S, Nataraj V, Bethell S, Remuninan M, Encinas L, Jervis P, Cammack N, Bhatt A, Kruse U, Bantscheff M, Futterer K, Barros D, Ballell L, Drewes G and Besra G (2016). THPP target assignment reveals EchA6 as an essential fatty acid shuttle in mycobacteria. *Nature Microbiology* In Press

v. Table of Contents

i.	Abstract	**ii**
ii.	Acknowledgements	**iii**
iii.	Declaration	**v**
iv.	Publications	**vi**
v.	Table of Contents	**vii**
vi.	Figures and tables	**xi**
vii.	Abbreviations	**xiv**
CHAPTER 1.	General Introduction	**1**
1.1	Tuberculosis: Disease, Incidence and Pathogenesis	**2**
1.2	Treatment Strategy	**5**
1.3	Approaches to Drug Discovery	**9**
1.4	*In Vivo* Pre-clinical Screens and Clinical Drug Assessment	**13**
1.5	Newly Discovered Anti-tubercular Agents	**14**
1.5.1	Bedaquiline	**16**
1.5.2	Nitroimidazoles	**18**
1.5.3	SQ109 and MmpL3 inhibitors	**20**
1.5.4	Benzothiazinones	**24**
1.5.5	Oxazolidinones	**25**
1.6	The future for TB Drug Discovery	**27**
CHAPTER 2.	The imidazo[1-2-*a*]pyridines inhibit mycobacterial oxidative phosphorylation by targeting the *b* subunit of the cytochrome bc_1 complex	**31**
2.1	Introduction	**32**
2.2	Materials and methods	**35**
2.2.1	MIC Determination of the IP Compounds in *M. bovis* BCG	**35**
2.2.2	Generation of *M. bovis* BCG Mutants Resistant to IPs	**35**
2.2.3	Genomic DNA Extraction and Genome Sequencing	**36**
2.2.4	Recombinant DNA Manipulations	**37**
2.3	Results	**39**
2.3.1	MICs of IP Compounds (1, 3 and 4) in *M. bovis* BCG	**39**
2.3.2	Target Identification of the IP Chemical Family	**40**
2.3.3	Target Validation by Overexpression of QcrB in *M. bovis*	**40**

2.4 Discussion **44**

CHAPTER 3. Investigations into the apparent promiscuous TB drug target mycobacterial membrane protein large 3 (MmpL3) **48**

3.1 Introduction **49**

3.2 Materials and methods **51**

3.2.1 *M. bovis* BCG strains **51**

3.2.2 Growth Curves with *M. bovis* BCG with and without MmpL3 overexpression in the presence of varying concentrations of putative MmpL3 inhibitors **52**

3.2.3 Generation of spontaneous resistant mutants using *M. bovis* BCG pMV261A-*mmpL3* **52**

3.2.4 Whole genome sequencing of spontaneous resistant mutants **53**

3.2.5 Target validation by *in vitro* ribosomal inhibition assay **53**

3.2.6 Analysis of FAMEs and MAMEs of *M. bovis* BCG treated with putative MmpL3 inhibitors **54**

3.3 Results **54**

3.3.1 Overexpression of MmpL3 causes increased sensitivity to putative MmpL3 inhibitors **54**

3.2.2 Analysis of FAMEs and MAMEs of *M. bovis* BCG treated with putative MmpL3 inhibitors **58**

3.3.3 Sequencing of spontaneous resistant mutants generated against BM635 indicates 16S rRNA as the target **59**

3.3.4 Validation of mycobacterial 16S rRNA as the cellular target of BM635 **61**

3.4 Discussion **63**

CHAPTER 4. EchA6 as the Target of the Tetrahydropyrazolopyrimidine (THPP) anti-tubercular drug series **66**

4.1 Introduction **67**

4.1.1 Mycolic acids **67**

4.1.2 Known inhibitors of mycolic acid biosynthesis **71**

4.1.3 New Direction **73**

4.2 Materials and methods **74**

4.2.1 General methods **74**

4.2.2 Assessment of chronic and acute efficacy in murine TB models **75**
4.2.3 Preparation of *M. bovis* BCG cytosolic extract **76**
4.2.4 Chemoproteomics **76**
4.2.5 Generation and characterisation of a conditional *echA6* mutant in *M. bovis* BCG **77**
4.2.6 EchA6 recombinant protein production & purification **78**
4.2.6.1 *E. coli* strains **78**
4.2.6.2 Plasmids & primers **79**
4.2.6.3 Transformation by heatshock **81**
4.2.6.4 Expression of EchA6 **81**
4.2.6.5 Purification of EchA6 by IMAC **82**
4.2.7 ITF ligand binding assays **83**
4.2.8 X-ray crystallography of EchA6 **84**
4.2.9 EchA6 overexpresser **87**
4.2.10 SDM of EchA6 **88**
4.3 Results **88**
4.3.1 Target identification **88**
4.3.2 The *echA6* gene is essential **92**
4.3.3 EchA6 overexpression causes resistance to a THPP compound **94**
4.3.4 EchA6 interacts with key components of mycobacterial FAS-II **96**
4.3.5 ITF ligand binding assays **97**
4.3.6 SDM of EchA6 **104**
4.3.7 *In vivo* validation of EchA6 interaction with GSK951A **107**
4.3.8 Crystallography of EchA6 **109**
4.4 Discussion **113**
CHAPTER 5. Identification of novel inhibitors of *M. tuberculosis* drug targets by target-specific high throughput phenotypic screens **117**
5.1 Introduction **118**
5.1.1 GuaB2 **119**
5.1.2 MurC **120**

5.1.3 Antigen 85A (FbpA) **121**
5.1.4 DHFR (DfrA) **122**
5.1.5 DapF **125**
5.1.6 DapE **126**
5.1.7 KasA **127**
5.1.8 HadAB **128**
5.1.9 MabA **129**
5.2 Materials and methods **130**
5.2.1 Strains, transformation and culture **130**
5.2.2 HTS of overexpresser strains in single shot **131**
5.2.3 Dose response validation of hits **132**
5.2.4 Data analysis **132**
5.3 Results **133**
5.3.1 Z-factor **133**
5.3.2 GuaB2 **134**
5.3.3 MurC **136**
5.3.4 Antigen 85A (FbpA) **139**
5.3.5 DHFR (DfrA) **140**
5.3.6 DapF **142**
5.3.7 DapE **143**
5.3.8 KasA **144**
5.3.9 HadAB **145**
5.3.10 MabA **146**
5.4 Discussion **146**
CHAPTER 6. General Discussion **149**
CHAPTER 7. References **155**

vi. Figures and tables

Figure 1.1:	Estimated TB incidence rates, 2012 (WHO 2013)	**3**
Table 1.1:	Drug Profiles	**8**
Figure 1.2:	Methods of Drug Discovery	**12**
Table 1.2:	Drug Profiles of recently discovered anti-TB agents	**15**
Figure 1.3:	The Drug Discovery Pipeline	**30**
Figure 2.1:	Representation of the functional activity of the Ubiquinol-cytochrome *c* reductase (Cytochrome bc_1 complex or Complex III) in the electron transport chain	**33**
Table 2.1:	IP compounds identified to target QcrB	**39**
Figure 2.2:	Cross-resistance of *M. bovis* BCG mutants to IP compounds	**42**
Figure 2.3:	Fragments of the *qcrB* gene cluster that were cloned into pMV261	**43**
Figure 2.4:	The overexpression of QcrB, QcrCAB and CtaE-QcrCAB in *M. bovis* BCG leads to an increase of MIC against IP compound 3 to > 16 x the MIC of WT	**43**
Figure 2.5:	Ribbon diagram of QcrB illustrating the locus of the resistance conferring mutation T313A in relation to the Myxothiazol binding site (Myx)	**46**
Figure 3.1:	The chemical diversity of proposed MmpL3 inhibitors	**49**
Figure 3.2:	Diagram of the locations of SNPs in resistant mutants generated against putative MmpL3 targeting compounds	**50**
Figure 3.3:	Growth Curves of MmpL3 overexpresser with a dose response of THPP, Spiro, BM635, Adamantyl Urea, C215 and SQ109	**56-58**
Figure 3.4	Analysis of FAMEs and MAMEs of *M. bovis* BCG treated with putative MmpL3 Inhibitors	**59**
Figure 3.5:	Generation of spontaneous resistant mutants of *M. bovis* BCG pMV261A-*mmpL3* against BM635	**61**
Figure 3.6:	In vitro cell-free expression and inhibition of mCherry	**63**
Figure 4.1:	Schematic representation of FAS-I and FAS-II biosynthesis in mycobacteria	**71**
Table 4.1:	Primers used in this study	**80**
Table 4.2:	Conditions used for EchA6 crystal production	**85**

Table 4.3: Crystallography software used to solve EchA6 structures **85**
Table 4.4: Crystallographic data and refinement statistics **86**
Figure 4.2: Efficacy of GSK951A over an 8-week period against an established murine model of *M. tuberculosis* chronic infection **89**
Table 4.5: The THPP compounds and their respective MICs **89**
Figure 4.3: Chemoproteomics profiling identifies the putative enoyl-CoA hydratase EchA6 as target of the THPP series (work performed by Cellzome, Heidelberg, Germany) **91**
Figure 4.4: Essentiality of *echA6* **93**
Figure 4.5: Overexpression of *M. tb* EchA6 causes increased resistance to THPP GSK951A **95**
Figure 4.6: [^{14}C]-acetate labeling of cultures of *M. bovis* BCG strains containing pVV16 and pVV16-*echA6* **96**
Figure 4.7: Protein-protein interaction screen using the bacterial two-hybrid system-BACTH and EchA6 with components of FAS-II **97**
Figure 4.8: SDS-PAGE gel showing the purification of EchA6 from clarified lysate following recombinant expression by *E. coli* BL21 (DE3) transformed with pET28a-*echA6* **98**
Figure 4.9: Sequence alignment of *M. tb* EchAs **99**
Figure 4.10: Sequential additions of acyl-CoAs results in a decrease in fluorescence maxima **100**
Figure 4.11: ITF binding assay of EchA6 with THPP compounds **101**
Figure 4.12: EchA6 competition assay with C_4-CoA (a) and C_{20}-CoA (b) and GSK951A **102**
Table 4.6: Summary of the binding affinities of all ligands tested with EchA6 **103**
Table 4.7: Summary of the binding affinities of all ligands tested with point mutated EchA6 **105**
Figure 4.13: SDM of *M. tb* EchA6 amino acids Leu75 (a), Ile76 (b), Asp131 (c) and Trp133 (d) to Ala affects THPP GSK951A binding, but maintains C_{20}-CoA binding with reduced affinity **106**
Figure 4.14: SDM of *M. tb* EchA6 amino acid Gln107 to Ala increases affinity for THPP GSK951A and maintains C_{20}-CoA binding **107**
Figure 4.15: The ED_{99} of GSK951A and INH was calculated in a murine model of *M. tb* acute infection **109**

Figure 4.16: EchA6 crystals that gave the *apo*-EchA6 crystal structure (0.1M Tris pH 8.5, 60% v/v polypropylene glycol 400) **111**
Figure 4.17: Comparison of the mode of THPP compound binding EchA6 **112**
Figure 4.18: Model of the physiological role of EchA6 in mycobacterial fatty acid metabolism **115**
Figure 5.1: The folate pathway around dihydrofolate reductase (DHFR) that reduces dihydrofolate (DHF) to tetrahydrofolate (THF), a precursor to the pyrimidine nucleotide threonine monophosphate (TMP) **123**
Figure 5.2: Phenotypic validation of the MoA of the THT compounds as inhibitors of *M. tb* DHFR, following their identification by *in silico* drug discovery **124**
Figure 5.3: Lysine/*meso*-diaminopimelate (mDAP) synthesis pathway from L-aspartate incorporating the DapA-F enzymes **126**
Table 5.1: The Z' values for each overexpresser HTS **134**
Table 5.2: Results of GuaB2 overexpresser HTS **135**
Table 5.3: Results of MurC overexpresser HTS **137**
Table 5.4: Results of FbpA overexpresser HTS **139**
Table 5.5: Results of DfrA overexpresser HTS **141**
Table 5.6: Results of DapF overexpresser HTS **142**
Table 5.7: Results of DapE overexpresser HTS **143**
Table 5.8: Results of KasA overexpresser HTS **144**
Table 5.9: Results of HadAB overexpresser HTS **145**
Table 5.10: Results of MabA overexpresser HTS **146**
Figure 5.3: A summary of the distribution of 284 hits identified in a target-specific phenotypic HTS of 10,000 known inhibitors of *M. tb* **148**

vii. Abbreviations

AcpM – Acyl carrier protein
ADC – Albumin, dextrose and catalase
ADME – Adsorption, distribution, metabolism and excretion
ADP – Adenosine diphosphate
AG – Arabinogalactan
AMP – Adenosine monophosphate
ATc – Anhydrotetracycline
ATP – Adenosine triphosphate
BTZ – Benzothiazinone
cfu – Colony forming unit
CMC – Computational medicinal chemistry
cpm – Counts per minute
DAP – Diaminopimelic acid
DHF – Dihydrofolate
DHFR – Dihydrofolate reductase
DMSO – Dimethyl sulfoxide
DNA – Deoxyribonucleic acid
DOTS – Directly observed treatment short-course
DPA – Decaprenylphosphoryl arabinose
DPR – Decaprenylphosphoryl-ribose
EBA – Early bactericidal activity
EchA – Enoyl-Coenzyme A
EDTA – Ethylenediaminetetraacetic acid
EMB – Ethambutol
ETC – Electron transport chain
ETH – Ethionamide
FAMEs – Fatty acid methyl esters
FDA – Food and Drug Administration
FoR – Frequency of resistance
gDNA – Genomic DNA
GMM – Glucose monomycolate
GMP – Guanosine monophosphate
GSK – GlaxoSmithKline
HEPES – (4-(2-hydroxyethyl)-1-piperazineethanesulfonic acid)
HIV – Human immunodeficiency virus
HTS – High throughput screen[ing]
IC_{50} – 50% inhibitory concentration
IMAC – Immobilised metal ion affinity chromatography
IMP – Inosine monophosphate
IMPDH – Inosine monophosphate dehydrogenase
INH – Isoniazid
IP – Imidazo[1-2-a]pyridine
IPA – Imidazopiridine amide
IPTG – β-D-1-thiogalactopyranoside
ITF – Intrinsic tryptophan fluorescence
LAM – Lipoarabinomannan

LBDS – Ligand-based drug screening
LM – Lipomannan
LTBI – Latent TB infection
mAGP – Mycolyl arabinogalactan-peptidoglycan complex
MAMEs – Mycolic acid methyl esters
MDR-TB – Multi-drug resistant TB
MFS – Major facilitator superfamily
MIC – Minimal inhibitory concentration
MmpL3 – Mycobacterial membrane protein large 3
MoA – Mode of action
MTZ – Metronidazole
NADP(H/+) – Nicotinamide adenine dinucleotide phosphate
NIAID – National Institute of Allergy and Infectious Diseases
NMR – Nuclear Magnetic Resonance
OADC – Oleic acid, albumin, dextrose and catalase
OD – Optical density
PAGE – Polyacrylamide gel electrophoresis
PAINS – pan-assay interference compounds
PAS – *Para*-amino salicylic acid
PCR – Polymerase chain reaction
PG – Peptidoglycan
PIM – Phosphatidylinositol mannoside
PZA – Pyrazinamide
Q – Ubiquinone
QH_2 – Ubiquinol
QSAR – Quantitative structure-activity relationship
RMP – Rifampicin
RND – Resistance, Nodulation and Division
SBDS – Structure-based drug screening
SDM – Site directed mutagenesis
SDS – Sodium dodecyl sulfate
SNP(s) – Single nucleotide polymorphism(s)
Spiro – N-benzyl-6',7'-dihydrospiro[piperidine-4,4'-thieno[3,2-c]pyran]
TB – Tuberculosis
TDM – Trehalose dimycolate
TDR-TB – Totally-drug resistant TB
THF – Tetrahydrofolate
THPP – tetrahydropyrazolo[1,5-*a*]pyrimidine-3-carboxamide
TLC – Thin-layer chromatography
TLM – Thiolactomycin
TMM – Trehalose monomycolate
TraSH – Transposon site hybridisation
WGS – Whole Genome Sequencing
XDR-TB – Extensively-drug resistant TB
XMP – Xanthosine monophosphate
Z' – Z-factor

CHAPTER 1

General Introduction

1.1 Tuberculosis: Disease, Incidence and Pathogenesis

Mycobacterium tuberculosis (*M. tb*), identified in 1882 by Robert Koch as the etiological agent of the disease tuberculosis (TB), is a historic pathogen that has plagued the earth for the last 9000 years, evolving alongside mankind (Hershkovitz *et al.* 2008). One third of the world's population are asymptomatically infected with a latent form of *M. tb,* which carries a 10% lifetime risk of reactivation into an active infection. Drug susceptible TB is curable in 95% of cases following 6 months of treatment, however there remains a 5% chance of relapse to an active infection. Despite the advent of new therapies, TB remains a global problem, with 8.7 million newly confirmed cases and 1.4 million deaths in 2011, equating to approximately one death every 22 seconds. The highest incidence of TB is found in developing countries where high population density and poor sanitation provide the greatest opportunity for the transmission of disease. Approximately, 80% of the world's TB cases occur in twenty-two high burden countries, the most prominent of which are India, China, South Africa and the Russian Federation (WHO) (Figure 1.1).

TB is an infectious disease spread by inhalation of aerosolised sputal droplets from a cough or sneeze of an infected individual, where droplets are 2-5 μm in diameter and contain 1-3 bacilli (Riley 1957). It is a disease that is predominantly prevalent in immuno-compromised or immuno-suppressed individuals (Escombe *et al.* 2009) and therefore there is a high incidence of TB co-infection amongst individuals infected with human immunodeficiency virus (HIV). In 2011, one third of HIV positive individuals (33 million) had a TB co-infection and accounted for 25% of the global mortality rate (350,000) (Getahun *et al.* 2010). There is also a high risk of TB

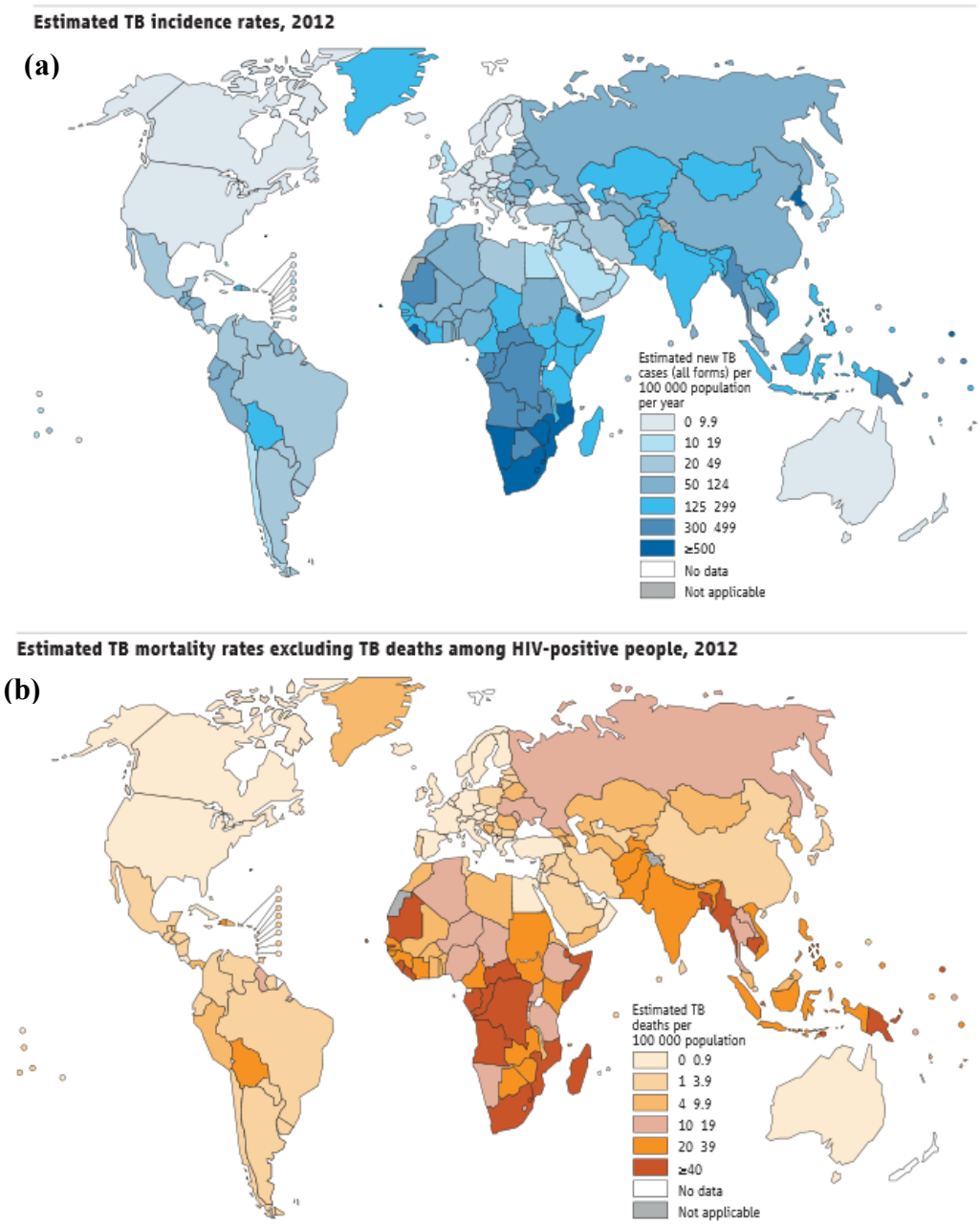


Figure 1.1: Estimated TB incidence rates, 2012 (WHO 2013). (a) The data illustrates the range of incidence throughout the world, where the UK TB incidence is estimated to be 10-19 cases per 100,000, South Africa shows an incidence of ≥500 cases per 100,000 per year. (b) Estimated TB mortality rates excluding TB deaths among HIV-positive people, 2012 (WHO 2013). This diagram illustrates the disparity between incidence and mortality depending on the country in question. UK < 1 death per 100,000, where as South Africa > 50 deaths per 100,000.

infection in individuals who are immuno-compromised due to treatment with anti-cancer or anti-diabetic drugs.

M. tb infection can exist as either an actively replicating (active) or non-replicating (latent). Of individuals infected with TB, the active disease develops in 10% of individuals, leading to symptomatic infection of *M. tb* most commonly in the lung. However, 41% of active TB infections in England and Wales are considered to be extra-pulmonary and have been known to infect the pleural cavity, the meninges, the pericardium, the skeleton, and the skin (miliary TB), as well as the lymphatic, gastrointestinal and genitourinary systems (Dinnes *et al.* 2007). Latent TB infection is not contagious and carries no associated clinical symptoms of infection, however reactivation of TB occurs in 5-10% of individuals infected with a latent TB infection at some point during their lifetime where the immune system of the infected individual is no longer able to sustain the management of the infection. In healthy immunocompetent individuals infected with pulmonary *M. tb*, the primary site of *M. tb* infection is contained by the formation of a complex aggregation of cells of the host immune system, known as a granulomatous lesion. This system of bacterial containment has been observed to be mutually beneficial to both the host and the bacteria. Preventing the dissemination of active infection and suppressing the growth capabilities of *M. tb* leading to latency is of clear benefit to the host. However, the granuloma provides a comfortable environment for the bacteria and nutrient availability that allows for the maintenance of the latent infection (Ramakrishnan 2013). The evolution of this system of suppression combined with the ability of *M. tb* to hijack this system for its own benefit and survival serves to better illustrate the millennia old struggle between mankind and *M. tb*.

1.2 Treatment Strategy

Today, some *M. tb* strains have evolved the ability to combat the last 70 years of antibiotic development, from the early days of streptomycin treatment (Crofton *et al.* 1948), to the routinely used four drug, first-line treatment regimen used for the last 40 years (isoniazid [INH], rifampicin [RMP], ethambutol [EMB] and pyrazinamide [PZA] (Goble *et al.* 1993). MDR-TB infections have created a demand for the development of second-line antibiotics (aminoglycosides, polypeptides, fluoroquinolones, thioamides, cycloserine and terizidone), and with the subsequent emergence of extensively drug resistant (XDR-TB), and TDR-TB, respectively, the demand remains for the discovery of new anti-TB drugs (Velayati *et al.* 2009; Udwadia *et al.* 2012; Zumla *et al.* 2013). The current treatment strategy for drug sensitive *M. tb* infections is routinely used in combination with anti-retroviral drugs for both pulmonary and extra-pulmonary infections of *M. tb* in HIV positive individuals. This highly effective treatment strategy follows a well-defined 6 months of a directly observed treatment short-course (DOTS) (Zwarenstein *et al.* 1998), comprising 2 months of all four first line Group 1 anti-TB drugs (INH, RMP, PZA and EMB) followed by 4 months of two drugs (INH and RMP) and results in a >95% cure rate in patients treated under the DOTS program (WHO 2010). However, drug-drug interactions between anti-retroviral drugs and first line anti-TB drugs, often results in toxicity and around 10% of diagnosed cases of *M. tb* infection are MDR-TB strains (WHO 2010).

MDR-TB and XDR-TB treatment regimens include a combination of eight to ten second-line antibiotics, only four of which were originally designed to treat TB and last up to 18-24 months (Ghandi *et al.* 2010). Second line anti-TB drugs consist of the injectable aminoglycosides (Group 2, such as streptomycin, kanamycin and amikacin), injectable polypeptides (Group 2, such as capreomycin and viomycin), oral and injectable fluoroquinolones (Group 3, such as ciprofloxacin, levofloxacin, moxifloxacin, ofloxacin and gatifloxacin), and Group 4 drugs, such as thioamides, cycloserine, terizidone. Groupings are determined by drug class, efficacy, potency and toxicity. The Group 1 compounds are the four first line antibiotics, whereas Group 5 compounds are third line antibiotics, considered experimental with unclear efficacy and undefined roles (e.g. clofazimine and linezolid) (Falzon *et al.* 2011). These antibiotics are summarised in Table 1.1. TDR-TB was first documented in 2012, and is defined as strains of *M. tb* that exhibit total resistance to all current first and second line anti-TB drugs (Udwadia *et al.* 2012). Acceptance of compounds into routine usage following approval by the Unites States Food and Drug Administration (FDA) varies dramatically from country to country, therefore resistance to all available first and second line drugs may vary by definition. Furthermore, as research and development programs produce ever more clinically relevant compounds, the term 'total drug resistance' will inevitably become obsolete.

Due to the lengthy replication time of *M. tb*, individual patient strain culture and subsequent drug susceptibility screening of second line antibiotics is an extensive process, often taking several months to obtain results. However, advancement in the sensitivity of molecular biological techniques has opened the door to personalised treatment of drug resistant TB. High throughput drug resistance screening utilising

sputum cultures and polymerase chain reaction (PCR) based analysis of resistance confirming mutations has proved effective in the detection of INH and RMP resistance, with results in 1-2 days (Barnard *et al.* 2008). Due to the high incidence of MDR-TB in areas of the world where culture and technical analysis equipment are still unavailable, the traditional method for the rationalisation of a second line treatment strategy is used for >95% of cases, taking into account a number of factors: demographic of TB drug resistance in the local area, previously administered antibiotics, secondary medical conditions and the patient's tolerance for previously administered drugs (Zumla *et al.* 2013). As a result of the limited availability of specifically designed anti-TB drugs for the treatment of MDR-TB and the limited availability of personalised treatment, around 30% of MDR-TB patients undergoing treatment are not cured of their infection (Mitnic *et al.* 2003).

Table 1.1: Drug Profiles

Drug	Discovered	Group	Family	Target	Mode of Action (MOA)
Isoniazid (INH)	1952	1	Isonicotinylhydrazine (INH)	Enoyl-[acyl-carrier-protein] reductase	Inhibits mycolic acid synthesis
Rifampicin (RMP)	1963	1	Rifamycin	RNA polymerase, β-subunit	Inhibits transcription
Pyrazinamide (PZA)	1954	1	Pyrazine-2-carboxamide	S1 component of 30S ribosomal subunit	Inhibits translation and trans-translation, acidifies cytoplasm
Ethambutol (EMB)	1961	1	Ethambutol	Arabinosyl transferase	Inhibits arabinogalactan biosynthesis
Para-amino salicylic acid (PAS)	1948	2	Aminosalicylic acid (ASA)	Dihydropteroate synthase	Inhibits folate biosynthesis
Streptomycin	1944	2	Aminoglycoside	S12 and 16S rRNA components of 30S ribosomal subunit	Inhibits protein biosynthesis
Capreomycin	1963	2	Aminoglycoside	Interbridge B2a between 30S and 50S ribosomal subunits	Inhibits protein synthesis
Kanamycin	1957	2	Aminoglycoside	30S ribosomal subunit	Inhibits protein synthesis
Amikacin	1972	2	Aminoglycoside	30S ribosomal subunit	Inhibits protein synthesis
Viomycin	1972	2	Tuberactinomycin (Aminoglycoside)	Binds RNA	Inhibits protein synthesis
Ofloxacin	1980	3	Fluoroquinolone	DNA gyrase and DNA topoisomerase	Inhibits DNA supercoiling
Ciprofloxacin (INN)	1983	3	Fluoroquinolone	DNA gyrase and DNA topoisomerase	Inhibits DNA supercoiling
Levofloxacin	1987	3	Fluoroquinolone	DNA gyrase and DNA topoisomerase	Inhibits DNA supercoiling
Moxifloxacin	1989	3	Fluoroquinolone	DNA gyrase and DNA topoisomerase	Inhibits DNA supercoiling
Gatifloxacin	1999	3	Fluoroquinolone	DNA gyrase and DNA topoisomerase	Inhibits DNA supercoiling
Ethionamide	1961	4	Thioamide	Enoyl-[acyl-carrier-protein] reductase	Inhibits mycolic acid biosynthesis
Terizidone	1965	4	Alanine analogue	L-alanine racemase and D-alanine ligase	Inhibits peptidoglycan synthesis
Cycloserine	1955	4	Alanine analogue	D-alanine racemase and ligase	Inhibits peptidoglycan synthesis
Clofazimine	1957	5	Riminophenazine	Unknown	Unknown

1.3 Approaches to Drug Discovery

The urgent demand for new TB drugs stems from a number of short falls in the current four-drug treatment regimen. Primarily, the six month duration of treatment for a drug susceptible active infection of *M. tb* carries a lengthy pill burden with a high dosing frequency that requires the DOTS strategy to ensure the patient's full compliance in completing the course following a substantial time period symptom free. Secondly, the emergence of XDR-TB and the increasing incidence of such infections highlights the importance of developing alternative antibiotics capable of killing such strains. Finally, more antibiotics are required that can be effectively used in combination with anti-retroviral therapy (Koul *et al.* 2011). There also exists a set of guidelines for medicinal chemistry of newly designed compounds termed Lipinski's 'rule of 5,' so called because of the existence of each rule containing a number which is a factor of 5. This rule aims to provide an assessment of a chemical in terms of its likelihood to be suitable for human consumption by evaluating four features of that compound. The rules are: not more than 5 hydrogen bond donors; not more than 10 hydrogen bond acceptors; a molecular mass less than 500 daltons; an octanol-water partition coefficient (log*P*) not greater than 5 (measure of the difference of solubility of the compound in two phases) (Lipinski *et al.*1997).

The challenge of overcoming these obstacles has forced drug development groups to rethink their approach to the development of anti-TB compounds resulting in a recent considerable change of tack in the approach to the discovery of new antibiotics. Fueled by the advancement of technology (high throughput robotics and next generation sequencing), research teams are favouring a top-down high throughput

strategy over the more traditional bottom-up target based approaches. Although, the start-up and running costs of high throughput drug screening campaigns are considerably higher than the costs involved in a target based approach, the accelerated rate of identification of many new compounds with potent (nM) anti-TB activity has only been achievable through high throughput screening (HTS). The classical HTS approach to antibiotic discovery comprises the screening of an extensive compound library against whole bacterial cells to identify hits by growth inhibition, known as a phenotypic screen. Compound libraries can be either commercially available, such as Exquiron Biotech's library of 250,000 lead-like compounds or privately collated, such as the set of 2.5 million compounds held by GSK in Tres Cantos, Madrid. Following the identification of 'hits' (compounds which inhibit cell growth), the minimal inhibitory concentration (MIC) of successful inhibitors can be determined for bacteria in liquid culture by exploring the 'hit' in a dose response format. Subsequently, the MIC of the compound is determined on solid media and this information is used to select for spontaneous resistant mutants by plating a high cell titer (traditionally 10^8 cells) against the hit under investigation at concentrations that far exceed the MIC (5, 10 or 20 times the MIC). Genomic DNA is then prepared from resistant isolates and whole genome sequencing (WGS) performed along with the reference 'parental' strain. WGS alignment of the mutant and reference genomes is then able to highlight single nucleotide polymorphisms (SNPs), which indicate the potential mechanism of apparent growth inhibition or cell death by the 'hit' compound. This process is known as drug-to-target drug discovery and it has some limitations. Many new targets that have been discovered by this method are found to be inhibited by a wide variety of drugs of different classes and chemical scaffolds and have therefore been termed 'promiscuous' targets (Lechartier *et al.* 2014). An example of this is the

Mycobacterial membrane protein large 3 (MmpL3), a transmembrane protein that transports trehalose monomycolate, which has been implicated as the cellular target of a wide variety of drugs (SQ109, AU1253, THPP, SPIRO, BM212, C215 and the indoleamides) by the drug-to-target drug discovery method (Tahlan *et al.* 2012; Grzegorzewicz *et al.* 2012; Remuinan *et al.* 2013; La Rosa *et al.* 2012; Stanley *et al.* 2012; Lun *et al.* 2013). Other limitations of the phenotypic screening approach include the lack of upfront knowledge regarding the mode of action (MoA) of the inhibitory compound, and creating *in vitro* growth conditions that accurately represent infection *in vivo* as some compounds behave differently depending on the composition of the growth media (Pethe *et al.* 2010). Despite these limitations, the drug-to-target method of drug discovery has had unparalleled success in the last 10 years, producing the only new anti-TB drug for over 40 years to make it into the clinic for the treatment of MDR and XDR-TB, the ATPase inhibitor, Bedaquiline (formerly TMC207), which received FDA approval in 2012 (Matteelli *et al.* 2010) (discussed in detail in Chapter 1.5.1 of this thesis).

The opposing method of drug discovery is the target-to-drug approach, whereby inhibitors are designed *de novo* to a pre-determined drug target. This may take the form of fragment-based screening, *in silico* drug design or the re-engineering of existing scaffolds with well documented targets, otherwise known as reverse pharmacology. The re-engineering of chemical scaffolds from historic drug classes aims to improve compound potency, circumvent resistance mechanisms, improve drug safety, pharmacology and bactericidal activities. This reverse pharmacology has yielded a number of new compounds with potent activity against TB that have proved successful in Phase I and II clinical trials. The re-engineering of the 1,2-ethylene

diamine antibiotic EMB led to the development of SQ109, a potent compound with activity against both drug susceptible TB and MDR-TB in three Phase I and one Phase II clinical trial in Africa. SQ109 has also been shown to increase the efficacy of the Group 1 anti-TB drugs INH and RIF when used in combination (Tahlan *et al.* 2012; Rayasam 2013). In spite of the success of the SQ109 campaign, reverse pharmacology efforts with the fluoroquinolones have resulted in increased resistance to gatifloxacin and moxifloxacin (Agrawal *et al.* 2009). The notion of circumventing existing resistance mechanisms with novel compounds by medicinal chemistry efforts is hampered by the speed and complexity of emerging resistance mechanisms. On balance, of the drug discovery methods discussed above, efforts to discover new chemical scaffolds with potent inhibitory activity, low toxicity, and a low frequency of mutation following HTS has the most favorable chance of success in the development of clinically relevant anti-TB compounds (Figure 1.2).

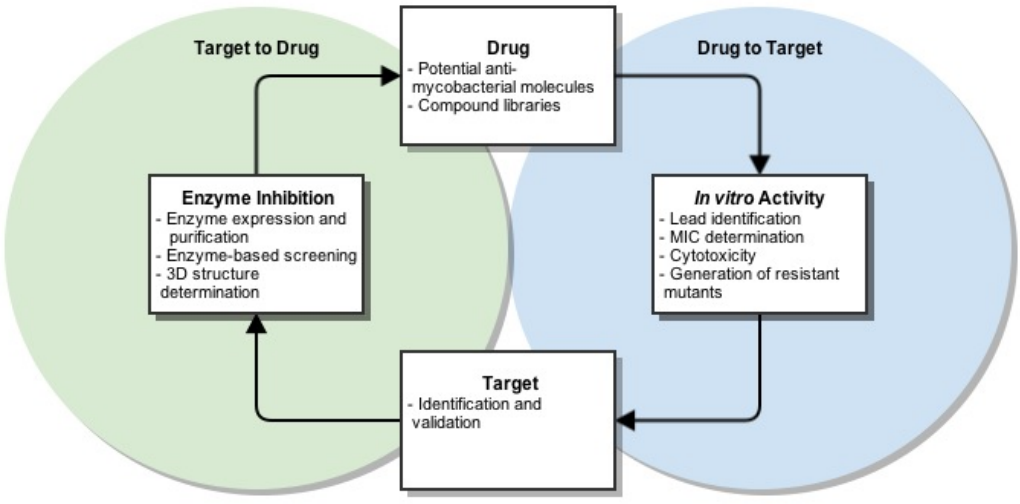


Figure 1.2: Methods of Drug Discovery. This figure illustrates the two different approaches to drug discovery and how they can be combined to provide a work flow encompassing both phenotypic (drug-to-target) and chemical proteomic (target-to-drug) methods, circumventing false positive target speculation.

1.4 *In Vivo* Pre-clinical Screens and Clinical Drug Assessment

Following the identification of the MoA of an anti-TB compound, its drugability must be assessed prior to the consideration of clinical usage. This often takes place in an animal model, where the effects of the compound *in vivo* can be observed. However, data obtained through a murine model is not directly representative of the human system, and therefore acts as a guide to the pharmacodynamic potency (*in vivo* activity in clearing an infection), toxicological profile and the pharmacokinetic absorption, distribution, metabolism and excretion (ADME) characteristics of the compound (Balani *et al* 2005). With its relatively inexpensive running costs and ability to provide detailed information about the bactericidal and clearing potency of single and combination therapy, the murine model remains an essential tool in drug development (Andries *et al.* 2010). Due to the metabolic and physiological differences between active and latent TB infection, and a lack of mechanistic understanding of the causes of reactivation, murine models have been developed in an attempt to simulate latent TB infection in humans (Shi *et al.* 2011). Other models that have distinct advantages over mouse models in TB drug development include monkeys, rabbits and guinea pigs. Testing in one *in vivo* model does not provide sufficient conclusions about how a drug will behave in human clinical trials. Therefore, multiple models are routinely used following initial trials in mice as they provide a better understanding of the pathogenesis of *M. tb* infection in humans, such as pleural granulomatous lesions (Koul *et al.* 2011).

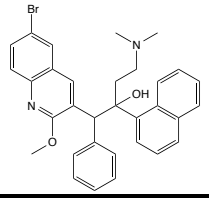
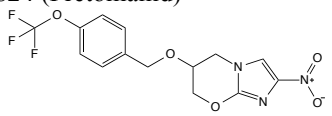
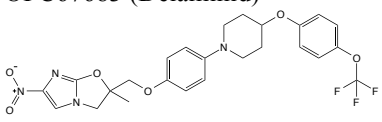
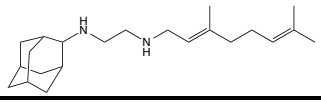
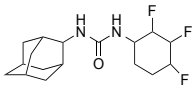
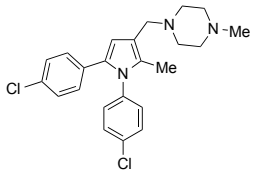
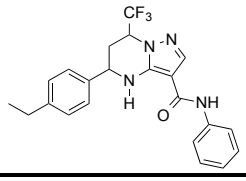
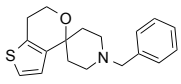
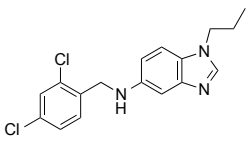
Clinical trials in humans of newly developed anti-TB compounds are grouped into phases. Phase I clinical trials are known as early bactericidal activity (EBA) trials

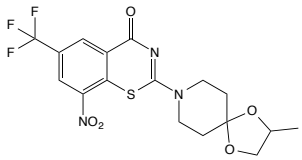
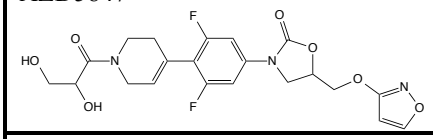
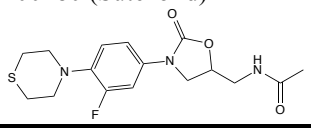
whereby the patient is dosed for a period of 2 to 5 days and the bacterial load in patient's sputum samples is measured for reduction (Donald *et al.* 2008). EBA studies are restricted to this limited time-point to avoid the possibility of the development of bacterial resistance to the trial compound (Koul *et al.* 2011). Phase II trials of a compound are dependent on the successful outcome of Phase I, and involve the dosing of the experimental drug in addition to the existing regimen for 8 weeks and drug potency is indicated by improved rate of sputal sterilisation. This trial can be extended to a longer time period (6-12 months) providing the safety aspects and the activity of the compound are satisfactory. For MDR-TB, the Phase II clinical trial can extend to 12-24 months, and for drug susceptible and MDR-TB patients, regular monitoring of progress towards sterilisation is conducted for 2 years post-treatment in order to recognise any relapse at the earliest possible moment. Finally, Phase III clinical trials are designed to support the eventual licensing of an anti-TB agent as a drug for use in the regular treatment of TB infections (Schluger *et al.* 2007).

1.5 Newly Discovered Anti-TB Agents

In this chapter, new anti-TB compounds in pre-clinical and clinical development will be reviewed. A summary of these compounds is presented in Table 1.2.

Table 1.2: Drug Profiles of recently discovered anti-TB agents

Compound	Discovered	Group	Family	Target	Mode of Action (MoA)
Bedaquiline 	2005	5	Diarylquinoline	ATP synthase	Inhibits generation of ATP by the F_0F_1 ATP synthase
PA-824 (Pretomanid) 	2006	5	Nitroimidazole	Multiple targets	Pro-drug. Activated to produce reactive nitrogen species leading to cellular toxicity
OPC67683 (Delaminid) 	2006	5	Nitroimidazole	Multiple targets	Pro-drug. Activated to produce reactive nitrogen species leading to cellular toxicity
SQ109 	2005	5	1,2-ethylenediamine	MmpL3	Inhibition of mycolic acid biosynthesis
AU1235 	2012	5	Adamantyl Urea	MmpL3	Export of trehalose monomycolate (TMM) *via* MmpL3
BM212 	2007	5	1,5-diarylpyrrole	MmpL3	?
THPP 	2013	5	THPP	MmpL3	Export of trehalose monomycolate (TMM) *via* MmpL3
Spiro 	2013	5	Spiro	MmpL3	Export of trehalose monomycolate (TMM) *via* MmpL3
C215 	2012	5	Benzimidazole	MmpL3	Inhibition of mycolic acid biosynthesis

BTZ043 	2009	5	Nitro-benzothiazinone	DprE1	Pro-drug, suicide inhibitor of DprE1. Inhibits arabinogalactan (AG) and lipoarabinomannan (LAM) biosynthesis
AZD5847 	2014	5	Oxazolidinones	50S Ribosomal Subunit	Protein synthesis inhibitor
PNU-100480 (Sutezolid) 	2009	5	Oxazolidinones	50S Ribosomal Subunit	Protein synthesis inhibitor

1.5.1 Bedaquiline

Bedaquiline (Sirturo™, TMC207), from the compound family of diarylquinolines (DARQs), has been identified as an inhibitor of both drug-sensitive and drug-resistant *M. tb* (Table 1.2). It was first recognised as a potential anti-TB compound in a whole cell phenotypic HTS campaign. Resistant mutants were generated against the compound in both *M.tb* and *Mycobacterium smegmatis,* and demonstrated a frequency of resistance (FoR) of 5 x 10^{-8} and 1 x 10^{-8} respectively, comparable to the FoR observed for RIF (Heep *et al.* 2001). Sequencing of genomic DNA extracted from these mutants identified SNPs in the *atpE* gene (Rv1305), and not in *gyrA* (Rv0006) and *gyrB* (Rv0005) (DNA gyrase), in which SNPs relating to quinolone resistance are commonly found (Andries *et al.* 2005). The *atpE* gene encodes the *c* subunit of the F_0 subunit of the F_0F_1 ATP synthase complex that generates ATP from ADP using the proton motive force from oxidative phosphorylation in the electron transport chain (Curtis 1987). The target was confirmed when *M. smegmatis* transformed with a construct constitutively expressing *atpE*Δ-D32V and *atpE*Δ-A63P

demonstrated resistance to TMC207 (Andries *et al.* 2005). An attractive characteristic of TMC207 is that it shows equal potency against dormant (non-replicating) and replicating mycobacteria with the same target specificity for the essential ATP synthase. This was somewhat unexpected due to the dramatically decreased availability of cellular ATP due to the considerable down regulation of the ATP synthase during dormancy. This led to potent bactericidal activity against non-replicating cells in which well-balanced bioavailability of ATP for energy metabolism is critical for maintaining the dormant-state (Koul *et al.* 2008). Further studies in a murine model of both actively replicating and latent *M. tb* infection showed significant inhibitory activity of TMC207. The mouse model also identified that the bactericidal activity was equipotent whether TMC207 was used as part of a combination treatment regimen or in monotherapy; the dose could be decreased by 50% if used in combination with the standard regimen but still maintained the same kill kinetics (Lounis *et al.* 2008). Significant success was observed in Phase I clinical trials of TMC207 assessing EBA in combination with a standard treatment regimen for drug susceptible TB, which lead directly to Phase II clinical trials with the addition of TMC207 to the standard treatment of MDR-TB. This trial found a significant improvement on the conversion of sputum samples from culture-positive to culture-negative in patients who received TMC207 (48% conversion to culture-negative) in combination with standard treatments as opposed to the control group, who received a placebo (9% conversion to culture-negative) (Diacon *et al.* 2009). This extremely high potency, along with the comparatively lengthy half-life of the compound validated the ATP synthase as a significant target for the development of future anti-mycobacterial agents with TMC207 as a highly promising anti-TB candidate. TMC207 is the first drug with a novel MoA approved by the FDA for the

treatment of TB since 1971. However, during clinical trials, out of 189 individuals included in the trial there were 36 fatalities, with 6 from the placebo group, resulting in an 11.4% increased risk of death for those administered TMC207 compared to a 2.5% in the control group. It was found that many patients in the trial group experienced QTcF prolongation as a side effect of the drug. Nevertheless, TMC207 was approved for use on a case-by-case basis for the treatment of MDR-TB (Centers for Disease Prevention and Control 2013).

1.5.2 Nitroimidazoles

The first compound from the nitroimidazole family to be tested against *M. tb* was metronidazole (MTZ). MTZ is a pro-drug that is reduced by ferrodoxin to a mixture of nitroso-intermediates, which react with cystedine residues to form sulfinamides and thioesters in the active site of many catalytic enzymes in the bacterial cytoplasm. It was selected because of its well documented activity against anaerobic bacteria. *M. tb* infections that are in latency are considered to have originated from hypoxic anaerobic growth conditions that induces the latent metabolic state. In a cynomolgus macaque model of TB infection, MTZ was used with and without combination with INH and RIF. As MTZ only has antimicrobial activity against latent non-replicating *M. tb*, it was expected that its incorporation into the regular treatment regimen may improve the efficacy of combating latent infections in order to prevent reactivation of the disease. It was found that 2 months of treatment with MTZ was as effective as a two month treatment with INH and RIF in combination or a six month treatment of INH alone in preventing the reactivation of a latent TB infection (LTBI) (Lin *et al.* 2012). The nitroimidazole compound family has been further explored in the

treatment of TB by the development of two other pro-drugs, known as PA-824 (Pretomanid) and OPC67683 (Delamanid).

PA-824 is activated by a F_{420} deazaflavin-dependent nitroreductase (Ddn) that is only present in the *M. tb* genome, making it only effective against *M. tb*. The compound produces reactive nitrogen species following its activation and targets non-replicating cells by nitric oxide inhibiting the cytochrome *c* oxidase and poisoning the bacterial respiratory system (Manjunatha *et al.* 2009). Following successful EBA studies, Phase II clinical trials have begun with PA-824 where the drug is being incorporated into existing treatment strategies, as well as recently established drug combinations (including bedaquiline and moxifloxacin) to treat both drug susceptible and MDR-TB (Diacon *et al.* 2012).

The second recently produced nitroimidazole, Delamanid (Matsumoto *et al.* 2006), also inhibits cellular growth by the production of reactive nitrogen species via reduction from Ddn. However, this compound has also been implicated in the inhibition of mycolic acid biosynthesis, an essential constituent of the mycobacterial cell wall. Delamanid has been shown to be a highly potent compound, with MICs ranging from 6-24 $ng.ml^{-1}$ and is active against both drug susceptible and MDR-TB with greater potency than PA-824 (Matsumoto *et al.* 2006). EBA trials have shown that Delamanid can substantially improve the rate of generation of culture-negative sputum samples (Gler *et al.* 2012). Delamanid has overtaken PA-824 and is currently in Phase III clinical trials with the aim of being incorporated into an optimised treatment regimen for MDR-TB and XDR-TB (Skripconoka *et al.* 2012).

1.5.3 MmpL3 inhibitors

Due to the relative lack of efficacy of EMB compared to the other Group 1 anti-TB drugs, an opening remained for an alternative 1,2-ethylenediamine compound with improved activity. A compound library of 60,000 analogues of the 1,2-ethylenediamine scaffold was synthesised and screened in a HTS phenotypic campaign against *M. tb*. Of the hits generated, one proved the most significant in terms of its potential as a drug candidate, SQ109 (Protopopova *et al.* 2005). Attempts to generate spontaneous resistant mutants against this compound met with continuous failure, however the examination of analogous compounds led to the generation of spontaneous mutants that were cross resistant to SQ109. These resistant mutants contained SNPs in a gene that encoded the Mycobacterial membrane protein large 3 (MmpL3), a transport protein that has been widely documented as a transporter of the essential cell wall constituent, TMM (Tahlan *et al.* 2012; Li *et al.* 2014). There has been some investigation into the synergistic effects of combining SQ109 with other agents, such as bedaquiline. It was found that the combined use of SQ109 and bedaquiline had the effect of significantly improving the bactericidal effects of the compounds used separately and also decreased the respective MIC of each compound (Reddy *et al.* 2010). SQ109 is presently undergoing Phase II EBA clinical trials, where the drug is administered for a short initial period in combination with standard first-line treatment regimens.

The bactericidal adamantyl urea AU1253 was identified by a phenotypic screen of 12,000 chemical scaffolds from a commercially available compound library (LeadScreen™) using *M. tb* with a very promising MIC of 0.3 μM. AU1253 was

shown to also be equally active against MDR-TB and spontaneous resistant mutants of *M. tb* strains were generated against AU1253 at 2-4 times the MIC with a FoR of 4 $x10^{-9}$ (Grzegorzewicz *et al.* 2012). These mutants were subsequently sequenced and a SNP (G^{758} to A^{758}) identified in *mmpL3*, translating to an amino acid substitution (G253E) that was present in all resistant mutants generated against AU1253. Further validation of MmpL3 as the cellular target of AU1253 was conducted through cell wall lipid analysis by thin layer chromatography (TLC). It was identified that although the biosynthesis of mycolic acids was not inhibited by AU1253, the translocation of TMM into the cell wall was affected, thus indicating a MoA for AU1253 in inhibiting TMM export by MmpL3 (Grzegorzewicz *et al.* 2012). Structurally it can be noted that SQ109 and AU1253 have similar chemical properties, which may account for their similarities in terms of MoA.

Another compound that has arisen from a phenotypic screening approach is BM212, a 1,5-diarylpyrrole derivative, which has been shown to have potent activity against both drug susceptible and MDR-TB strains (La Rosa *et al* 2012). The MIC of BM212 was shown to be 0.78 and 1.5 $\mu g.ml^{-1}$ for *Mycobacterium bovis* BCG and *M. tb,* respectively. Based on a similar strategy as with AU1253, *M. bovis* BCG and *M. tb* spontaneous resistant mutants were generated with FoR of 1.7 $x10^{-8}$ and 2 x 10^{-9}, respectively. The genomes of the resistant mutants were sequenced and multiple SNPs were identified in *mmpL3* (La Rosa *et al* 2012). All mutants sequenced contained an L320P mutation in the sixth predicted trans-membrane domain of MmpL3, however many other non-synonymous mutations were present in different resistant mutants. It was also demonstrated that the resistance mutations found in MmpL3 did not induce a drug efflux response, and therefore it is unlikely MmpL3

functions as a drug efflux mechanism (La Rosa *et al* 2012). The limitation of BM212 in terms of progression as an anti-TB drug is the high toxicity associated with the compound. Attempts are underway to re-engineer the BM212 scaffold to improve the toxicity profile of the compound (Biava *et al.* 2007). Recently tested analogues of BM212 proved highly efficacious in an acute murine model of TB infection. These improved BM212 derivatives were shown to be equipotent to many of the currently employed drugs routinely used in the treatment of *M. tb* with MICs reduced from 5 μM to 0.16 μM of the parent compound, with one compound (BM579) possessing improved cytotoxicity in a HepG2 cell line (Poce *et al.* 2013). The MoA of BM212 remains to be reported.

The tetrahydropyrazolo[1,5-a]pyrimidine-3-carboxamide (THPP) and N-benzyl-6',7'-dihydrospiro[piperidine-4,4'-thieno[3,2-c]pyran] (Spiro) chemical series were both identified as inhibitors of *M. tb* as part of a GSK led HTS campaign (Remuinan *et al.* 2013). The two compound series (THPP and Spiro) were found to inhibit *M. tb* at 0.3 μM. The generation and sequencing of spontaneous resistant mutants revealed SNPs in *mmpL3*, and the identification of MmpL3 as the target of the THPP and Spiro compounds was further validated by radio-labelled [^{14}C]-acetate uptake experiments and TLC lipid profilling, identifying that treatment with both THPP and Spiro compounds lead to the intracellular accumulation of TMM in *M. bovis* BCG (Remuinan *et al.* 2013). These compounds and analogues of them with both improved and decreased activity profiles were examined in a murine model of acute TB infection (Remuinan *et al.* 2013). The compounds now form part of a group of 177 small molecule inhibitors of *M. tb* that are publicly accessible through a GSK-led

directive, termed, "Open-source Drug Discovery," to further TB drug discovery, by giving groups worldwide access to these anti-TB leads (Ballel *et al.* 2013).

A screening campaign of 20,502 compounds selected from the extensive compound library of the Broad Institute yielded C215 (*N*-(2,4-dichlorobenzyl)-1-propyl-1*H*-benzo[*d*]imidazol-5-amine), a compound from the benzimidazole family that demonstrated potent anti-TB activity in a HTS phenotypic screen. Resistant mutants were selected at 2x and 10x the MIC and their genomes sequenced. Their *g*DNA was found to contain SNPs that mapped to *mmpL3* in the following loci: L320P, T667A, V684A and V51A. The validation of MmpL3 as the target of C215 was validated by the use of [^{14}C]-acetate uptake experiments and TLC analysis examining fatty acid methyl esters (FAMEs) and mycolic acid methyl esters (MAMEs) in mycobacteria following exposure to the C215 compound. They identified a significant decrease in the amounts of labelled FAMEs and MAMEs following exposure of cells to a range of C215 concentrations from 1 to 10 times the MIC. However, the MIC was not stated in the publication (Stanley *et al.* 2012).

Indoleamides have also been found to inhibit MmpL3 and have been shown to have potent activity against both drug susceptible and MDR-TB. Using the same method as all the other MmpL3 inhibitors (excluding SQ109), the target was identified by the sequencing of spontaneous resistant mutants. Mutants resistant to the indoleamides were found to contain a single conserved SNP in *mmpL3* at position S228T mapping to the fourth predicted trans-membrane domain of MmpL3. Further characterisation of the inhibitory effects of the indoleamides was conducted in a murine model of TB infection and found that the indoleamides are orally bioavailable, remaining at

concentrations higher than the MIC in the lung for nearly 24 hours post administration (Lun *et al.* 2013).

1.5.4 Benzothiazinones

The benzothiazinone (BTZ) inhibitors are to date, one of the most potent anti-TB compounds with MICs described in the range of 0.1 – 30 $ng.ml^{-1}$ against *M. tb*. This is a significant improvement from the Group 1 drugs (Makarov *et al.* 2006) (e.g. INH has an MIC of 0.02 to 0.2 $\mu g.ml^{-1}$ and the MIC of RIF is >1 $\mu g.ml^{-1}$). In the initial BTZ screening process, over 30 compounds demonstrated MICs below 50 $ng.ml^{-1}$ against *M. tb* (Zhang *et al.* 2005). The lead BTZ compound, BTZ043, was found to be equipotent against all clinical isolates of both MDR and XDR-TB, with bactericidal activity that can reduce colony forming unit (cfu) counts by 1000 times in the primary 72 hours of treatment. Target identification was conducted by two independent genetic approaches. Firstly, using a cosmid library to identify resistance-conferring genes, and secondly, by the isolation of resistant strains of *M. bovis* BCG and *M. smegmatis,* the *g*DNA of which was sequenced. Both methods indicated the target of BTZ was *Rv3790*, which encodes decaprenylphosphoryl-β-D-ribose oxidase (DprE1) (Makarov *et al.* 2009). DprE1 works in combination with decaprenylphosphoryl-D-2-keto erythro pentose reductase (DprE2) and catalyses the epimerisation of decaprenylphosphoryl-ribose (DPR) to decaprenylphosphoryl arabinose (DPA), a sugar precursor to arabinogalactan (AG) and lipoarabinomannan (LAM), both essential cell wall components in mycobacteria (Mikusova *et al.* 2005; Jankute *et al.* 2015). Further investigation into the MoA has identified a likely secondary killing mechanism of BTZ. This dual-killing mechanism may be indicative of the high

potency of these compounds. This secondary mechanism is the result of chemical synthetic lethality, preventing the cellular recycling of decaprenyl phosphate and the accumulation of DPR and consequent mycobacterial growth inhibition (Grover *et al.* 2014). The structural elucidation of the mode of inhibition of BTZ has also been completed, identifying the MoA as suicide inhibition by covalent binding of BTZ to a conserved cysteine residue 378 in the active site of DprE1. This paves the way forward for medicinal chemistry efforts to further improve BTZ (Batt *et al.* 2012; Grover *et al.* 2014). Other nitro-aromatic compound families have been identified that covalently bind the same Cys378 of DprE1, including dinitrobenzamide (DNB1), benzoxyguinoxaline (VI-9376) and a nitro-triazole (377790) (Zumla *et al.* 2013).

1.5.5 Oxazolidinones

The oxazolidinone chemical series were first discovered as potent inhibitors of Gram-positive bacteria in 1987 by DuPont Pharmaceuticals (Slee *et al.* 1987). Ten years later, upon re-examining the series, Pharmacia identified linezolid as the lead compound and entered it into pre-clinical development (Ford *et al.* 1997). The high potency of linezolid against Gram-positive bacteria is likely due to its MoA of inhibiting protein synthesis by binding the 50S ribosomal subunit and preventing subsequent complexation with the 30S subunit; identified by the sequencing of linezolid-resistant isolates (Kloss *et al.* 1999). Linezolid displayed considerably high anti-mycobacterial activity *in vitro* against clinical isolates (Huang *et al.* 2008) and was approved by the FDA for treatment of vancomycin-resistant *Enterococcus faccium* infections (FDA Center for Drug Evaluation and Research, 2001). Therefore, it was trialed for incorporation into the treatment strategy for MDR and XDR-TB

(Lee *et al.* 2012). Linezolid was not recommended for prolonged treatment of drug resistant *M. tb* infections due to the considerable side effects such as severe neuropathy and haematological issues. However, a statistical assessment of 11 clinical trials documented for linezolid treatment for XDR-TB found an improvement over existing regimens (Fortun *et al.* 2005; Cox *et al.* 2012). Efforts have been made to further develop the oxazolidinones for incorporation into TB treatment regimens and the eventual improvement of the toxicological performance of the oxazolidinone chemical scaffold. A new compound, AZD5847 (AstraZeneca), has demonstrated improved extracellular and intracellular *in vitro* bactericidal activity against *M. tb* compared to linezolid, as well as delivering promising results in terms of efficacy in combination with first line TB drugs (Bakasubramanian *et al.* 2014). Animal trails with AZD5847 have been conducted in both mice and dogs by AstraZeneca, and an EBA 14 day clinical trial (Phase 2a) has been performed by National Institute of Allergy and Infectious Diseases (NIAID) (Butler, AstraZeneca). Despite reports that the compound was well tolerated and completion of the EBA trial, the results are yet to be published. The oxazolidinones have also been explored by Pfizer, who have developed Sutezolid (PNU-100480), a molecule with similarly improved *in vitro* characteristics to AZD5847 over linezolid. Improved bactericidal activity and pharmacokinetics were observed with PNU-100480 in a murine model compared to linezolid (Williams *et al.* 2009). Furthermore, the results of a pharmacokinetics and whole-blood bactericidal activity clinical trial with PNU-100480 and linezolid have been published. This trial shows PNU-100480 was well tolerated at 1000 mg doses, compared to the linezolid maximum recommended treatment dose of 300 mg, with comparable bactericidal efficacy to linezolid at 300 mg and a two log reduction of cfu

at 600 mg. These results indicate that maximal bactericidal efficacy of PNU-100480 is possible while maintaining sub-toxic concentrations (Wallis *et al.* 2010).

1.6 The Future for TB Drug Discovery

The demand to develop new anti-TB drugs that are able to combat the evolving strains of drug resistant *M. tb,* that can reduce treatment duration and can eventually lead to better control over the global incidence of TB has never been greater. The advancement of technology has driven a change in the classical approach to drug discovery and has catalysed the development of a number of potent compounds with novel MoA that are able to circumvent current bacterial mechanisms of resistance. The employment of large-scale high cost HTS techniques has accelerated the identification of new chemical scaffolds with proven activity. Advancement in WGS technologies has revolutionised the identification of targets of antibiotic compounds and provides a foundation for the validation of their MoA. Improved models of disease are making it possible to better understand how antibiotics respond *in vivo*, in terms of their ability to combat infection, as well as their chemical effects on the infected host, allowing for a greater understanding of how compounds will behave in clinical trials. Despite these considerable advancements, many of these compounds never make it into the TB drug development pipeline due to poor *in vivo* activity, toxicological restraints, high FoR, unsuitability, poor half-life, insufficient bioavailability, lack of efficacy against latent infection or unsafe side effects. As a result, only one novel compound has been accepted by the FDA for the treatment of TB in the last 40 years, and side-effects of this compound when used in the clinic

have rendered it only suitable for the treatment of MDR-TB infections. Therefore, despite progress, we are still far from a long-term solution to the treatment of TB.

Not only has there been a change in strategy, but also a change in attitude. In 2013, scientists from GSK made a series of 177 chemical scaffolds discovered by a phenotypic screen globally available for any group that felt their technology and ideas could further develop these compounds into possible anti-TB drugs. This novel compound sharing initiative, termed "Open-source Drug Discovery," is aimed at improving the global pooling of resources to speed up the drug development process and motivate an expansion of the global effort to eradicate this disease (Ballell *et al.* 2013). The unparalleled progress in the whole cell phenotypic screening method of TB drug discovery profoundly demonstrates the effectiveness of this approach. A top-down strategy to drug development, although more costly than conventional approaches, holds the greatest statistical chance of success in a fixed time point. As compound libraries become more extensive and HTS technology advances, the output of screening campaigns in terms of hit identification will continue to grow. This technology is also highly translatable to other microbial diseases, for example considerable success attributed to whole cell phenotypic HTS, has been made in the development of antimalarial drugs in recent years (Bowman *et al.* 2014). Although, this approach to the development of TB drugs is the most widely followed at present, work is still continuing to identify the drug development methods of the future.

Computational medicinal chemistry (CMC) is a method of *in silico* drug discovery where hits can be identified more rapidly than conventional laboratory based approaches. There are two main sub-divisions of CMC, structure-based drug

screening (SBDS) and ligand-based drug screening (LBDS). The former involves the use of docking simulation software that can screen a collection of virtual compounds against the target protein structure. The latter involves pharmacophore modeling and quantitative structure-activity relationship (QSAR) in order to identify molecules of likely biological significance. This method is also dependent on X-ray crystallographic and/or Nuclear Magnetic Resonance (NMR) structural solution of the target protein and three dimensional chemical modeling of the chemical scaffolds undergoing screening. CMC serves as a powerful tool for the identification of ligands that are able to overcome known resistance mechanisms. A number of compounds have been found by this approach that are able to bind InhA, the target of INH, irrespective of resistance conferring mutations within the InhA protein. (Koseki *et al.* 2014).

In the hunt for novel anti-TB compounds, some groups are turning to ancestral sources of medication for a modern solution. Medicinal plants have been used for many hundreds of years, and their rich diversity of chemical compounds makes them a lucrative hunting ground for the next generation of antibiotics. This ethnobotanical approach to drug discovery has been implemented in the search for new drugs active against *M. tb*. Natural products have a considerable stake in the drug development market; 48.6% of FDA approved drugs from 1981-2010 and 74.8% of drugs that protect against infection are products from natural sources or have been adapted from such products (Newman *et al.* 2012). Phenotypic whole cell HTS of libraries of natural products have yielded a number of peptides and polyketides that show potent activity against *M. tb* H37Rv, with MICs ranging from 0.025 $\mu g.ml^{-1}$ for Nocardithiocin (peptide) produced by *Nocardia pseudobrasiliensis* IFM 0757 (a

bacteria found in soil), 0.12 μg.ml^{-1} for Trichoderin A (peptide) produced by *Trichoderma* sp. 05F148 (a marine sponge), and 2.52 μg.ml^{-1} for Biscogniazaphilone A (polyketide) produced by *Biscogniauxia formosana* (an endophytic fungus) (Alvin *et al.* 2014).

With the plethora of multi-directional research currently underway to discover the next anti-TB drug, and the constant emergence of new technologies, for the first time, the scientific community has the chance to regain control of transmission and treatment of TB. A continuous pipeline of new drugs with novel targets will allow us to halt the emergence and spread of resistant strains of *M. tb*, and will bring us one step closer to the ultimate goal of total eradication of TB, a disease that brings death and suffering to millions worldwide.

The aim of this thesis was to shed light into the MoA of anti-TB compounds identified in phenotypic HTS. The importance of this work in TB drug development is exemplified by the Drug Discovery pipeline (Figure 1.3). In this model, MoA elucidation is the precursor to 'hit-to-lead' medicinal chemistry where the physiochemical properties of the compound-target interaction can be explored to improve the inhibitory effect of the compound, whilst also improving the drug-like characteristics of the molecule. In this thesis a number of novel MoA have been identified and as a result, this work serves as a solid foundation for the future of TB drug development.

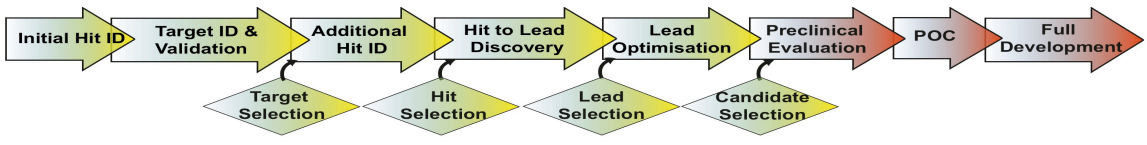


Figure 1.3: The Drug Discovery Pipeline.

CHAPTER 2

The imidazo[1-2-*a*]pyridines inhibit mycobacterial oxidative phosphorylation by targeting the *b* subunit of the cytochrome bc_1 complex

2.1 Introduction

Chemical agents that disrupt the bacterial electron transport chain (ETC), preventing oxidative phosphorylation and subsequent adenosine tri-phosphate (ATP) biosynthesis could show considerable promise as antibiotic compounds. However their toxicological effects on mammalian systems has rendered them in dangerous territory in antibiotic drug discovery. The complexity of the ETC and the multitude of essential proteins that are required for proton translocation in order to sustain the proton motive force which drives the F_0F_1 ATP synthase and subsequent cytoplamsic ATP concentrations, makes this pathway a wealth of potential antibiotic targets. As a ubiquinol-cytochrome *c* reductase, the cytochrome bc_1 complex (complex III of the ETC) functions by coupling electron transfer to the transfer of a proton across the membrane, contributing to the proton electrochemical gradient that powers the F_0F_1 ATP synthase and subsequent oxidative phosphorylation. This occurs through the oxidation of two ubiquinols (QH_2) to two ubiquinones (Q), and the reduction of an iron-sulfur cluster, releasing four protons from the ubiquinols into the periplasm. The iron-sulfur cluster subsequently reduces cytochrome c_1 with two electrons, and reduces BL haem, which passes the electrons to the BH haem where one ubiquinol is reduced to one ubiquinone, using two protons from the cytoplasm. Inhibition of the cytochrome bc_1 complex has been previously identified by the compound myxothiazol, which competitively inhibits at the ubiquinol binding site (Q_o site). This is summarised in Figure 2.1.

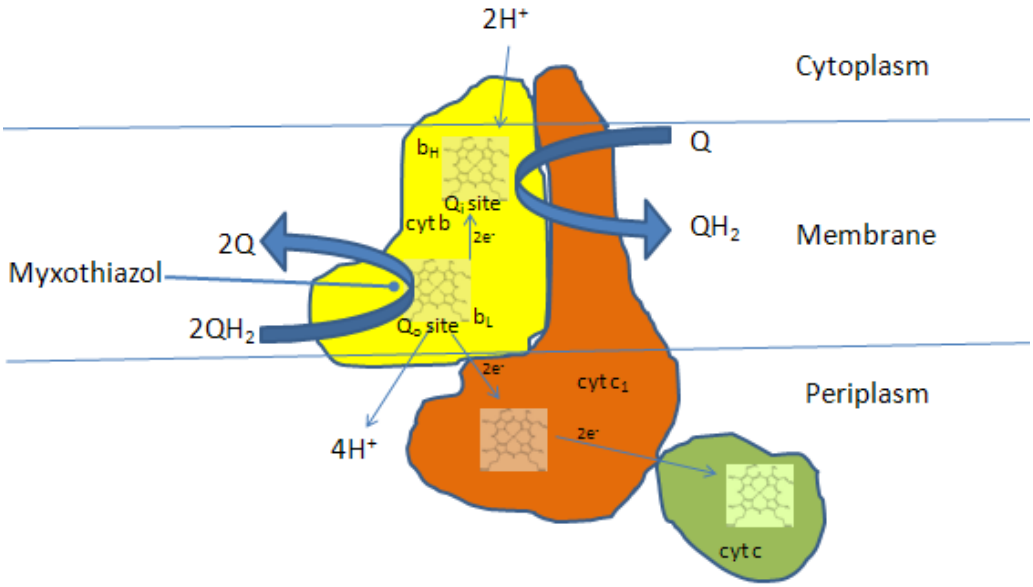


Figure 2.1: Representation of the functional activity of the Ubiquinol-cytochrome *c* reductase (Cytochrome *bc*$_1$ complex or Complex III) in the electron transport chain. The oxidation of two Ubiquinols (QH_2) to two Ubiquinones (Q) is coupled to the net translocation of two protons (H^+) from the cytoplasm to the periplasm, contributing to the electrochemical proton gradient (proton motive force) that drives ATP synthesis by the F_0F_1 ATP synthase.

Imidazo[1,2-*a*]pyridine-3-nitroso and imidazo[1,2-*a*]pyrimidine-3-nitroso hits were identified to inhibit *M. tb* QcrB with promising MICs of 3.13 and 0.78 μg.ml^{-1}, respectively (Abrahams *et al.* 2012). These compounds were found to display poor solubility and toxicological constraints when tested in a VERO cell line (Anaflous *et al.* 2004). Another series, the imidazo[1,2-*a*]pyridine-3-hydrazones have also been synthesised, however this compound family displayed no significant inhibitory activity against *M. tb* H37Rv when tested *in vitro* at concentrations up to 20 times the MIC of RIF (0.031 μg.ml^{-1}) (Kasimogullari *et al.* 2004). The 3-amino-imidazo[1,2-*a*]pyridines are potent inhibitors of *M. tb* (MIC in the region of 0.76 μM) and were found to target glutamine synthetase, a mycobacterial drug target that is essential for the metabolism of nitrogen, as well as cell wall biosynthesis (Odell *et al.* 2009). The

2,7-dimethylimidazo[1,2-*a*]pyridine-3-carboxamides and 2,7-dimethylimidazo[1,2-*a*]pyrimidine-3-carboxamide compounds were also found to display considerable potency against *M. tb* with MIC values of ≤ 1 μM (Moraski *et al.* 2011). The pharmacokinetic properties of these compounds were investigated and it was established they display many drug-like properties, in addition to potent efficacy against MDR-TB and XDR-TB (Moraski *et al.* 2011).

Following a HTS campaign against *M. tb* in a whole cell phenotypic assay against an extensive library (GSK, Tres Cantos), compounds with an imidazo[1-2-*a*]pyridine (IP) scaffold were identified with potent MICs against *M. tb*. We characterised the target of the hit 2,6-dimethyl-N-(4-(trifluoromethyl)benzyl)imidazo[1,2-*a*]pyridine-3-carboxamide (IP 3), along with three other less potent IP compounds. Using spontaneous resistant mutants and WGS we identified mutations in the *b* subunit of the cytochrome bc_1 complex (ubiquinol cytochrome *C* reductase) of the mycobacterial ETC, denoted QcrB. These studies were further validated by overexpression of the target in order to observe a change in MIC of the compound.

2.2 Materials and Methods

2.2.1 MIC Determination of the IP 1,3 and 4 in *M. bovis* BCG

The MICs of IP compounds 1, 3 and 4 were determined against *M. bovis* BCG grown aerobically in Middlebrook 7H9 liquid media (Difco) containing 0.05 % (v/v) Tween-80, 0.25 % (v/v) glycerol, supplemented with 10 % (v/v) ADC: albumin (1.25 % w/v), dextrose (0.5 % w/v) and catalase (7.5×10^{-4} % w/v) (Sigma-Aldrich). Cultures were grown at 37°C and 180 rpm. *M. bovis* BCG MIC determination was conducted on Middlebrook 7H11 agar (Difco) containing 0.5 % (v/v) glycerol and supplemented with 10 % (v/v) OADC: oleic acid (1.25×10^{-2} % v/v), albumin (1.25 % w/v), dextrose (0.5 % w/v) and catalase (1×10^{-3} % w/v) (Sigma-Aldrich). This was determined by plating a serial dilution of cells onto 7H11 agar containing a range of concentrations of compounds in a dose response format. The numbers of bacterial cells plated was calculated by OD_{600} (assuming OD_{600} of 1.0 is approximately equal to 2.5×10^8 cells.ml^{-1}) and 10^4, 10^3, 10^2 and 10^1 cells were spotted onto each plate. The plates were wrapped in Parafilm® and aluminum foil and were incubated at 37°C for 4-6 weeks until growth inhibition could be recorded. The MIC was defined as the lowest concentration of compound at which cell growth was completely inhibited.

2.2.2 Generation of *M. bovis* BCG Mutants Resistant to IP 1, 3 and 4

Resistant mutants of *M. bovis* BCG were generated by plating 10^8 cells from a liquid culture grown to mid-log (OD_{600} 0.8-1.0) onto 7H11 solid media containing 5x MIC of each IP compound. Suspected mutant colonies were transferred into 7H9 liquid

media and grown up without antibiotic selection before being plated back on to 7H11 solid media containing 5x MIC of compound, along with the parental wild-type (WT) strain of *M. bovis* BCG. This was repeated on compound negative media as a growth control. Both plates were incubated at 37^{o}C for 4-6 weeks. Confirmed mutants were re-cultured into 50ml of 7H9 containing 2x MIC of compound in order to maintain resistance selection. Glycerol stocks of these mutants were prepared by flash freezing 1ml of mid-log cultures with 25% glycerol in liquid nitrogen and storage at -80^{o}C. The remaining culture was used for *g*DNA extraction and sequencing.

2.2.3 Genomic DNA Extraction and Genome Sequencing

The extraction of *g*DNA was conducted from 25-50 ml of mid-log *M. bovis* BCG (WT or mutant) culture. The culture was pelleted by centrifugation at 3,500 rpm for 30 minutes at room temperature. The pellet was subsequently re-suspended in 450 µl GTE buffer containing 50 mM glucose, 25 mM Tris.HCl pH8 and 10 mM ethylenediaminetetraacetic acid (EDTA) pH 8, and 1 mg.ml^{-1} lysozyme was added before incubation overnight at 37^{o}C without agitation. The following day sodium dodecyl sulphate (SDS) was added to a total concentration of 1.67 % in addition to 0.5 mg.ml^{-1} of Proteinase K. Following incubation for 3 hours at 55^{o}C, 0.16 mg.ml^{-1} RNAse A was added and the temperature reduced to 37^{o}C for 30 minutes. To this, 1.2 M sodium chloride and 1 ml chloroform:isoamylalcohol (24:1, v/v) was added and mixed by inversion. Following centrifugation at 13,000 rpm for 10 minutes, the aqueous layer was extracted and washed twice more with 1 ml chloroform:isoamylalcohol (24:1, v/v) followed by a wash with 0.7 x volume of chilled isopropanol. Following a 30 minute centrifugation at 13,000 rpm, isopropanol

was removed and the DNA pellet washed with 700 μl of 70 % (v/v) ethanol at 4^{o}C and following a further 30 minute centrifugation at 13,000 rpm, ethanol was removed and the pellet left to dry at room temperature for 15 minutes before being re-suspended in 20 μl of elution buffer from a Qiagen Miniprep Kit. The purity of the sample was assessed with 1 % (w/v) agarose gel electrophoresis and all *g*DNA was stored at -20^{o}C. Both parental WT *g*DNA and mutant *g*DNA were sequenced in tandem on the Illumina platform (University of Warwick) with a total of 7 samples.

2.2.4 Recombinant DNA Manipulations

Standard procedures of molecular genetics were followed during the cloning process (Sambrook *et al.* 1989). All reference data for sequences of *M. bovis* BCG genes was obtained from xBASE (Chadhuri *et al.* 2008). All oligonucleotide primers and sequencing of constructs was performed by Eurofins MWG Operon, Ebersberg, Germany. In order to overexpress QcrB in *M. bovis* BCG, three constructs were made containing the genes: *qcrB, qcrCAB* and the gene cluster *ctaE-qcrCAB* in the mycobacterial overexpression vector pMV261 with a kanamycin resistance cassette for transformant selection. These genes were amplified by polymerase chain reactions (PCR) using Phusion High-Fidelity DNA polymerase (New England Biolabs) using *M. bovis* BCG WT *g*DNA as a template. Fragment sizes of 1.7 kb (*qcrB*), 3.8 kb (*qcrCAB*) and 4.6 kb (*ctaE-qcrCAB*) were cloned into the mycobacterial overexpression vector pMV261(Kan) using *Bam*HI and *Hind*III restriction sites which were prepared using FastDigest restriction endonucleases (Fermentas) and ligated with T4 DNA Ligase (New England Biolabs). All constructs were verified by sequencing and diagnostic digest with 1 % agarose gel electrophoresis.

Oligonucleotide Primers:

Primer	Sequence (5'-3')
qcrB sense	GATCGATC**GGATCC**AATGAGTCCGAAACTGAGTCC
qcrB anti-sense	GATCGATC**AAGCTT**CTAGTGCTCGCCGTCTGG
qcrCAB sense	GATCGATC**GGATCC**AATGACGAAACTGGGGTTCACC
qcrCAB anti-sense	GATCGATC**AAGCTT**CTAGTGCTCGCCGTCTGG
ctaE-qcrCAB sense	GATCGATC**GGATCC**GATGGTCCCATGAGGATCAAC
ctaE-qcrCAB anti-sense	GATCGATC**AAGCTT**GTGCTTGATTTGCCCGGTTC

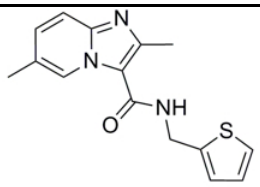
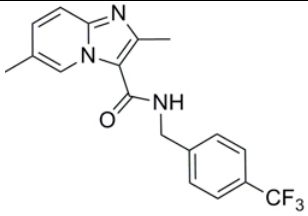
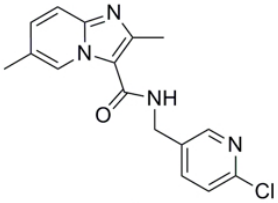
These constructs were subsequently electroporated into electrocompetent *M. bovis* BCG cells that had been prepared by centrifugation of 100 ml of mid-log BCG culture (4000 rpm at 4^{o}C) and a subsequent 3 rounds of washes of the pellet with ice-chilled 10 % glycerol. After the final wash, the supernatant was removed and the cells resuspended in 2 ml of 10 % glycerol. These electrocompetent cells were either stored in 250 μl aliquots by flash freezing in liquid nitrogen and prolonged storage at -80^{o}C or were used freshly for transformation by electroporation. The electroporation was conducted by combining 1 μl of plasmid construct (pMV261, pMV261-*qcrB*, pMV261-*qcrCAB* and pMV261-*ctaE.qcrCAB*) with 200 μl of electrocompetent *M. bovis* BCG cells in a sterile Gene Pulsar electroporation cuvette with a 0.1 cm gap between plates (Bio-Rad). Following 10 minutes incubation at 4^{o}C, cells were pulsed with 1800 Volts twice before returning to 4^{o}C incubation. The cuvette contents (200 μl) were transferred to 2.8 ml of Middlebrook 7H9 media and incubated without agitation at 37^{o}C overnight, before plating 20, 50 and 100 μl of transformation mix onto selective Middlebrook 7H11 media containing antibiotic respective to the plasmid resistance cassette (kanamycin at 25 μg.ml^{-1}). Plates were stored at 37^{o}C for 3-4 weeks. Colonies were picked into Middlebrook 7H9 media with selective antibiotic (25 μg.ml^{-1} kanamycin) and grown at 37^{o}C until mid-log before being plated back on to 7H11 solid media containing a range of concentrations of IP compound 3 (0, 1, 2, 4 and 8 μM, respectively) and incubated for 3-4 weeks at 37^{o}C.

2.3 Results

2.3.1 MICs of IP 1, 3 and 4 in *M. bovis* BCG

IP 1 was the initial hit compound from the HTS whole cell phenotypic campaign conducted at GSK (Tres Cantos), and IP 3 and 4 were compounds with altered functional groups in order to improve efficacy. IP 2 is a commercially available compound that was also found to inhibit *M. tb* H37Rv in the initial screen. Following a solid media dose response analysis of the MIC of the IP compounds against *M. bovis* BCG, the most effective compound was found to be IP 3 with an MIC of 0.5 μM against *M. bovis* BCG. This compound also showed lead potency against *M. tb* H37Rv, conducted by GSK during the HTS screen. A table of MIC values and structures of the IP compounds tested is shown below in Table 2.1.

Table 2.1: IP compounds identified to target QcrB

IP Compound Number	IP Compound Structure	MIC (μM)	
		M. tuberculosis H37Rv	*M. bovis* BCG
1		0.2	1
3		0.03	0.5
4		5	5

2.3.2 Target Identification of the IP Chemical Family

The identification of the physiological target of the IP inhibitors is the first step to elucidation of the MoA of the compounds in mycobacteria. Using the MICs for the compound (as indicated in Table 2.1), spontaneous resistant mutants were generated to the IP compounds by screening 1 x 10^8 cells at 5x MIC. The FoR of these compounds was 2, 3 and 1 in every 1 x 10^8 for IP 1, 3 and 4, respectively. WGS analysis of the *g*DNA extracted from each of the resistant mutants identified 16 SNPs compared to the WT *M. bovis* BCG parental strain. Of these 16 SNPs, 5 were considered to be the result of laboratory bacterial storage conditions, and 5 were predicted to be synonymous mutations or potential insertions/deletions. Only one mutation in the remaining 6 was found to be consistently present in all mutants but absent in the WT, encoding a single base change from ^{937}ACC>^{937}GCC (translating to the amino acid substitution of T313A) in the gene encoding *qcrB*, the b subunit of the ETC ubiquinol cytochrome C reductase. It was predicted that this mutation signals the target of the IP inhibitors as QcrB, and may affect inhibitor binding or cellular drug accumulation, thus equipping mutants with the ability to survive 5x MIC of the compounds.

2.3.3 Target Validation by Overexpression of QcrB in *M. bovis* BCG

In order to confirm the conserved SNP ^{937}AAC>^{937}GCC confers resistance to the IP compounds, mutants selected against each compound were screened for cross-resistance to each of the other IP inhibitors at 5x MIC with a WT *M. bovis* BCG control. The results indicated a cross-resistance phenotype of each of the mutants to

each IP inhibitor irrespective of which compound the mutants were raised against. This confirms the amino acid substitution from threonine to alanine at the 313 position of QcrB conveys resistance to the IP compounds (Figure 2.2).

Following the identification of QcrB as the putative target of the IP compounds, further validation was required in order to confirm the MoA of these drugs. This was conducted by the cloning of varying lengths of the QcrB gene cluster (Figure 2.3) into the constitutive mycobacterial overexpression vector pMV261 and subsequent transformation by electroporation into *M. bovis* BCG.

M. bovis BCG strains containing each of these constructs were plated onto Middlebrook 7H11 solid media containing a dose response (0 x, 2 x, 4 x 8 x and 16 x MIC) of the most potent of the IP compounds, compound 3 (0, 1, 2, 4 and 8 μM respectively). As a control, an empty pMV261 vector strain was also prepared and plated. The results indicated that the overexpression of QcrB, QcrCAB and the complete gene cluster (CtaE-QcrCAB) in *M. bovis* BCG increased the MIC of IP compound 3 to >16x its original value of 0.5 μM, validating the target of these compounds as QcrB. This result is illustrated in Figure 2.4.

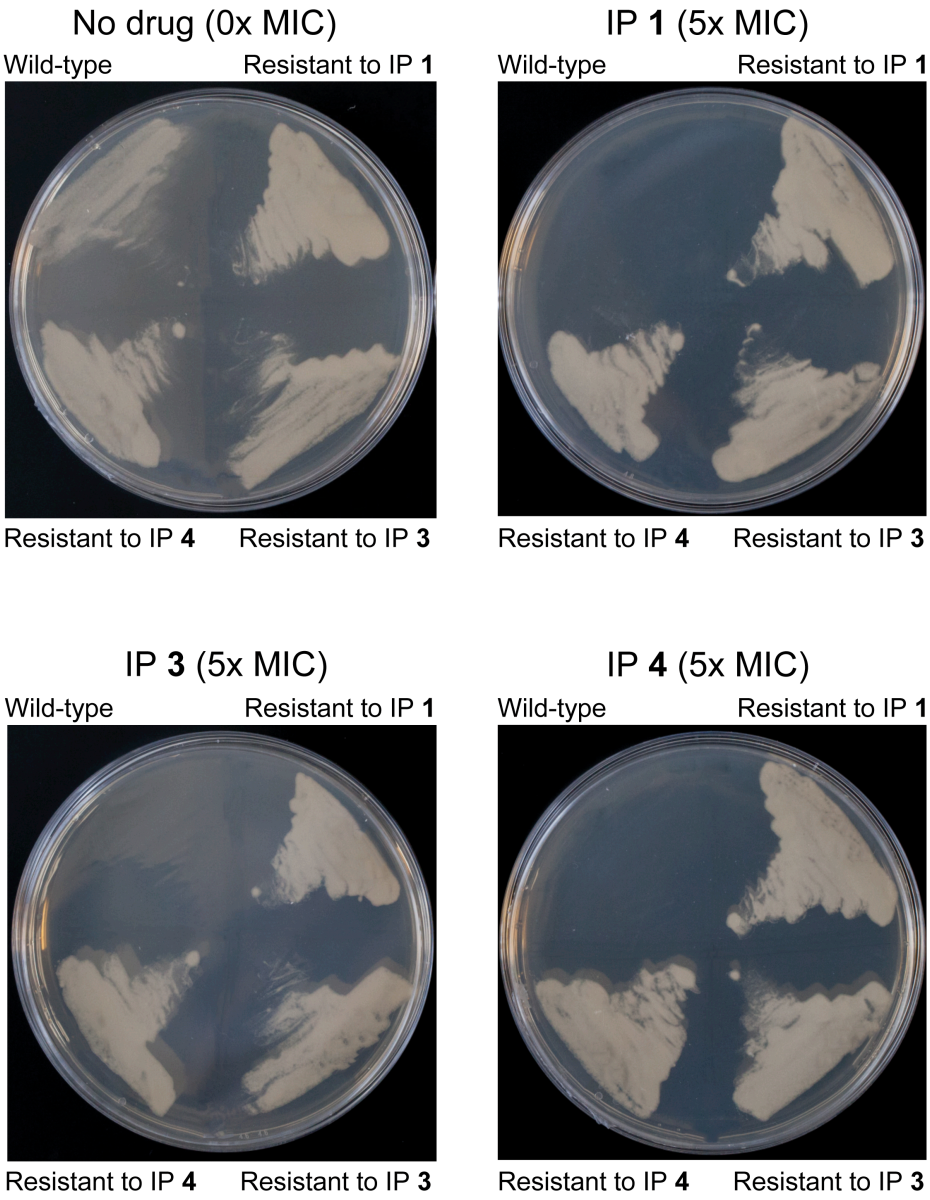


Figure 2.2: Cross-resistance of *M. bovis* BCG mutants to IP compounds. Mutants raised against IP compounds 1, 3 and 4 were tested for cross-resistance to each of the other IP compounds. This confirmed that the SNP in the *qcrB* gene at position ^{937}ACC>^{937}GCC conveys resistance to all three IP compounds tested. (Figure adapted from Abrahams *et al.* 2012).

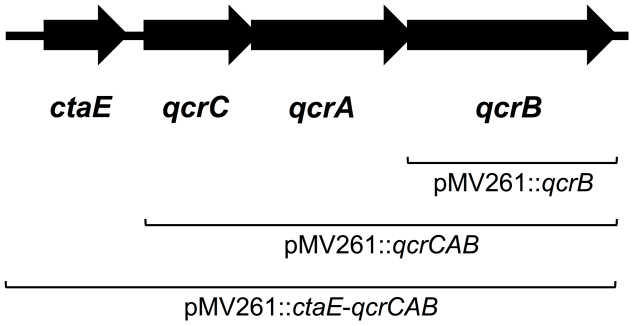


Figure 2.3: Fragments of the *qcrB* gene cluster that were cloned into pMV261. The resultant constructs were electroporated into *M. bovis* BCG and an MIC screen conducted to observe an increase in the MIC when QcrB is overexpressed and therefore validate the cellular target of the IP compounds as QcrB. (Figure adapted from Abrahams *et al.* 2012).

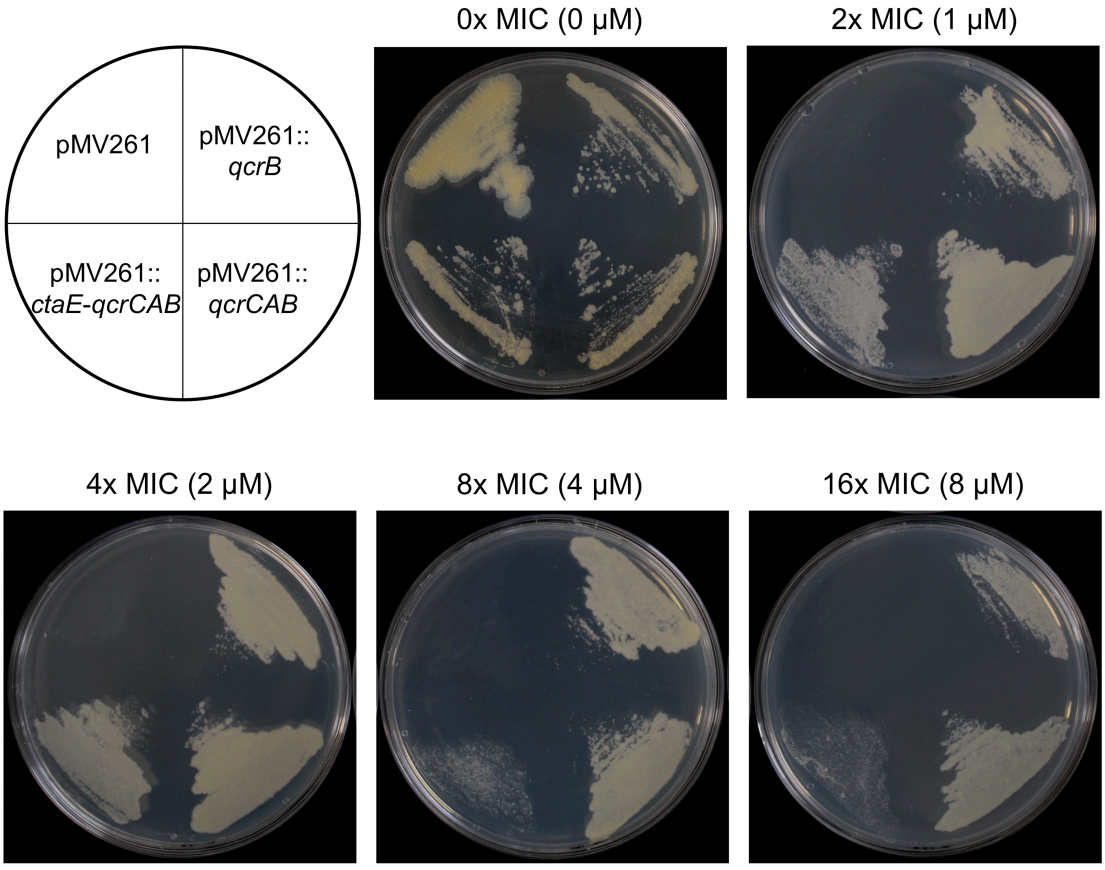


Figure 2.4: The overexpression of QcrB, QcrCAB and CtaE-QcrCAB in *M. bovis* BCG leads to an increase of MIC against IP compound 3 to > 16 x the MIC of WT. Varying lengths of the *qcrB* gene cluster were cloned into pMV261 and electroporated into *M. bovis* BCG, resulting in an increased tolerance to IP compound 3 and a validation of the QcrB target. (Figure adapted from Abrahams *et al.* 2012).

2.4 Discussion

Here we have identified a novel mycobacterial drug target and a series of compounds that show great promise as a foundation for future medicinal chemistry efforts. The essential *b* subunit of the cytochrome bc_1 complex forms a major component of mycobacterial respiration by the ETC, functioning as a ubiquinol-cytochrome *c* reductase, coupling electron transport to the translocation of protons, adding to the proton electrochemical gradient which drives ATP biosynthesis. There are three essential constituents to the cytochrome bc_1 complex, namely a cytochrome c_1, cytochrome *b* and a Rieske iron sulfur complex. The majority of inhibitors of the complex that have been previously identified for chemotherapeutic purposes function by way of an analogous structure to either the quinone or quinol substrate, competitively targeting the two catalytic domains of the integral membrane protein complex. Historically, antimycin was shown to be the first recognised inhibitor of QcrB and functions by binding the quinol (Q_i) site and competitively inhibiting the reduction of quinol to quinone and the subsequent oxidation of the cytochrome *b* subunit (Mitchell 1976). However, the most readily understood and well-documented inhibitor of QcrB is myxothiazol. Myxothiazol inhibits the reduction of *b* cytochromes by competitively binding the quinone (Q_o) binding site at high affinity ($K_d \leq 1$nM) (von Jagow *et al.* 1984). Other inhibitors have subsequently been shown to inhibit QcrB by the same mechanism as myxothiazol, such as Strobilurin A and Mucidin (von Jagow *et al.* 1986).

Three compounds from the IP family have been shown to inhibit QcrB by the generation of spontaneous resistant mutants that each contained the same base change

SNP (937ACC > 937GCC) at a position that corresponds to the amino acid substitution of a threonine to an alanine at position 313 (T313A). The crystal structure of the full cytochrome bc_1 complex from bovine heart mitochondria (Xia D *et al.* 1997) was used to determine whether or not resistance was a function of a change in catalytic activity caused by the amino acid substitution, however *in silico* mapping of the T313A mutation indicated the mutated residue is located proximally to the quinol binding site (Q_i). It is therefore likely that resistance occurs by a similar mechanism to Antimycin, competitively inhibiting the reduction of quinol to quinone (Figure 2.5).

Following the generation of resistant mutants against the three different IP compounds, it was necessary to demonstrate that the three compounds had the same mechanism of inhibition, therefore cross-resistance testing was conducted, confirming that all mutants were resistant to all compounds. Subsequent analysis of *M. bovis* BCG strains containing an overexpression construct, expressing various lengths of the *ctaE-qcrCAB* operon further validated QcrB as the true physiological target of IP compound 3 as an MIC shift (> 8 μM) was apparent, while a strain containing the empty plasmid remained sensitive to IP compound 3 (at 1 μM). The increased resistance to the IP compounds in the strains with increased cellular quantities of QcrB is due to the change in compound to target ratio, resulting in higher levels of uninhibited QcrB to function at a physiologically sustainable level. Literature previously indicated that QcrB, if expressed without QcrC would only be expressed at 10% efficiency, however our results show that this protein can be expressed independent of the other proteins in the operon. The IP compounds have considerable potential as a treatment for latent infections of TB, as well as active infections, due to their activity against an essential component of mycobacterial respiration.

Further investigative efforts regarding the IP compounds conducted by industrial partners to this work at GSK Tres Cantos, Madrid identified utilising their acute murine model of TB infection that these IP compounds deliver a bacteriostatic effect on mycobacterial proliferation (Abrahams *et al.* 2012).

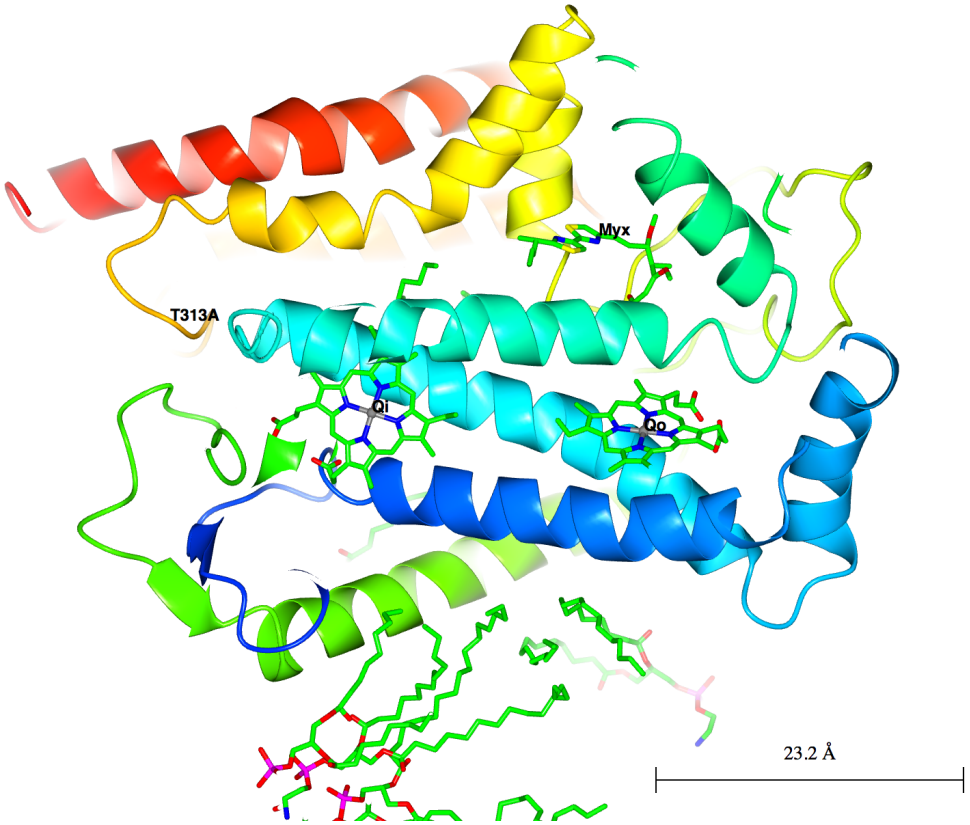


Figure 2.5: Ribbon diagram of QcrB illustrating the locus of the resistance conferring mutation T313A in relation to the Myxothiazol binding site (Myx). In this model the mutation does not occur within close proximity (> 30 Å) to the myxothiazol binding site, the quinone reactive site (Q_o), however falls proximally to the quinol binding site (Q_i) it is therefore likely that resistance occurs by a similar mechanism to antimycin, competitively inhibiting the reduction of quinol to quinone. This molecular mapping has utilized the structure of Bovine bc_1 in complex with Myxothiazol (Xia D *et al.* 2004). It must be noted that with only a 26% sequence identity between the bovine and mycobacterial QcrB proteins, and the absence of a myxothiazol bound crystal structure of greater homology, this model serves only as an indication to proximity of the two loci.

Subsequently, another group from the Institute Pasteur, Korea identified the imidazopyridine amide (IPA) compound series in a HTS of around 120,000 compounds utilising *M. tb* infected macrophages in order to not only test inhibitory activity, but also macrophage permeability of the compounds in a physiologically relevant environment. Their hit-to-lead optimisation produced 477 derivatives of the two hit IPAs and further optimisation lead to the development of Q203, a potent inhibitor of *M. tb* (MIC_{50} of 2.7 and 0.28 nM in liquid culture and in macrophages, respectively). They raised spontaneous resistant mutants in *M. tb* against Q203 and WGS analysis identified the same threonine 313 to alanine or isoleucine mutation in QcrB that was identified as the IP resistance conferring mutation in resistant isolates of *M. bovis* BCG. Due to the low potential for drug-drug interactions and positive pharmacokinetic profiling, as well as potency against hypoxic non-replicating *M. tb* in a chronic model of TB infection by disrupting bacterial ATP homeostasis, the Q203 compound has been proposed as a candidate for clinical trials (Pethe *et al.* 2013). Although, to date, a functional assay to test QcrB inhibition is yet to be developed.

CHAPTER 3

Investigations into the apparent promiscuous TB drug target mycobacterial membrane protein large 3 (MmpL3)

3.1 Introduction

In recent years, a considerable number of antimycobacterial compounds have been shown to inhibit the Resistance, Nodulation and Division (RND) superfamily transporter, MmpL3 by phenotyping methods, such as WGS (Tahlan *et al.* 2012; Grzegorzewicz *et al.* 2012; Remuinan *et al.* 2013; La Rosa *et al.* 2012; Stanley *et al.* 2012; Lun *et al.* 2013). These have been reviewed in Chapter 1.5.3.

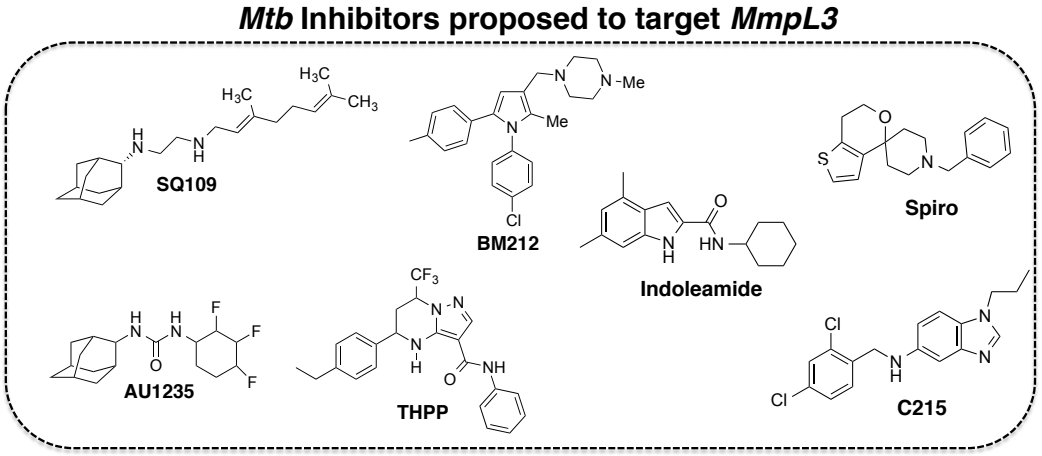


Figure 3.1: The chemical diversity of proposed MmpL3 inhibitors. The variety of different chemical scaffolds of inhibitors of MmpL3 which for the most part produce resistant mutants with mutations in the same transmembrane helix (not including SQ109), calls into question the validity of their MoA. This is further supported by the broad-spectrum activity of all the compounds except the indoleamide and adamantyl urea, which despite a resistant pheonotype arising from mutations in a similar locus to the others, are specific inhibitors of mycobacteria.

An alternative proposition as to the apparent MoA of the diverse range of compounds that have been deemed inhibitors of MmpL3 was proposed by Li *et al.* 2014, following the observation that some of the compounds showed broad-spectrum activity against non-mycolate synthesising bacterial and fungal pathogens (Figure 3.1). This is not the case for the indoleamide and adamantyl urea, as they appear to

have specificity to mycobacteria (Rao *et al.* 2013; Grzegorzewicz *et al.* 2012). This is most unexpected considering the proximity of SNPs in MmpL3 between adamantyl urea, THPP and BM212 in the fourth predicted transmembrane helix of the protein, demonstrating the resistance mechanism of these compounds is similar, making it highly unlikely MmpL3 is the primary target of these compounds, but more a facilitator of the resistance phenotype (Figure 3.2).

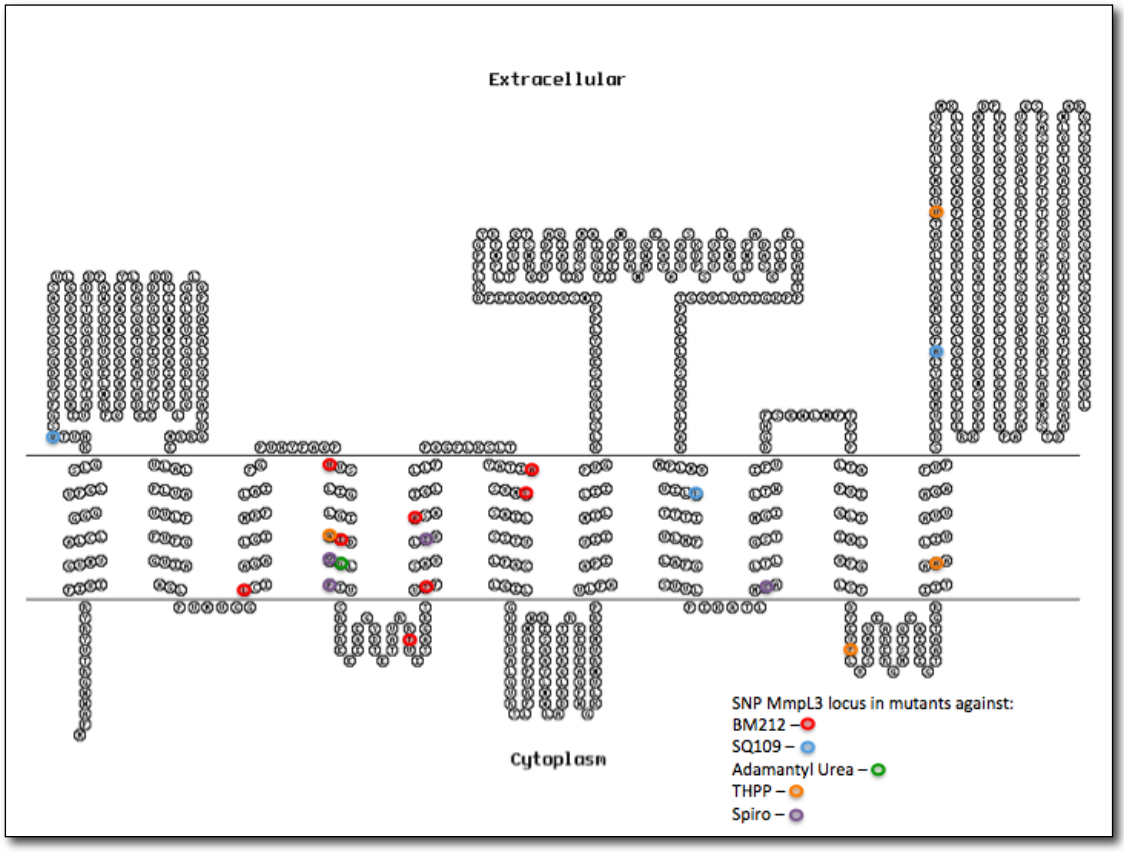


Figure 3.2: Diagram of the locations of SNPs in resistant mutants generated against putative MmpL3 targeting compounds. This diagram indicates the loci of SNPs in a map of the predicted trans-membrane domains of MmpL3. By the sequencing of resistant mutants generated against known inhibitors of *M. tb* growth, and the subsequent resistance conferring SNPs located in the *mmpL3* gene, MmpL3 has been identified as the cellular target of 7 chemically diverse anti-TB chemical scaffolds. The fourth predicted trans-membrane helix contains SNPs that convey resistance to all putative MmpL3 inhibitors except SQ109. This figure was generated using MEMSAT software that is copyrighted by Dr. David Jones (Jones *et al.* 1994).

Further evidence to the contrary is that SQ109, BM212 and THPP have activity against non-replicating *M. tb*, whereas adamantyl urea and the indoleamide do not. They suggest that the anti-mycobacterial activity of the MmpL3 compounds is due to their apparent dissipation of the transmembrane electrochemical proton gradient, supported by previous findings that RND transporters are associated with substrate export utilising a proton antiport mechanism (Li *et al.* 2014). Despite their observations of disruption of proton motive force by the proposed MmpL3 inhibitors, the unequivocal target for these compounds remains to be identified.

In this chapter a MmpL3 overexpressing strain of *M. bovis* BCG was used to probe MmpL3 as the molecular target of these aforementioned compounds. The overexpressing strain was also used to generate spontaneous resistant mutants, which were subsequently sequenced in an attempt to elucidate the true molecular target and confirm the involvement of MmpL3 in compound uptake.

3.2 Materials and methods

3.2.1 *M. bovis* BCG strains

An MmpL3 overexpresser plasmid was prepared by PCR amplification of the *mmpL3* gene from *M. tb* H37Rv genomic DNA, and subsequent digestion and ligation into the pMV261 vector containing an apramycin resistant marker at 30 $\mu g.ml^{-1}$. The construct was verified by sequencing (MWG Eurofins). Strains were prepared by electroporation of electrocompetent *M. bovis* BCG Pasteur with pMV261A-*mmpL3* and pMV261A following a standard protocol.

3.2.2 Growth Curves with *M. bovis* BCG with and without MmpL3 overexpression in the presence of varying concentrations of putative MmpL3 inhibitors

Growth curves were recorded using glass tubes (11 ml volume), which were sterilised by autoclaving. Each respective MmpL3 compound (Spiro, BM635, SQ109, Adamantyl Urea and C215) was added in a dose response format (0 to 2.4 x MIC of each compound against *M. bovis* BCG) and normalised for DMSO concentration, including a compound-free control in each case. Middlebrook 7H9 (2.7 ml; containing ADC, 0.05% Tween80) with apramycin (30 $\mu g.ml^{-1}$) to maintain plasmid selection, was combined with 0.3 ml of mid-log (OD_{600} = 0.4-0.6) bacterial culture. A bench top optical density meter was used to measure the OD_{600} of each culture every 24 hours from the first inoculation. Data was collected until stationary phase was reached in the compound-free control tubes and subsequently plotted on a XY-scatter plot (Excel).

3.2.3 Generation of spontaneous resistant mutants using *M. bovis* BCG pMV261A-*mmpL3*

Spontaneous resistant mutants were generated by plating 10^8 cfu *M. bovis* BCG pMV261A-*mmpL3* on Middlebrook 7H11 media supplemented with OADC (calculated following the assumption that OD_{600} = 1 = 2.5 x 10^8 $cfu.ml^{-1}$), containing 5x, 10x and 20x MIC of each respective compound. These plates were wrapped in parafilm and aluminum foil and incubated at 37^oC with 5% CO_2 and humidity for 4 weeks. Colonies were used to inoculate 3 ml of Middlebrook 7H9 containing ADC, 0.05% Tween80 and 2x MIC of each compound to maintain resistance. Once cultures

had reached mid-log, resistance was validated by plating on 7H11 at 0x, 5x and 10x MIC, along with the sensitive parental strain.

3.2.4 WGS of spontaneous resistant mutants

WGS was conducted as described in 2.2.3 Genomic DNA Extraction and Genome Sequencing.

3.2.5 Target validation by *in vitro* ribosomal inhibition assay

In order to validate the ribosome as the cellular target for BM635, a commercially available *in vitro* Protein Synthesis Reaction kit was used (PURExpress E6800, New England BioLabs) to constitutively express the fluorescent protein mCherry. The assay was conducted following the manufacturer's instructions in a 384 well florescence plate (Greiner) and fluorescent output was measured on a PHERAstar FS plate reader (BMG Labtech) by excitation at 575 nm and emission at 620 nm every 7.2 seconds, with 1000 reads in total up to two hours post-initiation of the assay. Data was compiled in PHERAstar Mars 4.0 (BMG Labtech) and presented in Microsoft Excel. Following completion of the assay, SDS-PAGE analysis of 5 µl of each sample was conducted by addition of an equal volume of protein sample/loading buffer (63.5mM Tris pH6.8, 0.4% w/v SDS, 5% v/v β-mercaptoethanol, 20% v/v glycerol and 2.5% w/v bromophenol blue) and boiled at 100^{o}C for 10 minutes. Each sample was then loaded in full onto a precast 12% SDS-PAGE gel (Bio-Rad) and run in a standard 1x Tris-glycine running buffer (Thermo Fisher Scientific) at 400V, 35mA

for 40 minutes. Gels were stained with Instant Blue (Expedeon) and photographed using a Gel Doc XR+ System (Bio-Rad).

3.2.6 Analysis of FAMEs and MAMEs of *M. bovis* BCG treated with putative MmpL3 inhibitors

A radioisotope labelled substrate incorporation assay was conducted to establish inhibitory effects of each MmpL3 compound on the biosynthesis of FAMEs and MAMEs. This assay was conducted as reported (Kremer *et al.* 2000).

3.3 Results

3.3.1 Overexpression of MmpL3 causes increased sensitivity to putative MmpL3 inhibitors

Growth curves of *M. bovis* BCG pMV261A-*mmpL3* and the corresponding empty vector strain in dose response with each of the putative MmpL3 inhibitors demonstrated that overexpression of MmpL3 increased sensitivity to each of the compounds. The exception to the rule was SQ109, wherein equal MICs were observed for both strains. This is contrary to observations with true physiological targets whereby overexpression of the compound target usually results in resistance to the compound being tested. In the case of the THPP compounds, the empty vector control, *M. bovis* BCG pMV261A, possessed an MIC of 0.96 μM, whereas the MmpL3 overexpressing strain, *M. bovis* BCG pMV261A-*mmpL3* was 0.64 μM.

A similar effect was observed with the Spiro compound, however the increased susceptibility was of a smaller magnitude. Growth of the empty vector strain was fully inhibited at 0.576 μM, where as the MmpL3 overexpresser was inhibited at 0.32 μM, equating to the MIC of the Spiro compound with *M. bovis* BCG. BM635 also gave a shift in MIC relating to increased sensitivity of the overexpresser strain. Growth of the empty vector strain was inhibited at 0.192 μM, whereas the MmpL3 overexpresser possessed an MIC corresponding to 0.08 μM. However, after 72 hours further growth, the MmpL3 overexpresser strain was inhibited at this concentration.

The adamantyl urea compound gave an MIC of 0.64 μM for the empty vector control. The MmpL3 overexpresser showed increased sensitivity. Cell lysis was observed at the latter stages of growth (from 192 hours) and the MIC of the MmpL3 overexpressing strain was 0.32 μM. The MmpL3 inhibitor with the least potency tested in these experiments was C215 with an MIC of 20 μM to fully inhibit growth of the empty vector strain, where as the MmpL3 overexpresser strain required 16 μM for complete inhibition. It is clear from the growth curves that there is impaired growth at 8 and 12 μM in the MmpL3 overexpressing strain compared to the empty vector, however as positive growth is observed throughout the time course, this cannot be counted as an MIC. Nevertheless, a fundamentally increased sensitivity to C215 is observed upon MmpL3 overexpression. The only compound that did not appear to behave as the others in terms of increased sensitivity upon MmpL3 overexpression was SQ109. In this instance, the MIC for both strains was equal at 2.8 μM. All growth curves are displayed in Figure 3.3.

(a)

THPP

μM	*M. bovis* BCG pMV261A								*M. bovis* BCG pMV261A-*mmpL3*							
	0	24	48	72	96	120	144	(hours)	0	24	48	72	96	120	144	(hours)
0	0.2	0.17	0.16	0.2	0.25	0.41	0.77		0.22	0.24	0.29	0.36	0.47	0.66	0.82	
0.32	0.17	0.17	0.12	0.16	0.19	0.28	0.53		0.22	0.23	0.28	0.29	0.29	0.33	0.35	
0.64	0.17	0.12	0.13	0.15	0.17	0.23	0.31		0.22	0.23	0.22	0.18	0.17	0.15	0.1	MIC
0.8	0.21	0.18	0.14	0.17	0.15	0.22	0.3		0.21	0.22	0.22	0.2	0.16	0.15	0.11	
0.96	0.18	0.18	0.12	0.1	0.11	0.15	0.18	MIC	0.22	0.23	0.23	0.2	0.16	0.15	0.11	
1.12	0.19	0.18	0.13	0.12	0.11	0.16	0.17		0.2	0.21	0.21	0.18	0.15	0.14	0.09	

Spiro

μM	0	24	48	72	144	168	192	216	(hours)	0	24	48	72	144	168	192	216	(hours)
0	0.12	0.18	0.29	0.48	1.25	1.69	1.86	1.72		0.15	0.32	0.54	0.85	1.75	2	1.97	1.91	
0.064	0.13	0.21	0.3	0.48	1.3	1.62	1.95	1.8		0.16	0.3	0.51	0.79	1.76	2	1.98	1.94	
0.128	0.13	0.21	0.28	0.47	1.23	1.64	1.97	1.79		0.14	0.32	0.57	0.95	1.97	2	2	1.81	
0.192	0.12	0.21	0.3	0.38	1.07	1.56	1.97	1.94		0.13	0.27	0.4	0.57	1.36	1.64	2	1.91	
0.256	0.13	0.19	0.26	0.3	0.84	1.25	1.73	2		0.14	0.25	0.34	0.36	0.65	1.03	1.56	1.98	
0.32	0.13	0.19	0.25	0.23	0.54	0.93	1.47	2		0.14	0.22	0.26	0.21	0.17	0.13	0.15	0.13	MIC
0.448	0.14	0.19	0.18	0.17	0.2	0.25	0.36	0.65		0.13	0.22	0.27	0.2	0.15	0.14	0.15	0.13	
0.576	0.13	0.18	0.2	0.18	0.13	0.13	0.12	0.12	MIC	0.16	0.21	0.29	0.23	0.16	0.17	0.15	0.14	
0.768	0.13	0.17	0.2	0.18	0.14	0.11	0.12	0.12		0.14	0.19	0.23	0.21	0.14	0.14	0.14	0.13	

BM635

μM	0	24	48	72	144	168	192	216	(hours)	0	24	48	72	144	168	192	216	(hours)
0	0.14	0.23	0.36	0.53	1.29	1.64	1.82	1.78		0.14	0.31	0.48	0.81	1.63	2	1.85	1.94	
0.016	0.13	0.2	0.34	0.53	1.31	1.76	1.86	1.81		0.15	0.29	0.58	0.87	1.71	2	1.83	1.86	
0.032	0.14	0.23	0.34	0.47	1.22	1.62	1.83	1.84		0.15	0.3	0.58	0.78	1.41	1.76	1.89	1.8	
0.048	0.14	0.24	0.42	0.44	1.05	1.29	1.88	1.75		0.14	0.29	0.49	0.56	0.82	0.92	1.18	0.71	
0.064	0.13	0.25	0.39	0.47	0.75	0.95	1.36	1.41		0.14	0.25	0.43	0.49	0.44	0.58	0.65	0.82	
0.08	0.13	0.24	0.35	0.27	0.52	0.78	1.17	1.71		0.15	0.27	0.4	0.49	0.31	0.29	0.3	0.29	MIC
0.112	0.12	0.22	0.3	0.2	0.21	0.27	0.49	0.85		0.14	0.2	0.28	0.27	0.12	0.09	0.11	0.09	
0.144	0.14	0.19	0.19	0.14	0.11	0.13	0.19	0.35		0.15	0.22	0.32	0.22	0.13	0.12	0.12	0.1	
0.192	0.13	0.19	0.21	0.17	0.1	0.11	0.11	0.11	MIC	0.14	0.29	0.25	0.17	0.11	0.09	0.09	0.11	

Adamantyl Urea

μM	0	24	48	72	144	168	192	216	(hours)	0	24	48	72	144	168	192	216	(hours)
0	0.17	0.13	0.15	0.18	0.62	1.18	1.75	1.78		0.22	0.25	0.3	0.39	0.83	1.09	1.27	1.26	
0.32	0.25	0.16	0.16	0.21	0.69	1.12	1.5	1.6		0.21	0.22	0.22	0.22	0.29	0.34	0.46	0.44	MIC
0.64	0.18	0.15	0.12	0.13	0.09	0.13	0.14	0.12	MIC	0.2	0.22	0.19	0.17	0.08	0.11	0.11	0.1	
0.8	0.17	0.13	0.11	0.12	0.05	0.08	0.1	0.08		0.19	0.21	0.21	0.16	0.07	0.09	0.09	0.07	
0.96	0.17	0.16	0.11	0.11	0.06	0.08	0.07	0.06		0.2	0.22	0.2	0.18	0.07	0.09	0.1	0.07	

C215

μM	0	24	48	72	144	168	192	216	(hours)	0	24	48	72	144	168	192	216	(hours)
0	0.11	0.19	0.24	0.36	1.08	1.41	1.72	1.6		0.17	0.21	0.33	0.53	1.15	1.46	1.64	1.59	
4	0.12	0.19	0.21	0.29	0.69	0.99	1.4	1.6		0.14	0.29	0.65	0.7	1.32	1.51	1.65	1.59	
8	0.13	0.17	0.17	0.21	0.43	0.64	0.96	1.43		0.13	0.21	0.18	0.2	0.32	0.37	0.45	0.56	
12	0.11	0.19	0.17	0.19	0.3	0.45	0.69	1.03		0.12	0.2	0.27	0.23	0.26	0.35	0.39	0.46	
16	0.11	0.17	0.19	0.18	0.21	0.24	0.33	0.5		0.13	0.21	0.27	0.19	0.16	0.16	0.14	0.14	MIC
20	0.11	0.19	0.2	0.18	0.21	0.18	0.22	0.24	MIC	0.12	0.2	0.24	0.2	0.17	0.12	0.13	0.1	
28	0.11	0.17	0.2	0.12	0.11	0.11	0.09	0.11		0.13	0.19	0.21	0.17	0.1	0.11	0.11	0.09	
36	0.11	0.18	0.17	0.14	0.11	0.09	0.1	0.1		0.12	0.21	0.22	0.17	0.13	0.12	0.12	0.12	

SQ109

μM	0	24	48	72	144	168	192	216	(hours)	0	24	48	72	144	168	192	216	(hours)
0	0.15	0.23	0.27	0.49	1.12	1.55	1.7	1.66		0.14	0.24	0.34	0.57	1.3	1.55	1.79	1.61	
0.4	0.15	0.25	0.24	0.38	0.95	1.39	1.64	1.75		0.13	0.22	0.31	0.45	1.14	1.32	1.67	1.7	
0.8	0.16	0.22	0.21	0.29	0.7	1	1.38	1.76		0.13	0.22	0.15	0.17	0.53	0.76	1.01	1.18	
1.2	0.14	0.21	0.21	0.22	0.34	0.48	0.81	1.17		0.12	0.19	0.17	0.13	0.4	0.57	0.79	1.12	
1.6	0.14	0.19	0.18	0.14	0.15	0.2	0.32	0.56		0.15	0.2	0.15	0.1	0.14	0.22	0.41	0.66	
2	0.14	0.21	0.23	0.2	0.16	0.17	0.24	0.39		0.13	0.2	0.21	0.21	0.16	0.16	0.27	0.39	
2.8	0.14	0.21	0.2	0.17	0.12	0.1	0.1	0.11	MIC	0.13	0.21	0.19	0.14	0.11	0.1	0.11	0.15	MIC
3.6	0.14	0.2	0.24	0.21	0.15	0.12	0.12	0.13		0.13	0.2	0.22	0.17	0.12	0.1	0.12	0.12	
4.8	0.14	0.2	0.22	0.18	0.14	0.13	0.15	0.13		0.16	0.21	0.2	0.22	0.12	0.11	0.12	0.15	

(b)

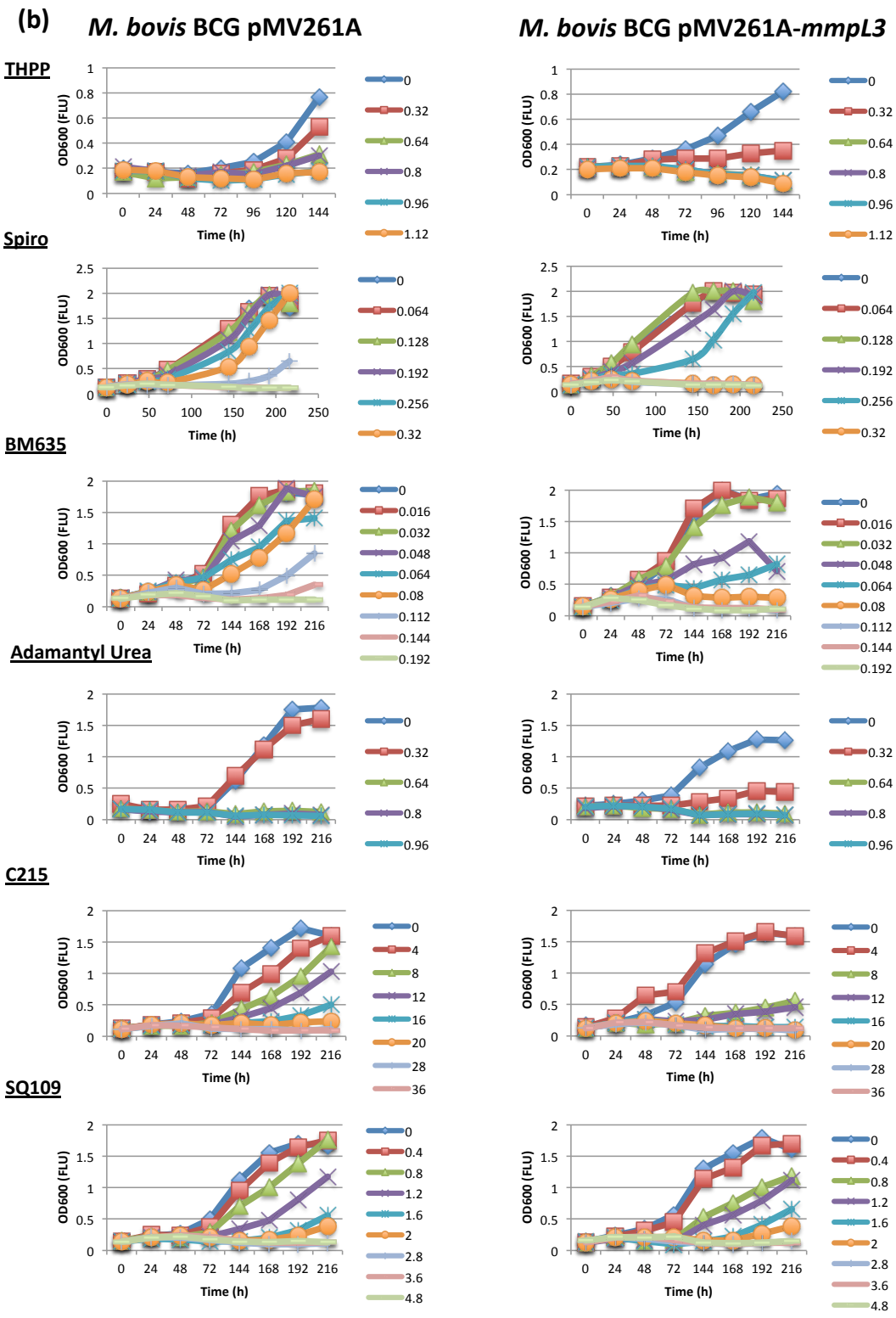

M. bovis BCG pMV261A
M. bovis BCG pMV261A-mmpL3
THPP
Spiro
BM635
Adamantyl Urea
C215
SQ109
OD600 (FLU)
OD 600 (FLU)
Time (h)
0
0.32
0.64
0.8
0.96
1.12
0.064
0.128
0.192
0.256
0.016
0.032
0.048
0.08
0.112
0.144
4
8
12
16
20
28
36
0.4
1.2
1.6
2
2.8
3.6
4.8

Figure 3.3: Growth Curves of MmpL3 overexpresser with a dose response of THPP, Spiro, BM635, Adamantyl Urea, C215 and SQ109. Growth curves were conducted in a dose response format respective to the MIC of the compound against *M. bovis* BCG. (a) depicts a heat map of the raw data (OD_{600} FLU) where green indicates highest and red indicates lowest OD_{600} value, respectively. (b) show these data presented as a growth curve over time. These data show a reduction in MIC from the empty vector control strain, *M. bovis* BCG pMV261A to the overexpresser strain, *M. bovis* BCG pMV261A-*mmpL3* for all compounds except SQ109 where MmpL3 overexpression does not appear to affect the MIC.

3.3.2 Analysis of FAMEs and MAMEs of *M. bovis* BCG treated with putative MmpL3 inhibitors

Using a previously published approach to observe the inhibition of mycolic acid biosynthesis, the effects of THPP, Spiro, BM635 and SQ109 compounds on FAMEs and MAMEs was determined (Kremer *et al.* 2000). The assay involves the metabolic incorporation of [^{14}C]-acetate into cell wall bound mycolates, which are hydrolysed and methyl esters are prepared and extracted. These are subsequently separated by TLC and visualised by autoradiography. It was found that a significant reduction in MAMEs can be observed at > 0.8 μM (the MIC) of THPP, and there was a similar outcome with the Spiro compound at > 0.32 μM to a lesser extent. BM635 treatment does not appear to reduce MAMEs until around 0.32 μM and SQ109 does not appear to show a reduction in MAMEs at or below 8 μM. These contrasting chemotypes from compounds presenting similar resistance phenotypes suggests MmpL3 may not be the sole physiological target of this broad range of anti-TB compounds.

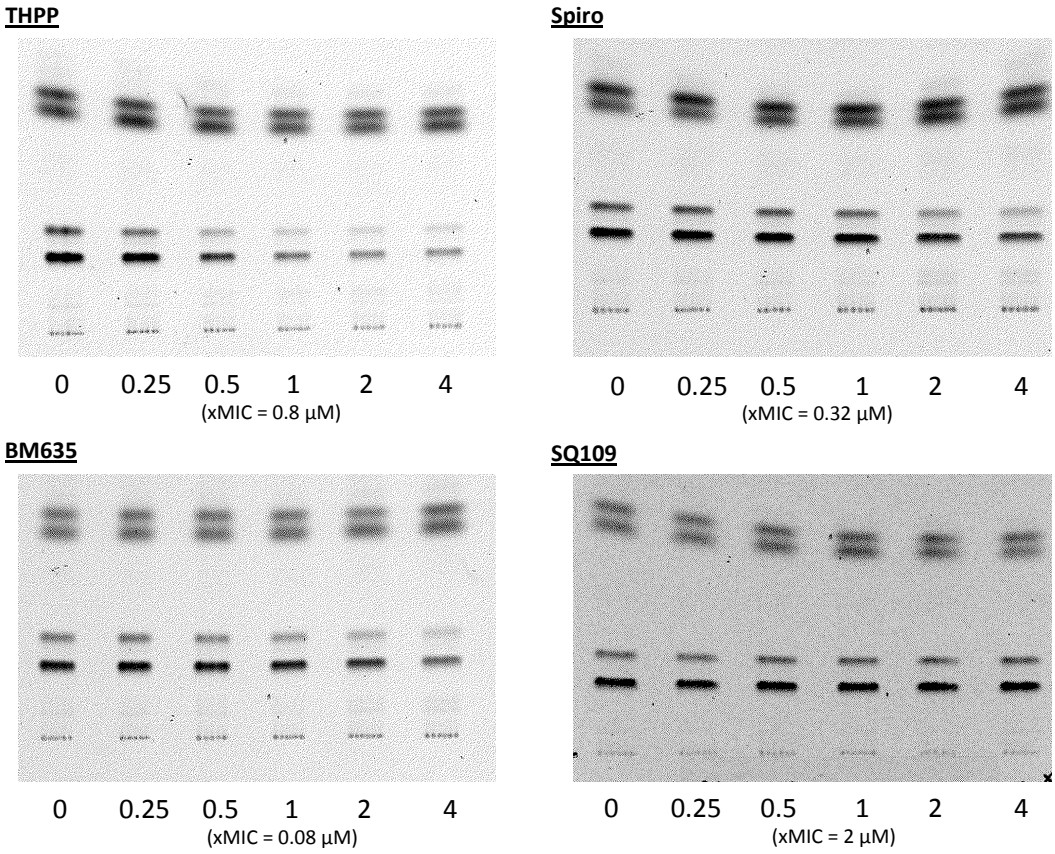


Figure 3.4 Analysis of FAMEs and MAMEs of *M. bovis* BCG treated with putative MmpL3 inhibitors. A significant reduction in MAMEs can be observed at > 1x MIC of THPP (0.8 μM), and a similar observation with Spiro compound at > 1x MIC (0.32 μM) at to a lesser extent. BM635 treatment does not appear to reduce MAMEs until around 4x MIC (0.32 μM) and SQ109 does not appear to show a reduction in MAMEs at or below 4x MIC (8 μM).

3.3.3 Sequencing of spontaneous resistant mutants generated against BM635 indicates 16S rRNA as a possible target

In order to identify the MoA of the most potent of the MmpL3 inhibitors, BM635, resistant isolates of *M. bovis* BCG containing a pMV261A-*mmpL3* plasmid were generated at 5x, 10x and 20x MIC, respectively. This gave a FoR of $1x10^{-8}$ cells at 22.4 μM, $5x10^{-8}$ cells at 11.2 μM and $24x10^{-8}$ cells at 5.6 μM. The resistance of 5

isolates from each of the 5x MIC and 10x MIC plates were validated by replica plating cultures of each isolate with and without BM635 selection at either 5 or 10x MIC, along with *M. bovis* BCG pMV261A-*mmpL3*. The results indicated that mutants 1 to 5 selected at 5x MIC, and mutants 2 to 5 selected at 10x MIC were all true resistant mutants (Figure 3.5). The *g*DNA of the resistant mutants was extracted and sequenced along with that of the *M. bovis* BCG pMV261A-*mmpL3* strain. A sequence alignment revealed a mutation with 100% coverage in the 16S ribosomal RNA (rRNA) of all resistant mutants that was not present in the *M. bovis* BCG pMV261A-*mmpL3* strain. The mutation, a nucleotide substitution of A to G at position 1400 (genome position 1499760), is synonymous with kanamycin resistance in *M. tuberculosis* (Suzuki *et al.* 1998). Two resistant isolates raised at 10x MIC, isolate 4 and 5, were shown to have an additional SNP in BCG_2282, a predicted transmembrane protein of unknown function, with 95% sequence homology to the Major Facilitator Superfamily (MFS) of *Streptomyces* sp., noted as "a large and diverse group of secondary transporters that include uniporters, symporters and antiporters," according to NCBI BLAST. It is further noted that MFS proteins may function as drug-efflux pumps to confer antibiotic resistance. It is possible that BCG_2282 may be a second compound uptake mechanism similar to MmpL3 that is mutated as a secondary resistance mechanism in the presence of high compound concentrations. This protein is also highly conserved, with 100% sequence homology in all strains of *M. tuberculosis*. Nevertheless, it is clear that with 100% frequency throughout all BM635 resistant mutants sequenced, and no discernible MmpL3-based resistance conferring mutations, the primary resistance phenotype appeared to be from the 16S rRNA mutation. This confirms the proposed mechanism of MmpL3 as a drug importer and not the drug target of BM635.

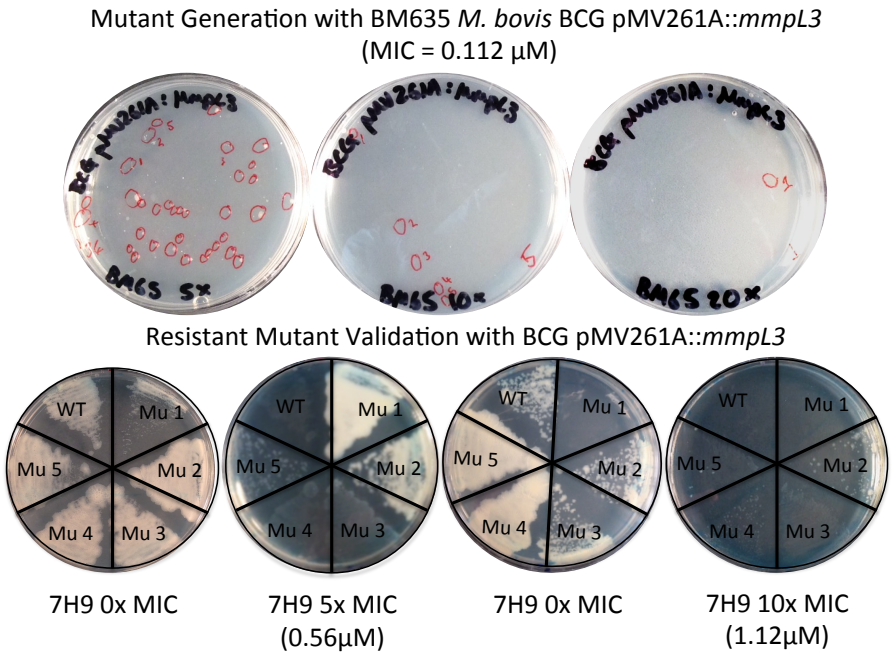


Figure 3.5: Generation of spontaneous resistant mutants of *M. bovis* BCG pMV261A-*mmpL3* against BM635. The upper panel shows the resistant isolates generated at 5x, 10x and 20x MIC of BM635. The lower panel shows the validation of the resistance phenotype by plating *M. bovis* BCG pMV261A-*mmpL3* along with the resistant isolates in the absence (0x MIC) and presence (5x or 10x MIC) of BM635. It is clear that growth of the *M. bovis* BCG pMV261A-*mmpL3* strain is fully inhibited at 5x and 10x MIC, whereas resistant isolates 1 to 5 at 5x MIC and isolates 2 to 5 at 10x MIC were able to grow at high compound concentrations.

3.3.4 Validation of mycobacterial 16S rRNA as the cellular target of BM635

In order to probe the potential target of BM635, the 16S rRNA, a novel ribosome inhibition assay was developed using constitutive expression of the fluorescent protein mCherry as an indicator of ribosome function. A commercially available kit (PURExpress, E6800, New England BioLabs) was used for expression, and kanamycin and INH were used as positive and negative controls for inhibition, respectively. A DMSO only control was also conducted and the DMSO concentration

was normalised to 2% in each assay. Each assay was initiated upon addition of 250ng of DNA, and fluorescence recorded at regular time intervals up to two hours after initiation. The results indicated that kanamycin at 10 μM was sufficient to fully inhibit mCherry expression from the outset of the assay. INH, as expected showed no reduction in mCherry expression at 10 μM and gave a similar output to the DMSO positive control, and at 100 μM, INH appeared to improve the expression of mCherry. This enhancement of protein expression was also seen in the presence of 10 μM BM635, however a marginal reduction was observed with BM635 at 100 μM. Subsequently samples were analysed by SDS-PAGE, and a clear band was observed at 28.8 kDa (molecular weight for mCherry) for assays conducted in the presence of INH and BM635, however no band was observed in the presence of kanamycin (Kan). A DNA-free negative control (-ve control) was also assayed and analysed by SDS-PAGE and likewise no band was present at 28.8 kDa (Figure 3.6). The results presented here provide clear evidence that the mycobacterial ribosome is unlikely to be the physiological target of BM635, and thus indicate the MoA of this compound is yet to be determined

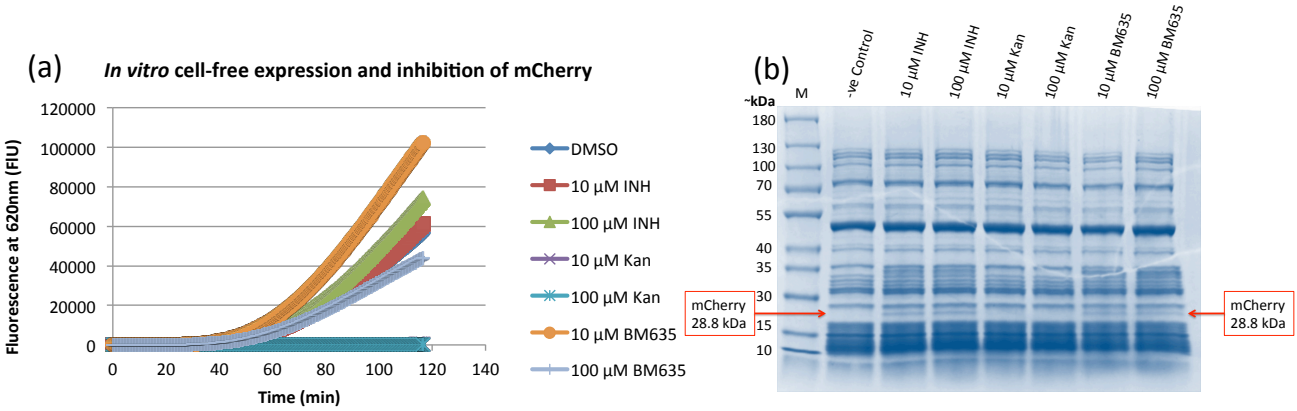


Figure 3.6: *In vitro* cell-free expression and inhibition of mCherry. Using the commercially available kit (PURExpress, E6800, New England BioLabs), and a plasmid for constitutive expression of the fluorescent protein mCherry, the ribosomal inhibitory activity of compounds was assayed. (a) Fluorescence was measured at 620 nm for two hours post-initiation in the presence of 10 and 100 µM of INH, Kan and the compound under investigation, BM635. Results were plotted directly for fluorescent output (FlU) over time (min). (b) SDS-PAGE was conducted with each assay reaction to observe mCherry expression by appearance of a band at 28.8 kDa.

3.4 Discussion

Here we have employed a basic molecular approach to unravel one of the present major stumbling blocks in TB drug discovery, an apparent promiscuous target and menace of phenotypic HTSs, the eponymous 'red herring' MmpL3 (Rayasam 2014). Overexpression of MmpL3 delivered the opposite result to what would be expected of drug target overexpression, resulting in an increased sensitivity, as opposed to providing resistance. Furthermore, THPP, Spiro, BM635 and SQ109 appear to have different dose-dependent effects on the biosynthesis of MAMEs, suggesting the MoA of each compound is different, despite the proximal loci of resistance-conferring mutations against these compounds in *mmpL3*. It therefore seems probable that MmpL3 acts in part as a means of drug uptake, possibly through a leaky channel

during the export of TMM and that resistance-conferring mutations reduce the leakiness of the channel and therefore uptake. This hypothesis is strongly supported by the evidence provided in Chapter 3.3.1 of this Thesis. By constitutively overexpressing MmpL3 in a multi-copy number plasmid, we hypothesised that it may be possible to circumvent MmpL3-based resistance, in favor of physiological target-based resistance development. WGS of resistant isolates provided 16S rRNA as the potential target for BM635, due to the presence of apparent resistance-conferring SNPs at a locus formally identified as being related to antimicrobial resistance. Experimental validation of ribosomal inhibition by BM635 was therefore necessary and attempts to reproduce a ribosomal inhibition assay involving [^{35}S]-labelled methionine reported in the literature were inconsistent (Grzegorzewicz *et al.* 2012). We developed the hypothesis of assaying the inhibition of *in vitro* cell-free protein expression, in a similar way to that reported in Salian *et al.* (2012). Using an intrinsically fluorescent protein in favour of the bioluminescent enzyme luciferase, which requires additional ATP and substrate in the reaction. Using constitutive expression of the fluorescent protein mCherry, we established that BM635 does not inhibit the ribosome and thus hypothesise that the previously observed mutations may have been driven by the presence of Apramycin for maintaining selection for a recombinant *M. bovis* BCG cell line containing the MmpL3 overexpression plasmid. The sequences are being re-analysed of the BM635 resistant isolates of the MmpL3 overexpressing *M. bovis* BCG in order to find possible clues as to the MoA from lower frequency mutations that were previous discounted, as well as continuing with the production and sequencing of other resistant mutants to the "MmpL3-targeting compounds". Despite these efforts, purely phenotypic approaches seem unlikely to shed light on the true MoA of these compounds. In Chapter 4, we use a

chemoproteomics approach for target identification that may provide a suitable alternative to phenotypic based MoA determination.

CHAPTER 4

EchA6 as the Target of the Tetrahydropyrazolopyrimidine (THPP) anti-tubercular drug series

4.1 Introduction

The highly complex cell wall is a key virulence factor of mycobacterial pathogenic strains, providing bacteria with a defensive shield against host immune responses. This complex superstructure that encapsulates mycobacteria is composed of cell wall proteins, phosphatidylinositol mannosides (PIM), lipomannan (LM) and lipoarabinomannan (LAM), as well as a mycolic acid layer covalently linked to an arabinogalactan (AG) layer, which is in turn linked to a peptidoglycan (PG) layer by a L-Rha-D-GlcNAc-P linker. The cell wall is split into two major segments, the mycolyl arabinogalactan-peptidoglycan (mAGP) complex forms the lower segment "cell wall core" and the upper segment is comprised of free lipids. The cell wall is scattered with cell wall proteins, PIM, LM and LAM. During fractionation of cell wall lysates, the mAGP complex can be separated from the soluble upper layer along with the proteins, PIM and LAM (Brennan 2003). The biosynthesis of these respective components is well documented, however the export of such components from the cytoplasm into the cell wall and the assembly of the superstructure remain of considerable interest and conjecture (Jankute *et al.* 2015).

4.1.1 Mycolic acids

The mycolic acids form a fundamental feature of the cell wall and thus the biosynthesis and regulation of this component plays a critical role in bacterial survival (Figure 4.1). Defined as long-chain (C_{70}-C_{90}) β-hydroxy fatty acids with a long α-alkyl side chain (Asselineau and Lederer 1950), three types of mycolates are found in

mycobacteria in varying relative abundance; α-mycolic acids (>70%) methoxymycolic acids (~15%) and ketomycolic acids (~15%) (Qureshi *et al.* 1984).

Mycolic acid biosynthesis involves a 5-step process commencing with (1) the synthesis of straight chain saturated fatty acids C_{20-26} that form the α-alkyl component. This is followed by (2) the synthesis of the meromycolate scaffold and (3) its subsequent modification to introduce other functional groups to the scaffold, (4) the final Claisden-type condensation is followed by a reduction and finally (5) mycolyltransferases to produce the mAGP complex, TMM and trehalose dimycolate (TDM) (Takayama *et al.* 1984).

(1) Short-chain fatty acid synthesis of the α and mero backbone

Short-chain *de novo* fatty acid synthesis occurs by FAS-I involving recurrent cycles of condensation, β-keto reduction, dehydration and enoyl reduction from an acetyl-CoA primer. These steps are catalysed by the individual subunits of the FAS-I complex: β-ketoacyl synthase, β-ketoacyl reductase, β-hydroxyacyl dehydratase and enoyl reductase. This cycle continues with a 2-carbon extension at each repetition until fatty acids ranging in C_{16-26} are reached (Takayama *et al.* 2005).

(2) Long chain fatty acid synthesis and the synthesis of meromycolates

The commencement of FAS-II biosynthesis is reliant upon the attachment of malonyl-CoA to an acyl carrier protein (AcpM) catalysed by FabD (malonyl-CoA:ACP transacylase), producing a malonyl-AcpM precursor. This acts as a primer for FAS-II biosynthesis as it undergoes condensation with palmitoyl-CoA from FAS-I, catalysed by FabH (β-ketoacyl-ACP synthase III), producing β-ketoacyl-AcpM as the starting

point of FAS-II (Choi *et al.* 2000). Reduction of the β-ketoacyl-AcpM by MabA (β-ketoacyl-ACP reductase) (Marrakchi *et al.* 2002) yields a β-hydroxyacyl-AcpM with the subsequent oxidation of an NADPH cofactor to $NADP^+$. Ensuing dehydration with a β-hydroxyacyl-ACP dehydratase (Had), catalysed by the heterodimeric proteins HadAB and/or HadBC (Sacco *et al.* 2007) produces the *trans*-2-enoyl-AcpM, which is reduced by the NADH-dependent InhA (enoyl-ACP reductase) (Marrakchi *et al.* 2000), producing an acyl-AcpM extended by two carbons. Products are cycled into the KasA/KasB β-ketoacyl-ACP synthases for further extension, which catalyse the condensation elongation of the acyl chain with malonyl-AcpM producing the β-ketoacyl-AcpM starting point (Schaeffer *et al.* 2001; Kremer *et al.* 2002). FAS-II cycling continues through rounds of reduction (MabA), dehydration (HadAB/BC), reduction (InhA) and condensation (KasA/KasB) until the acyl-chain length reaches $C_{54\text{-}64}$, yielding the saturated meromycolate moiety of mycolic acids.

(3) Modification of the meromycolate to introduce other functional groups

Modification to the meromycolate chain in order to introduce additional functional groups occurs through various processing steps including desaturation, *cis-/trans*-cyclopropanation, and the introduction of methoxy- and keto- groups (Bhatt *et al.* 2007). The process is thought to always commence with a desaturation step, catalysed by the desaturases DesA1-3 to produce an unsaturated meromycolate with *cis*- double bonds at both proximal and distal positions, providing sites for further modifications, such as cyclopropanation (Schroeder *et al.* 2002). Cyclopropanation is catalysed by cyclopropane mycolic acid synthase (CMAS-1) at the distal position and CMAS-2 at the proximal position (George *et al.* 1995). Methoxymycolic acids are produced by MmaA1-4, by the addition of a hydroxyl group at the distal desaturated position that

is subsequently methylated (Yuan *et al.* 1996). It has been proposed that the meromycolate modification leads to variations in cell wall fluidity and permeability as well as helping to protect mycobacteria from reactive oxygen species produced by the host immune system during infection (Yuan *et al.* 1995).

(4) Final Claisen-type condensation

The meromycolic acid, is subsequently activated by FadD32 (fatty acyl-AMP ligase) producing a meromycolyl-adenosine monophosphate (AMP), the substrate for condensation with the shorter α-alkyl chain (C_{22-24}) produced by FAS-I. This reaction is catalysed by Pks13 to produce a β-keto-α-alkyl mycolic acid (Trivedi *et al* 2004). Pks13 is a multifunctional enzyme with 4 distinct active sites, each catalysing a step in the condensation reaction. Firstly, the keto-synthase activity produces a thioester with the meromycolyl-AMP and a cysteine reside, resulting in a meromycolic acid and the reduction of AMP to ATP. The α-alkyl chain is loaded onto the acyl carrier protein by the acyltransferase, allowing the α-alkyl chain to make a nucleophilic attack on the carbonyl carbon of the meromycolic acid. The thioesterase activity then releases the β-keto-α alkyl mycolic acid product (Gavalda *et al.* 2009) and is followed by reduction culminating in the production of mature mycolic acids (Verela *et al.* 2012).

(5) Final deposition of mycolates via mycolyltransferase processes

The vast majority of mycolates synthesised within the cell end up esterified to the AG layer of the cell wall core catalysed by proteins from the antigen 85 complex (Belisle *et al.* 1997; Jackson *et al.* 1999). Some mycolates are also covalently bound to sugar

moieties to produce TMM, TDM and glucose monomycolate (GMM), that feature on the surface of the mycobacterial cell wall (Takayama *et al.* 2005).

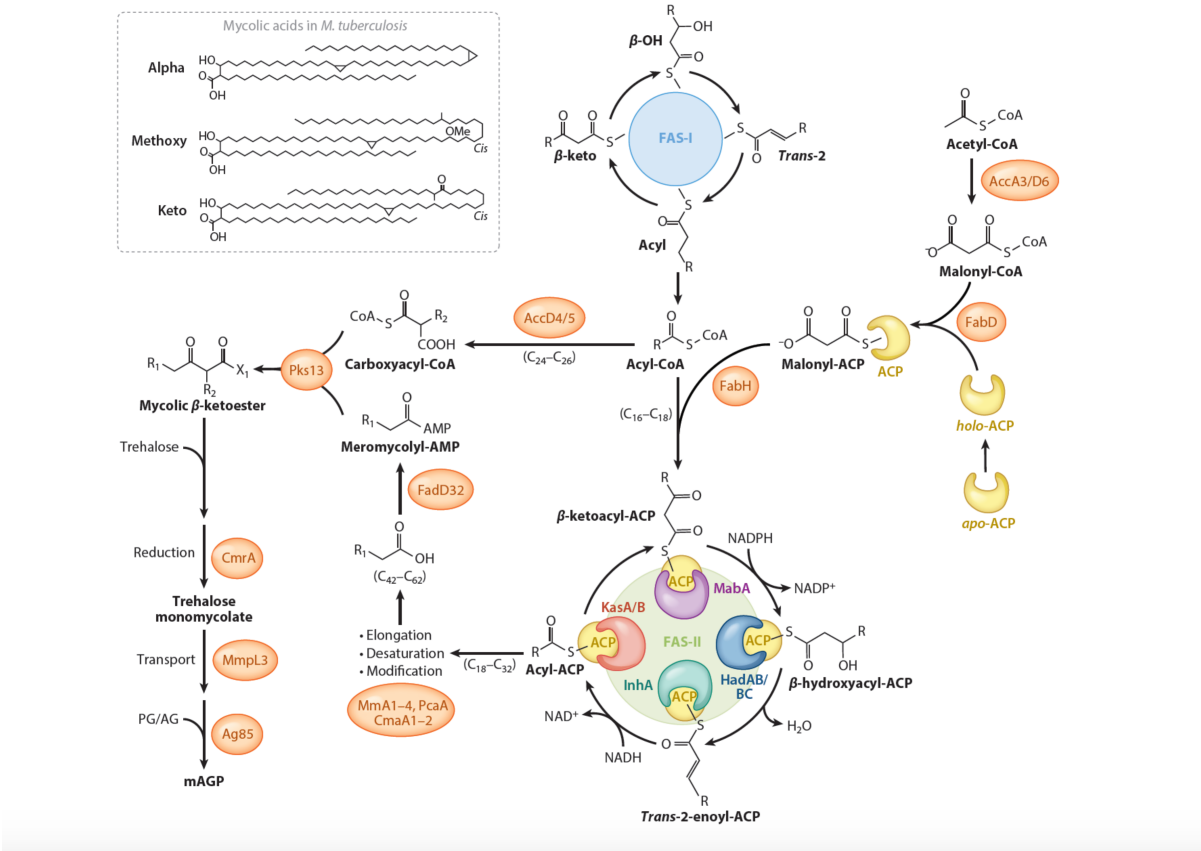


Figure 4.1: Schematic representation of FAS-I and FAS-II biosynthesis in mycobacteria. The biosynthesis commences with (1) the synthesis of straight chain saturated fatty acids $C_{20\text{-}26}$ that form the α-alkyl component of the mycolic acid. This is followed by (2) the synthesis of the meromycolate unit and (3) its subsequent modification to introduce other functional groups to the molecule, (4) the final Claisen-type condensation is followed by a reduction and finally (5) mycolyltransferases processes to produce the mAGP complex, TMM and TDM.

4.1.2 Known inhibitors of mycolic acid synthesis

The classic inhibitor of mycolic acid biosynthesis is INH. First identified as a potent inhibitor of *M. tb* in 1950s, INH has been used as a first line treatment for TB some

60 years, with efficacy against both *M. tb* and *M. bovis* BCG at 20 – 200 ng.ml^{-1}. The MoA of INH remained elusive for many years after the emergence of *M. tb* resistance to the drug. Initial examination of the genome of resistant clinical isolates led to the observation of resistance conferring mutations in *katG*, encoding a catalase-peroxidase enzyme (Zhang *et al.* 1994; Rouse *et al.* 1995). It was later discovered that KatG activates INH by oxidising it to the active form, isonicotinic acid, and that site directed mutants of the protein with a serine substituted for a threonine at position 315 (as was the most frequent mutation observed in clinical resistant isolates) became resistant to INH with a 70% decrease in the catalytic catalase peroxidase activity (Saint-Joanis *et al.* 1999). The role of KatG in activating INH was supported by the observation that overexpression of InhA in *M. bovis* BCG and *M. smegmatis* led to INH resistance. Ethionamide (ETH), a structural analogue of INH and also a pro-drug, was found to target InhA by the same method (Banerjee *et al.* 1994). There was however debate over the activation mechanism of ETH as INH resistant isolates with mutations in KatG were not found to be cross-resistant to ETH (Fattorini *et al.* 1999). It was later established that ETH is activated by EthA (Baulard *et al.* 2000). Subsequently, the MoA was proposed to be inhibition of *M. tb* β-ketoacyl-ACP synthase (KasA) due to the identification of mutations in two INH-resistant clinical isolates (out of the 28 resistant strains tested) that mapped to KasA but which lacked other mutations associated with INH resistance (Mdluli *et al.* 1996; Mdluli *et al.* 1998). However, studies conducted by Kremer *et al.* (2000) demonstrated that overexpression of KasA did not lead to a shift in the MIC of INH, whereas this was observed for thiolactomycin (TLM), a confirmed inhibitor of KasA. In all, mutations conveying resistance were found in five different genes in various *M. tb* resistant isolates that were sequenced (*katG, inhA, ahpC, kasA* and *ndh*). The final conclusion

as to the MoA of the primary target of INH was based upon the adherence of that putative target to the criteria for drug target assignment that a bactericidal drug target is a bacterial protein that (i) binds the drug, (ii) has its normal function inhibited by that drug and (iii) where inhibition of that protein's function leads to bacterial death. Only one of the proposed INH targets met all these criteria, therefore the MoA was concluded as pro-drug activation by KatG and subsequent inhibition of InhA function (Vilcheze *et al.* 2000).

4.1.3 New Direction

Following a HTS campaign at GlaxoSmithKline (GSK), Diseases of the Developing World (DDW), Madrid, the tetrahydropyrazolo[1,5-a]pyrimidine-3-carboxamide (THPP) series of compounds were identified as potent inhibitors of *M. tb*, and were proposed to target MmpL3, an integral membrane-spanning protein with 11 transmembrane domains that was recently identified as an exporter of TMM (Grzegorzewicz *et al.* 2012; Varela *et al.* 2012) (as discussed in Chapter 1.5.3). In this Chapter we have conducted a comprehensive analysis of the MoA of the THPPs. As indicated in the acknowledgements section, collaborators at Cellzome, GSK and members of the Besra Laboratory contributed certain aspects of the experimental design and implementation.

4.2 Materials and Methods

4.2.1 General methods

The measurement of the MIC for each tested compound, general antimicrobial activity, microsomal fraction stability, pharmacokinteic studies, HepG2 cytotoxicity assay, SDS-PAGE and Western blot were performed as described previously (Kremer *et al.* 2000; Kremer *et al.* 2002; Abrahams *et al.* 2012). *EchA6* (Rv0905) was cloned into the mycobacterial multi-copy plasmid pMV261 and its derivatives (Kremer *et al.* 2002); the site-directed mutant EchA6 Trp133Ala was generated using the plasmids containing wildtype *echA6* and QuikChange II (Agilent Technologies). MmpL3 (Rv0206c) was cloned into pMV261. The constructs were electroporated into either *M. bovis* BCG or *M. tuberculosis*. The primers are described in Table 4.1. The *in vitro* effect of GSK951A, TLM, and INH was studied by treating *M. bovis* BCG cultures at OD_{600} of 0.4 with inhibitor for 24 hours, followed by [^{14}C]-acetate labeling for 24 hours, and subsequent analysis of either total FAMEs and MAMEs (equal counts, typically 30,000 cpm), cell wall bound MAMEs (equal volumes, 5% aliquot), or cell envelope lipids (equal counts, typically 30,000 cpm) as described previously (Tahlan *et al.* 2012; Banerjee *et al.* 1994; Kremer *et al.* 2000; Kremer *et al.* 2002; Besra *et al.* 1994; Hu *et al.* 2010). Protein-protein interactions were studied using the bacterial adenylate cyclase based two-hybrid system as described in Karimova *et al.* 1998. Briefly, EchA6 (Rv0905) was cloned using the primers described in Table 4.1 into pUT18 in-frame with the T18 fragment, and the FAS-II genes cloned into pKT25 in-frame with the T25 fragment. The positive control pKT25 was fused to the Leucine Zipper of GCN4 co-transformed with pUT18C of the Leucine Zipper GCN4. The

negative control was pKT25 Zip co-transformed with empty pUT18 vector. The GSK in-house hydrophobicity assay was performed using 10 µl of a 10 mM DMSO stock solution diluted to 750 µl with octanol saturated pH 7.4 phosphate buffer and 160 µl buffer saturated octanol in a 96 well deep well block. Blocks were sealed and inverted for 3 sets of 50 inversions, then centrifuged at 300 *g* for 20 min. Both phases were quantified using generic gradient UV-HPLC.

4.2.2 Assessment of chronic and acute efficacy in murine TB models

The assessment of the chronic and acute efficacy in murine TB models was performed using specific pathogen-free, 8-10 week-old female C57BL/6 mice purchased from Harlan Laboratories and allowed to acclimate for one week. In the chronic model, mice (n = 3-7 mice/group) were intratracheally infected with 100 CFU/mouse and GSK951A formulated in 1 % aqueous methylcellulose and administered daily for 8 consecutive weeks, starting 6 weeks after infection. Lungs were harvested 24 h after the last administration. All lung lobes were aseptically removed, homogenised and frozen. Homogenates were plated in 10 % OADC-7H11 medium supplemented with activated charcoal (0.4 %) for 18 days at 37^{o}C. In the acute model (Rullas *et al.* 2010), mice were intratracheally infected with 50,000 cfu/mouse with all strains, and lungs harvested on day 9. GSK951A and INH (in water) were administered daily for 8 consecutive days, starting on day 1 after infection. All lung lobes were aseptically removed, homogenised, and plated in 10 % OADC-7H11 medium supplemented with activated charcoal (0.4 %) and grown for 18-25 days at 37^{o}C. Effective dose 99 % (ED_{99}), defined as the dose in mg/kg that reduced lung bacterial burden at day 9 after infection by 99 % (2 log.cfu) with respect to untreated.

4.2.3 Preparation of *M. bovis* BCG cytosolic extract

M. bovis BCG cell pellets were resuspended in lysis buffer (50 mM Tris-Cl, pH 7.4, 1 mM EDTA, 7.5 % glycerol, 150 mM NaCl, 25 mM NaF, 1 mM Na_3VO_4, 1 mM DTT, and 1 complete EDTA-free protease inhibitor tablet (Roche) *per* 25 ml). After sonication the samples were adjusted to 0.8 % Igepal-CA630 and extraction was completed by homogenisation using a Dounce homogeniser. After 45 min rotation at 4°C, the samples were subjected to centrifugation for 10 min at 20,000 *g* at 4°C. The supernatant was kept on ice, while the pellet was re-extracted with 1 volume of lysis buffer adjusted to 0.8 % Igepal-CA630. The pellet was resuspended using a long 20 gauge needle (2x), followed by rotation for 30 min at 4°C. After a centrifugation step as described above, both supernatants were pooled and subjected to centrifugation at 100,000 *g* for 1 h at 4°C. The final supernatant was snap frozen in liquid nitrogen and stored at -80°C.

4.2.4 Chemoproteomics

Sepharose beads were derivatised with GSK729A at various concentrations from 0.05 mM to 2 mM. Beads (35 µl) were washed and equilibrated in lysis buffer incubated at 4°C for 1 h with 1 ml (1 mg) *M. bovis* BCG cytosolic extract, which was pre-incubated with compound or buffer. Beads were transferred to disposable columns (MoBiTec), washed extensively with lysis buffer and eluted with SDS sample buffer. Proteins were alkylated, separated on 4-12 % NuPAGE (Invitrogen), stained with colloidal Coomassie, and quantified by isobaric tagging and LC-MS/MS. Digestion, labeling with TMT isobaric mass tags, peptide fractionation, and mass spectrometric

analyses were performed essentially as described in Bantscheff *et al.* 2011. The proteins .fasta file for *M. bovis* BCG was downloaded (May 11th 2011) from http://genome.tbdb.org/annotation/genome/tbdb/MultiDownloads.html and supplemented with the sequences of bovine serum albumin, porcine trypsin and mouse, rat, sheep and dog keratins. Decoy versions of all proteins were created and added. The search database contained a total of 11,492 protein sequences, 50 % forward, 50 % reverse. Criteria for protein quantification were: a minimum of 2 sequence assignments matching to unique peptides was required (FDR for quantified proteins <<0.1 %), Mascot ion score > 15, signal to background ratio of the precursor ion > 4, signal to interference > 0.5 (Savitski *et al.* 2010). Reporter ion intensities were multiplied with the ion accumulation time yielding an area value proportional to the number of reporter ions present in the mass analyser. Peptide fold changes were corrected for isotope purity as described and adjusted for interference caused by co-eluting nearly isobaric peaks as estimated by the signal-to-interference measure (Savitski *et al.* 2013). Protein quantification was achieved using a sum-based bootstrap algorithm (Savitski *et al.* 2011).

4.2.5 Generation and characterisation of a conditional *echA6* mutant in *M. bovis* BCG

A conditional mutant of the *M. bovis* BCG homologue of *M. tuberculosis echA6* was generated using the genetic tool CESTET (Brown *et al.* 2007; Rana *et al.* 2012). First, a recombinant *echA6* knockout phage was designed to replace the *M. bovis* BCG *echA6* homologue. The primers used for amplifying the left and right flanks to generate the allelic exchange substrate (Brown *et al.* 2007; Rana *et al.* 2012) are

provided in Table 4.1. Next, *Rv0905* was PCR amplified using the primers mdRv0905_F and mdRv0905_R (Table 4.1) and cloned downstream of the tetracycline promoter into the integrating vector pTIC6a to generate the plasmid pTIC6a-*Rv0905* (Brown *et al.* 2007; Rana *et al.* 2012). A merodiploid strain was then constructed by electroporating pTIC6a-*Rv0905* into *M. bovis* BCG. The resultant strain BCG-*Rv0905* was then transduced with *echA6* knockout phage. Transductants were selected on 7H10-agar plates containing 75 mg/ml hygromycin and 50 ng/ml anhydrotetracycline (ATc). One confirmed knockout strain was called Δ*BCG0957* and was used in a conditional depletion experiment to detect cell death as shown previously in minimal medium (Brown *et al.* 2007; Rana *et al.* 2012).

4.2.6 EchA6 recombinant protein production and purification

4.2.6.1 *E. coli* Strains

The recombinant protein production of EchA6 for purification and subsequent assay and crystallography work was conducted, using the improved Miroux and Walker strain of *E. coli* BL21 (DE3) (Miroux *et al.* 1996), which was chosen for its ability to culture a large titer of soluble recombinant protein and durability to the stress conditions associated with batch recombinant protein production. For cloning, *E. coli* TOP10 (Invitrogen) was selected. Both strains were grown in Luria Bertani (LB) broth from glycerol stock into 5ml and grown at 37^{o}C, overnight with 180 rpm shaking.

4.2.6.2 Plasmids and Primers

The *echA6* gene (*Rv0905*) was cloned into the his-tagged bacterial expression plasmid pET28a (Novagen), which contains a kanamycin resistance cassette (50 $\mu g.ml^{-1}$) for selection and an isopropyl β-D-1-thiogalactopyranoside (IPTG) inducible promoter. *E. coli* BL21 cells were subsequently transformed by heat shock and successful transformants selected on LB agar containing kanamycin at 50 $\mu g.ml^{-1}$.

The primers (Table 4.1) were used to amplify the *echA6* gene from *M. tb* H37Rv *g*DNA template by polymerase chain reaction (PCR) using Phusion High Fidelity DNA Polymerase (New England Biolabs) following the manufacturer's instructions. PCR products were purified using a QIAquick PCR Cleanup Kit (Qiagen) following the manufacturer's instructions. The PCR product and pET28a plasmid were subsequently digested using both *NdeI* (sense) and *HindIII* (anti-sense) fast digest restriction endonucleases (Thermo Scientific). The digested pET28a and PCR product were purified by 1% w/v agarose gel electrophoresis and stained using Ethidium Bromide (120V, 200mA for 30 minutes), extracted by incision using a Gel-Doc XR (Bio-Rad) imager and purified from the agarose using a QIAquick Gel Extraction Kit (Qiagen) following manufacturer's instructions. Quick-Stick DNA Ligase (Bioline) was used to ligate insert into digested plasmid and a transformation into *E. coli* TOP10 and plating of transformation mix onto selective LB agar used to identify successfully transformed cells. Colonies were used to inoculate LB broth containing 50$\mu g.ml^{-1}$ kanamycin and grown overnight. The plasmid was extracted by miniprep using a QIAprep Miniprep Kit (Qiagen) following manufacturer's guidelines. Plasmids were then sequenced for validation.

Table 4.1: Primers used in this study

Genes	Primer Sequence (5'-3')	Restriction site
EchA6 F_28a	CATGCATGCATATGATCGGTATCACCCAGGCAGA	NdeI
EchA6 R_28a	CATGCATGAAGCTTTTAAGCCCCTTGGAACTTCG	HindIII
TH_EchA6 F	CATGCATGTCTAGAAATGATCGGTATCACCCAGGC	XbaI
TH_EchA6 R	CATGCATGGGATCCTCAGCCCCTTGGAACTTCG	BamHI
TH_FabH F	ACTCTAGAGATGACGGAGATCGCCACGACC	XbaI
TH_FabH R	ATACGGTACCCGACCCTTCGGCATTCGCACCAC	KpnI
TH_KasA F	ACTCTAGAGGTGAGTCAGCCTTCCACCGC	XbaI
TH_KasA R	ATACGGTACCCGGTAACGCCCGAAGGCAAG	KpnI
TH_KasB F	ACTCTAGAGGTGGGGGTCCCCCCGCTTGC	XbaI
TH_KasB R	ATACGGTACCCGGTACCGTCCGAAGGCGATTGC	KpnI
TH_InhA F	ACTCTAGAGATGACAGGACTGCTGGAC	XbaI
TH_InhA R	ATACGGTACCCGGAGCAATTGGGTGTGCGC	KpnI
TH_MabA F	ACTCTAGAGGTGACTGCCACAGCCAC	XbaI
TH_MabA R	ATACGGTACCCGGTGGCCCATACCCATGCC	KpnI
TH_HadA F	ACTCTAGAGGTGGCGTTGAGCGCAGAC	XbaI
TH_HadA R	ATACGGTACCCGCGCAGCGCCATCAGAAAATCC	KpnI
TH_HadB F	ACTCTAGAGATGGCGCTGCGTGAGTTC	XbaI
TH_HadB R	ATACGGTACCCGCGCTAACTTCGCCGAGGC	KpnI
TH_HadC F	ACTCTAGAGATGGCGCTCAAGACCGATATC	XbaI
TH_HadC R	TAC CCG GGG CGC GGT CCT GAT GAC CTG CCC	SmaI
BCG_0957_LL	TTTTTTTTCCATAAATTGGTCCCATGCCGCCGTAGATTCTC	Van91I
BCG_0957_LR	TTTTTTTTCCATTTCTTGGTCCAGGGCCAGACCGTATTTCG	Van91I
BCG_0957_RL	TTTTTTTTCCATAGATTGGTCAACGACGACGGCGCTATC	Van91I
BCG_0957_RR	TTTTTTTTCCATCTTTTGGTCAGGAACCGTCCCGAGAAG	Van91I
mdRv0905_F	GATCGATCAAGCTTATGATCGGTATCACCCAGGC	HindIII
mdRv0905_R	GATCGATCATCGATTTAAGCCCCTTGGAACTTCG	ClaI
EchA6 F_pVV16	CATGCATGCATATGATCGGTATCACCCAGGCAGA	NdeI
EchA6 R_pVV16	CATGCATGAAGCTTAGCCCCTTGGAACTTCGGCG	HindIII
EchA6 F_pMV261	GATCGATCTGGCCAAGATGATCGGTATCACCCAGGC	MscI
EchA6 R_pMV261	GATCGATCAAGCTTTTAAGCCCCTTGGAACTTCG	HindIII
MmpL3 F_pMV261	GGCTGGCCAAGATGTTCGCCTGGTGGGGTCG	MscI
MmpL3 R_pMV261	GGCAAGCTTTTAAAGGCGTCCTTCGCGGC	HindIII
EchA6_SDM_CT223GC sense (Leu75Ala)	CGATTATCCCGACCGG**GC**CATCGAGCTGCACAAG	
EchA6_SDM_CT223GC anti-sense (Leu75Ala)	CTTGTGCAGCTCGATG**GC**CCGGTCGGGATAATCG	
EchA6_SDM_AT226GC sense (Ile76Ala)	CCCGACCGGCTC**GC**CGAGCTGCACAAG	
EchA6_SDM_AT226GC anti-sense (Ile76Ala)	CTTGTGCAGCTCG**GC**GAGCCGGTCGGG	
EchA6_SDM_CA319GC sense (Gln107Ala)	CAGCTTGCCATG**GC**ATGCGACCTGCGG	
EchA6_SDM_CA319GC anti-sense (Gln107Ala)	CCGCAGGTCGCAT**GC**CATGGCAAGCTG	
EchA6_SDM_A392C sense (Asp131Ala)	GTCTGGCCCTGG**C**TAACTGGAGCATC	
EchA6_SDM_A392C anti-sense (Asp131Ala)	GATGCTCCAGTTA**G**CCAGGGCCAGAC	
EchA6_SDM_TG397GC sense (Trp133Ala)	GCCCTGGATAAC**GC**GAGCATCCGCCG	
EchA6_SDM_TG397GC anti-sense (Trp133Ala)	CGGCGGATGCTC**GC**GTTATCCAGGGC	

4.2.6.3 Transformation by Heat Shock

All *E. coli* recombinant strains used in this work were transformed with the required plasmid by a heat shock method. Cells grown overnight in 20 ml LB broth were harvested by centrifugation at 5000 rpm at 4^{o}C for 20 minutes and resuspended in 10 ml 100 mM ice-cold calcium chloride. The cells were then rested on ice for 20 minutes after which, they were harvested once again and resuspended in 2.5 ml of 100 mM calcium chloride with 15% (v/v) glycerol. The competent cells were then divided into aliquots and flash frozen in liquid nitrogen and stored at -80^{o}C. For heat shock transformation, 50 µl of competent cells were defrosted on ice and transferred to a pre-chilled eppendorf tube containing 0.5 µl of plasmid and left on ice for 30 minutes. The cells were then heat shocked at 42^{o}C for 30 seconds, before returning to ice for a further 2 minutes. LB broth was added (250 µl) and the freshly transformed cells were incubated at 37^{o}C with 180 rpm shaking for 1 hour to allow for expression of the antibiotic resistance cassette(s). Varying volumes of cells (20, 50 and 100 µl) were then plated on LB agar containing relevant antibiotic and the plates stored at 37^{o}C overnight.

4.2.6.4 Expression of EchA6

Overnight cultures of *E. coli* BL21 pET28a-*echA6* were grown in LB broth under the selection of 50 µg.ml^{-1} kanamycin and were used to inoculate 1 L of LB broth with the same antibiotic selection as a 1:100 inoculation. These cultures were grown at 37^{o}C with 180 rpm shaking until an OD_{600} of 0.4 - 0.6 was reached, at which point recombinant protein production was induced using 1 mM IPTG and the temperature

decreased to 16°C in order to reduce stress on the host and improve native protein expression (Thomas and Baneyx 1996). Batch culture was continued at 16°C until 24 hours post-induction at which point cultures were harvested by centrifugation at 5000 rpm at 4°C, and the pellets were stored at -20°C for up to three months. Expression was confirmed by sodium dodecyl sulfate polyacrylamide gel electrophoresis (SDS-PAGE) and Western blot.

4.2.6.5 Purification of EchA6 by immobilised metal ion affinity chromatography (IMAC)

Cell pellets of *E. coli* BL21 pET28a-*echA6* that have been stored at -20°C were defrosted on ice and resuspended in 20 ml of lysis buffer (containing 50 mM sodium phosphate, 600 mM sodium chloride and 10 mM imidazole buffered to pH 8) and a complete EDTA-free protease inhibitor cocktail tablet (Roche) was added before placing on a rocker for 15 minutes. Cells were then sonicated on ice water with 10 cycles of 30 seconds sonication with 30 seconds cooling, before being centrifuged for 40 minutes at 15,000 rpm at 4°C to clarify the lysate.

For purification of the his-tagged EchA6 protein, a HisTrap HP column (GE Healthcare Life Sciences) fed by a peristaltic pump (flow rate of 1 $ml.min^{-1}$) was washed with deionised water for 20 minutes before being charged with a 0.1 M nickel chloride solution until the flow through was visibly green in colour. A further 10 minutes of deionised water removed any unbound nickel. Lysis buffer was introduced for 10 minutes prior to running through the clarified lysate, followed by each fraction of the imidazole gradient (50mM, 75mM, 100mM, 125mM, 150mM, 200mM,

300mM). All eluates were collected and kept on ice for sample analysis by SDS-PAGE at the end of purification. In order to prepare protein samples for SDS-PAGE, 6 μl of each fraction was added to the same volume of protein sample/loading buffer (63.5 mM Tris pH 6.8, 0.4% w/v SDS, 5% v/v β-mercaptoethanol, 20% v/v glycerol and 2.5% w/v bromophenol blue) and boiled at 100^{o}C for 10 minutes before being loaded in full onto a precast 12% SDS-PAGE gel (Bio-Rad) and run at 400V, 35mA for 40 minutes. Gels were stained with Instant Blue (Expedeon).

Imidazole fractions containing pure protein were dialysed overnight in 2 L of HEPES dialysis buffer (25mM HEPES, 10% Glycerol and 300mM NaCl buffered to pH8) at 4^{o}C, and for four hours the following day in a further 2 L of dialysis buffer. The protein was subsequently concentrated to around 25 mg.ml^{-1} using protein concentrator tubes (Thermoscientific) with 10 kDa exclusion (EchA6 has a molecular mass of 26.029 kDa).

4.2.7 Intrinsic Tryptophan Fluorescence (ITF) Ligand Binding Assays

ITF binding assays were conducted using purified EchA6 protein and varying chain length acyl-Coenzyme As and the THPP compounds. The protein concentration that was determined to give the optimal fluorescence signal was 3.75 μM. A Hitachi F7000 Fluorescence Spectrophotometer was used for the assays and spectra were measured at an emission (E_m) wavelength of 300-400 nm (with excitation (E_x) at 280 nm). The E_x and E_m slit-width was fixed at 5 nm. Each assay was conducted at 25^{o}C in a 1 ml crystal cuvette, containing 500 μl of protein (3.75 μM) in a buffer composed of 25 mM HEPES, 10% glycerol and 300 mM NaCl at pH 8. Ligand binding was

measured as a decrease in fluorescence maxima upon addition of an increasing stoichiometric molar ratio of ligand to protein (from 0.5 – 8.0 times) and DMSO concentrations were kept at < 0.6% for the acyl-CoA assays and < 2.0 for the THPP assays. All generated data was analysed using Prism 6 (GraphPad).

4.2.8 EchA6 X-ray Crystallography

EchA6 crystals were generated for both *apo*- (without ligand) and bound (THPP or C_{20}-CoA) conditions. A vapour diffusion method was used with the commercially available sparse matrix screens JCSG-*plus* and MIDAS (Molecular Dimensions). Each screen was conducted with 30 μl of each condition dispensed into a central reservoir of a 96- well sitting drop SWISSCI 3-lens plate, and dispensation of 0.15 μl of protein (at 20, 25 and 30 $mg.ml^{-1}$) into each of the three sitting drops combined with 0.15 μl of reservoir solution. A Mosquito nano-litre high throughput liquid dispensing robot (TTP labtech) was used to prepare each plate, which was subsequently sealed using ClearVue Sheets (Molecular Dimensions) and stored at $18^{o}C$. In order to obtain complexes (THPPs and C_{20}-CoA) a 3:1 molar ratio of ligand to protein was used. Conditions that yielded diffracting crystals are shown in Table 4.2.

Table 4.2: Conditions used for EchA6 crystal production

Complex	Condition	Cryoprotection
Apo-EchA6	0.1M Tris pH 8.5, 60% v/v polypropylene glycol 400	Not required
EchA6:C_{20}CoA	0.17M ammonium sulfate, 25% w/v PEG 4K, 15% v/v glycerol	Not required
EchA6:366A	0.1M Tris pH 8.5, 20% v/v ethanol	Not required
EchA6:059A	0.6M tri-sodium citrate	10 % glycerol
EchA6:572A	0.2M sodium chloride, 0.1M sodium cacodylate pH 6.5, 2M ammonium sulfate	10% ethylene glycol
EchA6:951A	0.1M sodium cacodylate pH 6.5, 0.1M tri-sodium citrate	20% glycerol

Diffraction data was collected initially using our in house X-ray facility (Rigaku MicroMax 007HF, VariMax optics, Saturn 994 CCD detector) and subsequently improved at Diamond Light Source, UK. Table 4.3 shows the software used for data analysis and model building and refinement, and the data and refinement statistics for each structure are shown in Table 4.4.

Table 4.3: Crystallography software used to solve EchA6 structures

Software	Function
XDS	Data reduction (Kabsch 2010)
XSCALE	Data reduction (Kabsch 2010)
CCP4 suite	Data analysis (CCP4 1994)
PHASER	Phases by molecular replacement with *M. tb* EchA6 (PDB: 3HE2) (McCoy *et al.* 2007)
COOT	Model building and refinement (Emsley *et al.* 2010)
REFMAC5	Model building and refinement (Murshudov *et al.* 1997)
PHENIX.REFINE	Model building and refinement (Adams *et al.* 2002)
SKETCHER	Ligand building (CCP4 1994)
PyMOL	Generation of figures (www.pymol.org)

Table 4.4: Crystallographic data and refinement statistics

X-ray diffraction data	***apo* EchA6**	**EchA6:C_{20}-CoA**	**EchA6: GSK366**	**EchA6: GSK059**	**EchA6: GSK572**	**EchA6: GSK951**	**EchA6: GSK729**
X-ray source	Diamond I04	Diamond I03	Diamond I04-1	Diamond I03	Diamond I03	In-house	Diamond I04-1
Wavelength (Å)	0.9795	0.9763	0.92	0.9763	0.9762	1.5414	0.92
Space group	$P3_221$	$P2_1$	$H3$	$P2_12_12_1$	$P2_12_12_1$	$P2_12_12_1$	$P6_3$
Cell parameters a,b,c (Å)	103.1, 103.1, 143.4	113.7, 51.4, 156.9, β = 106.7º	94.83, 94.83, 87.51	51.4, 116.6, 171.8	51.4, 116, 171.5	51.4, 119.2, 171.6	103.9, 103.9, 54.4
Molecules in asymmetric unit	3	6	1	3	3	3	1
Resolution (last shell) (Å)	89.3 - 1.91 (1.96 - 1.91)	108.9 - 2.4 (2.46 - 2.40)	47.4 - 1.7 (1.75 - 1.70)	85.9 - 2.61 (2.68 - 2.61)	96.1 - 2.23 (2.29 - 2.23)	48.9 - 2.7 (2.85 - 2.70)	51.9 - 1.43 (1.47 - 1.43)
Rmerge (%)[1)]	6.5 (70.4)	8.4 (49.9)	6.4 (53.0)	10.5 (59.2)	9.4 (67.4)	9.8 (35.9)	4.5 (67.5)
Total/unique observations	505752 / 68929	246225 / 68420	175974 / 31804	135533 / 31967	322214 / 50922	338678 / 29564	696415 / 61860
I/σ(I) [1)]	15.9 (2.7)	9.6 (2.1)	12.6 (2.7)	8.7 (2.0)	11.9 (2.9)	25.8 (7.3)	26.2 (3.5)
Completeness (%)[1)]	100 (100)	99.4 (99.5)	98.9 (99.3)	99.0 (99.4)	99.9 (99.8)	99.6 (97.5)	100 (99.9)
Multiplicity[1)]	7.3 (7.4)	3.6 (3.3)	5.5 (5.7)	4.2 (4.3)	6.3 (6.2)	11.5 (11.1)	11.3 (11.1)
Refinement							
Resolution range	89.3 - 1.91	108.93 - 2.4	47.4 - 1.7	85.9 - 2.6	96.07 - 2.23	48.9 - 2.7	51.9 – 1.50
Unique reflections	65376	64285	31794	31907	48273	29498	53631
R_{cryst} / R_{free} (%)	18.2 / 20.1	22.2 / 27.5	19.3 / 21.5	19.3 / 24.0	21.9 / 25.4	18.7 / 23.4	17.3 / 18.4
No of non-hydogen atoms	5610	11052	1927	5608	5606	5729	2096
Protein / Ligand / Solvent	5284 / - / 326	10793 / 138 / 121	1800 / 33 / 94	5419 / 87 / 102	5344 / 96 / 163	5452 / 168 / 109	1801 / 24 / 271
RMSD bonds / angles (Å / º)	0.006 / 0.976	0.008 / 1.20	0.006 / 1.2	0.009 / 1.13	0.009 / 1.38	0.009 / 1.38	0.006 / 1.14
Wilson B-factor ($Å^2$)	28.4	32.9	30	40.2	31.6	41.6	19.1
Overall average B-factor ($Å^2$)	32.5	30.3	34.5	47.8	40.4	27.6	23.2
Protein / Ligand / Solvent ($Å^2$)	32.5 / - / 33.5	30.3 / 34.1 / 23.2	34.7 / 34.8 / 31.5	47.9 / 49.2 / 36.1	40.4 / 38.5 / 39.7	26.7 / 56.6 / 23.7	21.7 / 20.6 / 33.4
RMSD B-factors	0.95	3.8	1.3	3.2	1.4	3.3	1.9
Ramachandran plot[2)] Favoured / allowed / disallowed (%)	97.4 / 2.5/ 0.1	96.7 / 3.6 / 0.1	97.1 / 2.9 / 0	95.8 / 4.0 / 0.2	96.9 / 3.0 / 0.1	95.6 / 4.4 / 0.0	97.9 / 2.1 / 0

[1)] Figures in parenthesis refer to last resolution shell. [2)] The Ramachandran plot statistics was calculated using Molprobity[50].

4.2.9 EchA6 Overexpresser

A mycobacterial pVV16-EchA6 (*Rv0905*) overexpression construct, expressing protein with a his-tag was prepared. Mycobacterial work was conducted in *M. bovis* BCG Pasteur. Liquid batch cultures of *M. bovis* BCG were grown in Middlebrook 7H9 media (Difco) supplemented with Albumin, Dextrose and Catalase (ADC) supplement (Sigma). These were grown at 37^{o}C with 180 rpm shaking until mid-log phase (OD_{600} 0.6-0.8) for plating or inoculation and stationary phase (OD_{600} 0.8-1.0) for the generation of competent cells for transformation by electroporation following a standard protocol.

The production of electro-competent mycobacteria for transformation by electroporation required a stationary phase culture (OD_{600} 0.8-1.0), which was made competent by repeated centrifugation at 4000 rpm at 4^{o}C with three washes of 20 ml glycerol (10% v/v) at 4^{o}C. Finally a 2 ml concentrate of cells in glycerol (10% v/v) was prepared. Into a pre-chilled electroporation cuvette, electro-competent *M. bovis* BCG cells (200 μl) were added to plasmid (1 μl). Cuvettes were electroporated at 1800V and the contents transferred to sterile falcon tube containing 7H9 media (2.8 ml) and rested at 37^{o}C, without shaking for 16-18 hours. Cells were then centrifuged at 25^{o}C and resuspended in fresh 7H9 media (200 μl) all of which was then plated on Middlebrook 7H11 agar (Difco) supplemented with oleic acid, albumin, dextrose and catalase (OADC) supplement (Sigma), containing kanamycin 25 $\mu g.ml^{-1}$ and stored at 37^{o}C for 14 days until transformant colonies appeared. Middlebrook 7H11 (OADC) plates containing THPP 951A were made for solid media dose response of the overexpressing strain *M. bovis* BCG pVV16-*echA6* compared to the empty vector

strain *M. bovis* BCG pVV16. Dose responses in liquid media were conducted using Middlebrook 7H9 (ADC). Solid media plates were incubated at 37^{o}C with 5% CO_2, and liquid cultures were incubated at 37^{o}C, 180 rpm shaking. Solid media dose responses were taken as an end point experiment, where as liquid media growth curve reading were taken every 24 hours until stationary phase was reached.

4.2.10 Site-Directed Mutagenesis (SDM) of EchA6

EchA6 was mutated in amino acids predicted to be important or related to inhibitor binding. The SDM was conducted using the pET28a-*echA6* vector as a template and a QuickChange II Site-Directed Mutagenesis kit (Agilent Technologies) following the manufacturers instructions. The primers used for SDM are displayed in Table 4.1.

4.3 Results

4.3.1 Target Identification

THPPs were prepared in a four-step synthetic route and the desired enantiomer separated by chiral-HPLC. GSK366A and GSK951A (Remuinan *et al.* 2013), and two novel THPP analogues GSK059A and GSK572A were included as tool compounds for MoA and structural studies (Table 4.5). All compounds were endowed with selective *M. tb* potency and were devoid of any significant cytotoxicity against HepG2 cell lines (Table 4.5). Compound GSK951A was progressed to a dose response analysis in a murine model of chronic TB infection (Figure 4.2), including a safety and pharmacokinetic profile (Remuinan *et al.* 2013). GSK951A showed a clear

dose response relationship similar to moxifloxacin, a reference drug. Thus, GSK951A combines potency in culture with *in vivo* activity and lack of cytotoxicity.

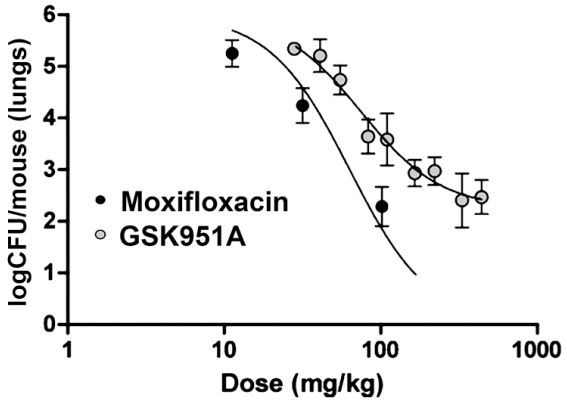
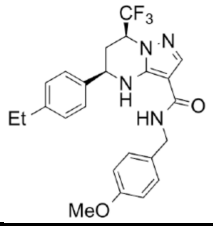
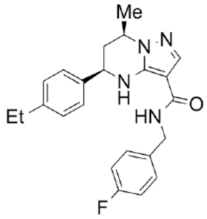
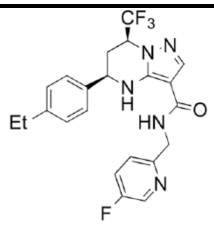
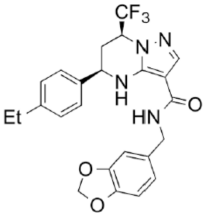


Figure 4.2: Efficacy of GSK951A over an 8-week period against an established murine model of *M. tuberculosis* chronic infection. Mean ± SD is shown for each treated mice group (*n* = 3-7 mice/group).

Table 4.5: The THPP compounds and their respective MICs

THPP Compound	THPP Compound Structure	Cytotoxicity HepG2	MIC (μM)	
			M. tb H37Rv	*M. bovis* BCG
GSK366A		>25 μM	0.3	n.d.
GSK059A		24.5 μM	0.16	n.d.
GSK572A		>25 μM	0.5	n.d.
GSK951A		>25 μM	0.16	0.8

Following the identification of the THPPs as putative MmpL3 inhibitors, collaborators at Cellzome (Heidelberg, Germany) applied a chemical proteomics strategy to identify the protein targets of the THPP lead compounds directly in *M. bovis* BCG extracts. They synthesised carboxylic acid analogues of the active and inactive THPP enantiomers suitable for immobilisation to Sepharose beads. Each type of bead was incubated with *M. bovis* BCG extracts under three different conditions: (i) in presence of vehicle, (ii) in presence of excess "free" active enantiomer analogue, and (iii) in presence of excess "free" inactive enantiomer analogue. The relative protein content captured by the beads from each sample was quantified by isobaric tagging of tryptic peptides and tandem mass spectrometry analysis of the combined peptide pools. A total of 152 different proteins were captured by the beads. However, target proteins for antibacterial activity would be expected to bind preferentially to beads derivatised with the active enantiomer analogue, a preference they probed by competition with free active *vs* free inactive enantiomer analogues. Relative quantification demonstrated that only a single protein showed a pronounced preference in their competition assay. The putative enoyl-CoA hydratase EchA6 showed robust (92%) inhibition by the active enantiomer analogue GSK729, but only insignificant (16%) inhibition by its inactive enantiomer analogue. Consistently, beads derivatised with the active analogue captured ~11 times more EchA6 compared to the inactive analogue (Figure 4.3).

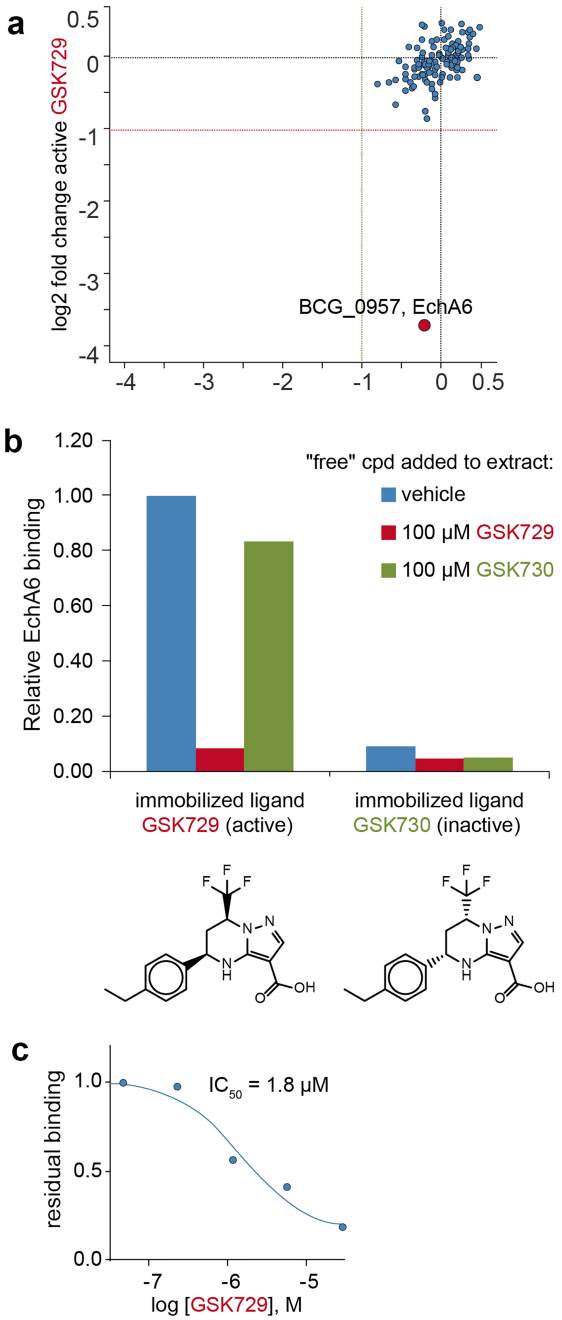


Figure 4.3: Chemoproteomics profiling identifies the putative enoyl-CoA hydratase EchA6 as target of the THPP series (work performed by Cellzome, Heidelberg, Germany). (a) EchA6 is captured from *M. bovis* BCG extracts with beads derivatised with GSK729. Capturing of EchA6 is inhibited by excess GSK729 (100 µM) but not by the inactive enantiomer analogue GSK730. No other proteins are affected by the addition of either compound. (b) EchA6 binds to beads derivatised with the active enantiomer analogue GSK729 but not the inactive enantiomer analogue GSK730. (c) Estimation of the affinity of GSK729 for EchA6. GSK729 inhibited the binding of EchA6 to GSK729-derivatised beads in *M. bovis* BCG extracts with an IC_{50} value of 1.8 µM.

In addition, MmpL3 (BCG_0243C) was not identified in pull-downs with the immobilised THPP analogues. MmpL3 was readily detected within the whole proteome analysis of the *M. bovis* BCG extract, which identified 1679 proteins. MmpL3 was detected with 261 peptides, placing it on position #70 on a list based on spectral counting as an approximate measure for abundance. Therefore it was inferred that the extracted MmpL3 protein did not bind to the immobilised ligands, which does not necessarily rule it out as a target, since it could be due to either steric hindrance by the linker on the compound, low affinity, or denaturation of the extracted MmpL3. Supporting the specificity of the GSK729-beads, in similar experiments performed with HepG2 cells, the beads did not capture the closest human EchA6 orthologue, ECH1. Moreover, no other proteins were captured by the GSK729-beads in a stereo-specific manner in this experiment. To allow estimation of the affinity of GSK729 for EchA6 in *M. bovis* BCG extracts, Cellzome optimised the concentration of immobilised ligands on the beads, and found that by lowering the ligand concentration from 2 mM to 50 μM, they avoided depletion of EchA6 from the extract. This enabled them to determine dose-dependent binding of EchA6 to GSK729 in *M. bovis* BCG extracts with an IC_{50} of 1.8 μM (Figure 4.3c).

4.3.2 The *echA6* gene is essential

The essentiality of *echA6* was established firstly by the failure of attempts to delete *echA6* in *M. tb*, *M. bovis* BCG and *M. smegmatis* by specialised transduction, and secondly by virtue of the CESTET system (Brown *et al.* 2007; Rana *et al.* 2012), through the generation of a merodiploid strain in *M. bovis* BCG that contained a second integrated copy of *echA6* (*Rv0905*) under the control of the inducible

tetracycline promoter. Following transduction of the merodiploid strain with the *echA6* knockout phage, Hyg^R conditional *echA6* knockouts were obtained on selective plates containing anhydrotetracycline (ATc) but not on those lacking ATc. One such transductant Δ*BCG0957* was selected for further work and was subjected to growth in liquid medium with and without ATc. As shown in Figure 4.4 (a), the strain grew normally in liquid medium with ATc, but showed cell lysis when grown in medium lacking ATc, hence demonstrating essentiality of *echA6*. To evaluate the effect of depletion of *echA6* on both mycolic acid and fatty acid synthesis in *M. bovis* BCG, MAMEs and FAMEs were prepared from cultures following labeling with [^{14}C]-acetate at day 15, and analysed by autoradiography TLC. As shown in Figure 4.4 (b), conditional depletion of *echA6* results in a reduction of α-MAMEs and keto-MAMEs, while the overall abundance of FAMEs remains largely unaffected, a classic hallmark of inhibitors targeting mycolic acid biosynthesis (Bantscheff *et al.* 2011; Cantaloube *et al.* 2011).

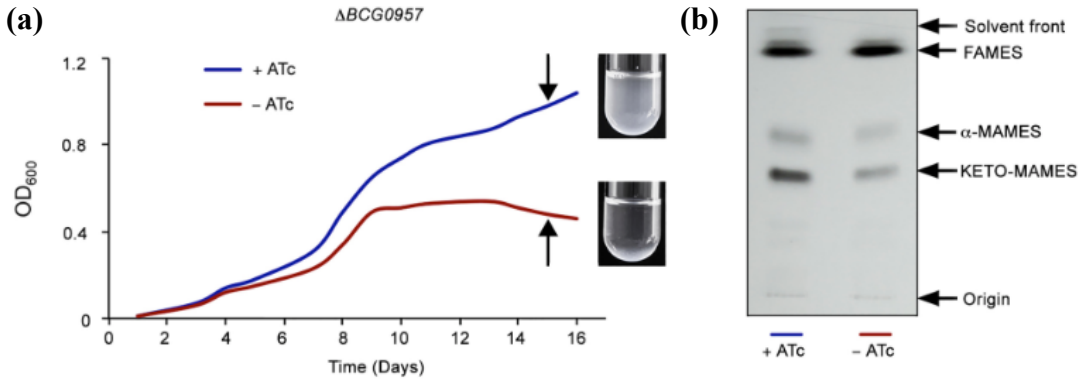


Figure 4.4: Essentiality of *echA6*. (a) Growth curves of *ΔBCG0957* in liquid media with or without ATc were performed in duplicate. (b) One culture of *ΔBCG0957* was labelled with [^{14}C]-acetate at day 15 indicated by the arrow on (a) for 24 hours with the corresponding total MAMEs and FAMEs isolated and equal counts for each sample subjected to TLC and exposed to Kodak X-Omat film. The second culture was monitored until cell lysis was observed as is shown in (a).

4.3.3 EchA6 overexpression causes resistance to THPP GSK951A

Whole-cell target engagement of GSK951A was established through resistance *via* overexpression of EchA6. *M. tb echA6* (*Rv0905*) was cloned into the multi-copy plasmid pVV16, which resulted in overexpression of his-tagged EchA6 as shown by Western Blot analysis as shown in Figure 4.5a. The MICs of the overexpresser pVV16-*echA6* and empty vector control pVV16 strains were established by dose response conducted on both solid (Figure 4.5b) and liquid media (Figure 4.5c). pVV16-*echA6* possessing an MIC of 1.60 μM on solid media and 2.00 μM on liquid media, in comparison to the pVV16 vector control of MIC 0.32 μM (in both media). Finally, [^{14}C]-acetate labeling of cultures of pVV16 and pVV16-*echA6* containing strains revealed an elevated synthesis of MAMEs (Figure 4.6a). We also observed the synthesis of cell wall bound MAMEs, which were less refractory to the addition of GSK951A at 1x MIC, using the pVV16-*echA6* strain in comparison to the pVV16 empty vector control (Figure 4.6b).

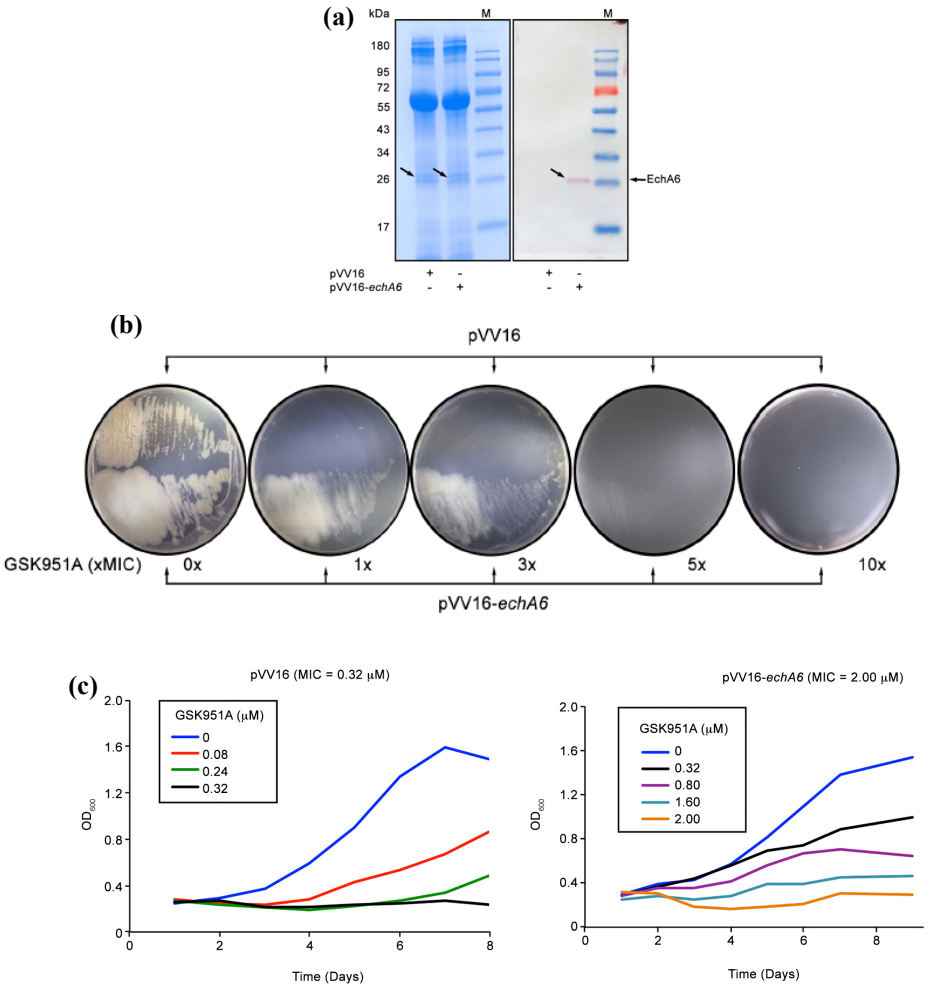


Figure 4.5: Overexpression of *M. tb* EchA6 causes increased resistance to THPP GSK951A. (a) Western blot validation of EchA6 overexpression. (b) A solid media dose response (0, 0.32, 0.96, 1.6 and 3.2 µM) of GSK951A with two strains of *M. bovis* BCG containing either pVV16-*echA6* or the corresponding empty plasmid pVV16. An MIC of ≤ 1.6 µM was observed with the EchA6 overexpresser compared to ≤ 0.32 µM with the empty vector. (c) A liquid media dose response of two strains of *M. bovis* BCG containing either pVV16-*echA6* or the corresponding empty plasmid pVV16. An MIC of ≤ 2.0 µM was observed with the EchA6 overexpresser compared to ≤ 0.32 µM with the empty vector.

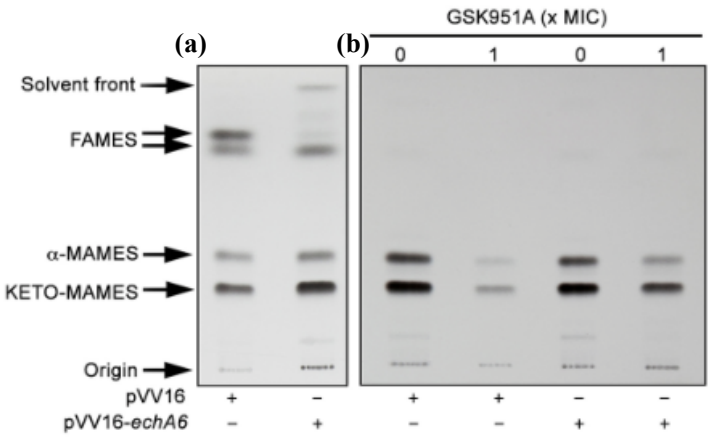


Figure 4.6: [^{14}C]-acetate labeling of cultures of *M. bovis* BCG strains containing pVV16 and pVV16-*echA6*. (a) The corresponding total MAMEs and FAMEs were isolated and equal counts were subjected to TLC and exposed on Kodak X-Omat film. (b) Cell wall bound MAMEs were also isolated from each strain with and without treatment with 0.32 μM GSK951A (1x MIC) and equal volumes were subjected to TLC and exposed to Kodak X-Omat film.

4.3.4 EchA6 interacts with key components of mycobacterial FAS-II

To further probe the possible interaction of EchA6 with components of FAS-II, a protein-protein interaction screen was conducted using the bacterial two-hybrid system-BACTH. Interestingly, preliminary evidence for EchA6 interacting with two specific components of FAS-II was found, including the β-ketoacyl-ACP synthase KasA, and the enoyl-ACP reductase InhA (Figure 4.7). No interactions were observed with either the β-ketoacyl-ACP synthase KasB, the heterodimeric hydroxyacyl-ACP dehydratase complex components, HadA, HadB, and HadC, the β-ketoacyl-ACP reductase MabA (FabG1), or the proposed FAS-I-FAS-II linking β-ketoacyl-ACP synthase III FabH. These findings indicate that EchA6 interacts primarily with specific components of the core multi-enzyme FAS-II complex, termed E1-FAS-II (Rullas *et al.* 2010).

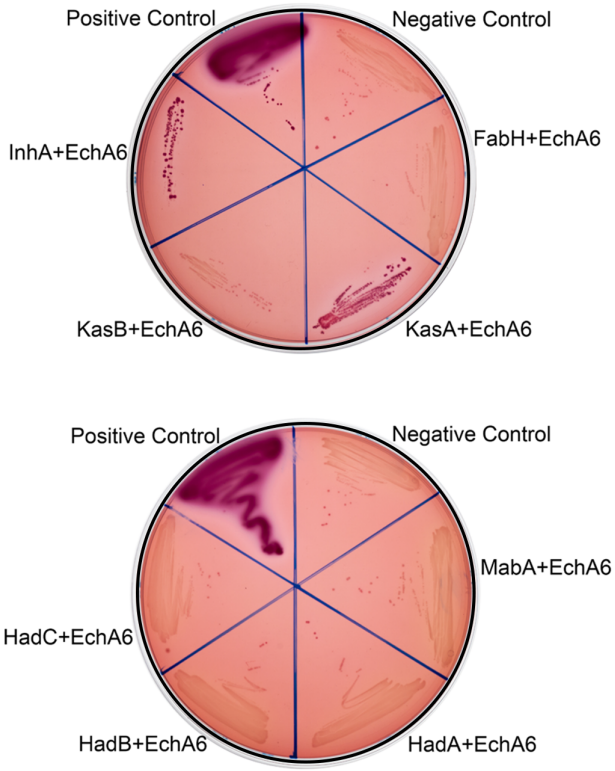


Figure 4.7: Protein-protein interaction screen using the bacterial two-hybrid system-BACTH and EchA6 with components of FAS-II. The positive control pKT25 was fused to the Leucine Zipper of GCN4 co-transformed with pUT18C of the Leucine Zipper GCN4. The negative control was pKT25 Zip co-transformed with empty pUT18 vector.

4.3.5 Intrinsic tryptophan fluorescence (ITF) ligand binding assays

M. tb echA6 was amplified by PCR and cloned into pET28a for recombinant protein production and subsequent use for assays and X-ray crystallography. Following expression in *E. coli* BL21 (DE3), recombinant EchA6 was purified from a clarified cell lysate and found to elute from the HisTrap HP column using 125-200 mM imidazole at a protein concentration of around 0.8 $mg.ml^{-1}$ (Figure 4.8).

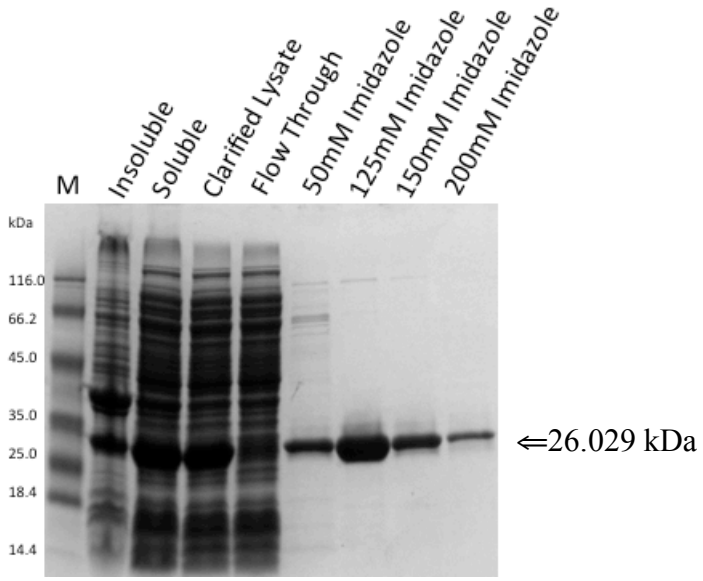


Figure 4.8: SDS-PAGE gel showing the purification of EchA6 from clarified lysate following recombinant expression by *E. coli* BL21 (DE3) transformed with pET28a-*echA6*. Protein was purified using a Histrap HP column (GE Healthcare Life Sciences) following manufacturers instructions and eluted with 125-200 mM imidazole.

An assay of EchA6 was required in order to determine whether or not the THPPs bind the protein and also if EchA6 binds acyl-Coenzyme As as would be expected due to its proposed activity as an enoyl-CoA hydratase (crotonase). Crotonases catalyse the addition of a water molecule across the double bond of *α,β*-unsaturated thioesters, corresponding to the second step of the catabolic fatty acid β-oxidation cycle. The functional enzymatic activity of an enoyl-CoA hydratase requires the presence of two key catalytic residues within the active site. A sequence alignment of *M. tb* EchA6 with other EchAs indicates that only 4 of the 21 EchAs proposed to be in the *M. tb* genome contained these functional carboxylic acid side chain amino acids in positions 144 and 164 that coordinate a water molecule for hydration to occur (Bahnson *et al.* 2002). Figure 4.9 shows a sequence alignment of all the *M. tb* putative EchAs and demonstrates the lack of catalytic residues at positions 144 and 164 in the amino acid sequence.

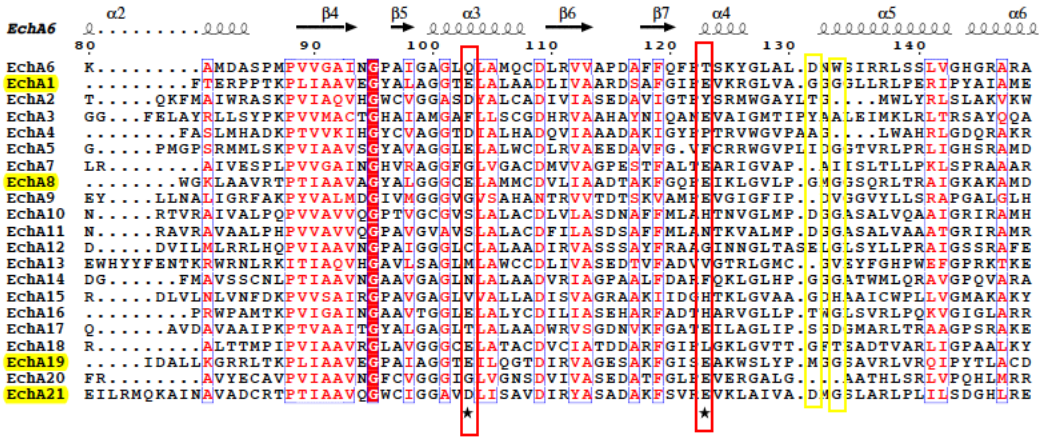


Figure 4.9: Sequence alignment of *M. tb* EchAs. Of the 21 EchAs present in the *M. tb* genome, only 4 have the residues required for catalytic activity. These EchA orthologues are highlighted in yellow and the residues required for catalytic activity are indicated within the red asterisked boxes. Conserved residues are indicated in red font and residues that interact with GSK951A in EchA6 are indicated within the yellow boxes.

Due to the absence of the required catalytic residues for crotonase enzymatic activity in EchA6, but the presence of four tryptophan residues in each monomer of EchA6, an assay was developed exploiting the intrinsic fluorescence of the tryptophan residues and the way in which that fluorescent signal changes upon ligand binding due to the change in microenvironment of tryptophan residues proximal to the binding site. Sequential additions of acyl-CoAs with acyl chains ranging in length from 4 to 20 carbons in length led to a decrease in fluorescence maxima. The acyl-CoA binding studies indicated that longer chains (C_{18} and C_{20}-CoA) bind EchA6 with a higher affinity (Table 4.6) and are therefore more likely to represent the physiological ligand of EchA6. These data are illustrated in Figure 4.10.

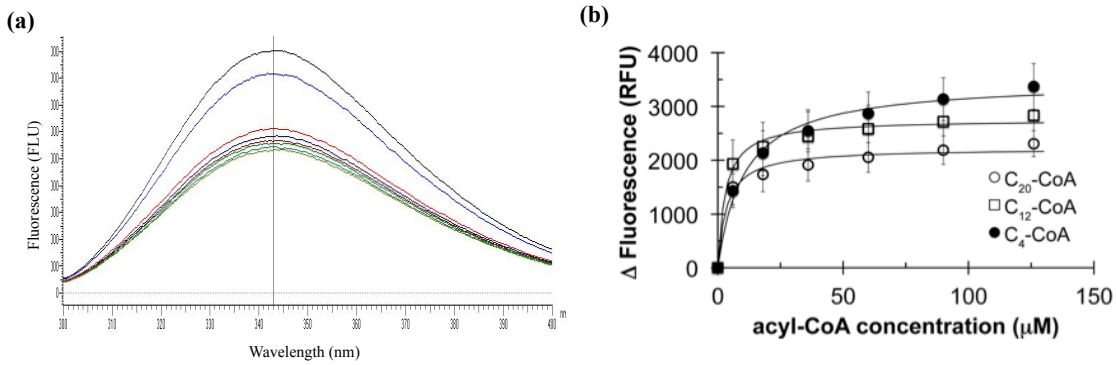


Figure 4.10: (a) Sequential additions of acyl-CoAs results in a decrease in fluorescence maxima. (b) Saturation binding curves for C_4-CoA (K_d = 10.4 ± 2.4 μM), C_{12}-CoA (K_d = 3.0 ± 1.1 μM), and C_{20}-CoA (K_d = 3.5 ± 0.4 μM) using an EchA6 ITF binding assay.

The same ITF binding assay was conducted with each of the THPP compounds. A clear correlation between compound activity against whole cells (MIC) and compound affinity (K_d) for EchA6 was apparent, where GSK572A (the active enantiomer of a THPP compound set) demonstrated a K_d of 1.9 ± 0.6 μM where as the inactive enantiomer of that compound, GSK573A gave a K_d of 285.8 ± 68.9 μM, demonstrating stereospecificity of the THPP:EchA6 interaction. The lead THPP compound, GSK951A gave a K_d of 0.45 ± 0.06 μM. The others, GSK366A and GSK059A gave K_ds of 5.6 ± 0.9 and 9.6 ± 1.9 μM, respectively (Figure 4.11; Table 4.6).

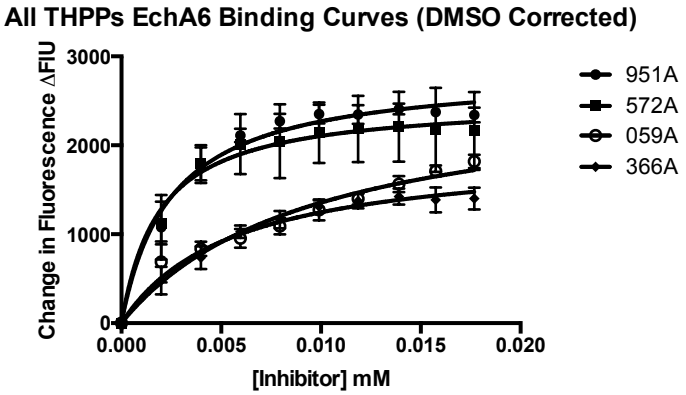


Figure 4.11: ITF binding assay of EchA6 with THPP compounds. Binding curves are shown for the active THPP compounds. Deducting the background ΔFlU generated by a DMSO control has normalised the data. The inactive enantiomer, GSK573A, is not shown. (Results were compiled using one-site specific binding data analysis in GraphPad Prism).

Following the identification of two distinctly different ligands that bind EchA6 with high affinities (C_{20}-CoA and GSK951A), a competition assay was conducted in order to determine if the THPP compounds perturbed C_{20}-CoA binding. Three concentrations of GSK951A were pre-incubated with EchA6 before sequential additions of C_{20}-CoA. The results of this binding assay clearly show that C_{20}-CoA binding is inhibited by GSK951A (C_{20}-CoA K_d = 10.2 ± 5.5 μM with GSK951A at 10 μM), and increasing inhibitor concentrations from 0.25 to 10 μM indicated a competition between the THPPs and C_{20}-CoA for the same EchA6 binding site. This experiment was repeated with C_4-CoA in order to further demonstrate that the observed competition is not totally dependent on a longer acyl-chain of the acyl-CoA ligand. No further inhibition of C_{20}-CoA binding was observed above 2.5 μM concentration of GSK951A, however C_4-CoA binding was observed at ≤ 10 μM. The results of this experiment are summarised in Figure 4.12. Table 4.6 summarises all of the binding data generated with EchA6.

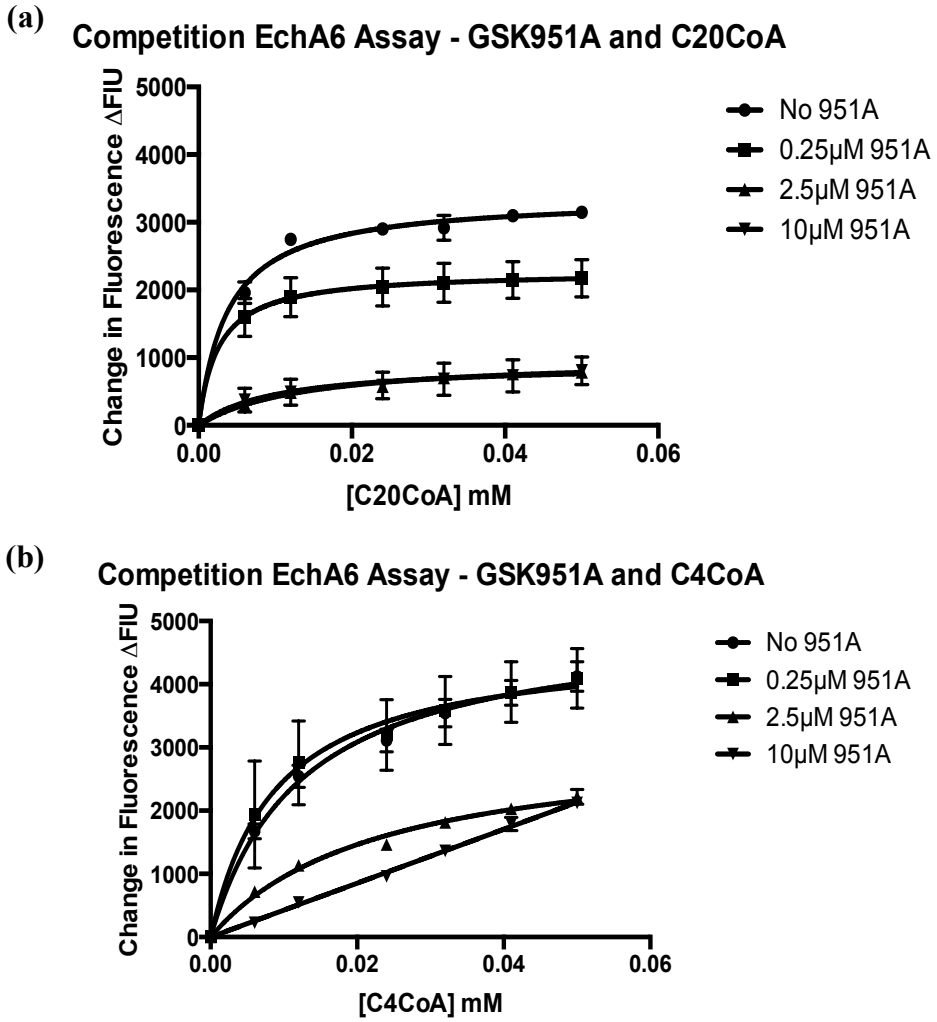


Figure 4.12: EchA6 competition assay with C_4-CoA (a) and C_{20}-CoA (b) and GSK951A. Binding data of C_4 and C_{20}-CoA in competition with GSK951A for EchA6. These data demonstrate that the greatest inhibitory effect of the compound is observed with the long chain CoA.

Table 4.6: Summary of the binding affinities of all ligands tested with EchA6

Ligand	K_d (μM)	
C_4-CoA	10.4 ± 2.4	
C_{12}-CoA	3.0 ± 1.1	
C_{14}-CoA	3.1 ± 0.9	
C_{16}-CoA	2.8 ± 1.4	
C_{18}-CoA	1.4 ± 1.3	
C_{20}-CoA	3.5 ± 0.4	
GSK951A	0.45 ± 0.06	
GSK366A	5.6 ± 0.9	
GSK059A	9.6 ± 1.9	
GSK572A	1.9 ± 0.6	
GSK573A	285.8 ± 68.9	
Competition C_{20}-CoA with GSK951A		**Fold increase of K_d relative to no drug**
0.25 μM drug	2.6 ± 0.9	0.7
2.5 μM drug	13.6 ± 2.1	3.8
10 μM drug	10.2 ± 5.5	2.9
Competition C_4-CoA with GSK951A		
0.25 μM drug	8.9 ± 2.7	0.86
2.5 μM drug	23.1 ± 2.8	2.2
10 μM drug	N.D.	-

N.D. – not determined due to failure of non-linear fitting

4.3.6 Site directed mutagenesis (SDM) of EchA6

Site directed mutagenesis (SDM) of *M. tb* EchA6 was conducted in order to determine which amino acid residues were essential for THPP binding. Amino acids were chosen for SDM based on their proximity and computer predicted interactions with the THPP compounds upon binding. Following mutation of the protein in the pET28a vector used for recombinant protein production as described above, five plasmids were obtained with the following mutations: CT223GC, AT226GC, CA319GC, A392C and TG397GC. These mutations related to the following mutations in the protein respectively: Leu75Ala, Ile76Ala, Gln107Ala, Asp131Ala and Trp133Ala. These proteins were expressed, purified and assayed following the same ITF binding assay method as used for the wildtype protein. Each mutant was assayed for C_{20}-CoA and GSK951A binding indicating the effect of each mutation on binding function and inhibition. Mutations of Leu75, Ile 76, Asp 131 and Trp133 to Ala resulted in a complete loss of THPP GSK951A binding but maintained C_{20}-CoA binding with K_ds of 8.7, 6.5, 12.5 and 141.7 μM, respectively with reduced affinity compared to wildtype EchA6 (K_d = 3.5 μM) (Summarised in Table 4.7) (Figure 4.13).

Table 4.7: Summary of the binding affinities of all ligands tested with point mutated EchA6

Binding of point mutant	K_d (μM)
EchA6 Gln107Ala + GSK951A	0.59 ± 0.3
EchA6 Gln107Ala + C_{20}-CoA	2.9 ± 1.2
EchA6 Leu75Ala + GSK951A	N.D.
EchA6 Leu75Ala + C_{20}-CoA	8.7 ± 1.1
EchA6 Ile76Ala + GSK951A	N.D.
EchA6 Ile76Ala + C_{20}-CoA	6.5 ± 0.64
EchA6 Asp131Ala + GSK951A	N.D.
EchA6 Asp131Ala + C_{20}-CoA	12.5 ± 4.85
EchA6 Trp133Ala + GSK951A	N.D.
EchA6 Trp133Ala + C_{20}-CoA	141.7 ± 15.3

Conversely, mutation of the Gln107 amino acid of *M. tb* EchA6 to an Ala resulted in a dramatically increased affinity of GSK951A binding and also a slight increase in C_{20}-CoA binding. The binding affinity for GSK951A increases with a change in K_d from 3.5 μM (EchA6 wildtype) to 0.6 μM (EchA6 Gln107Ala) and for C_{20}-CoA the affinity increases with a change in K_d from 3.5 μM (EchA6 wildtype) to 2.9 μM (EchA6 Gln107Ala) (Figure 4.14) (summarised in Table 4.7).

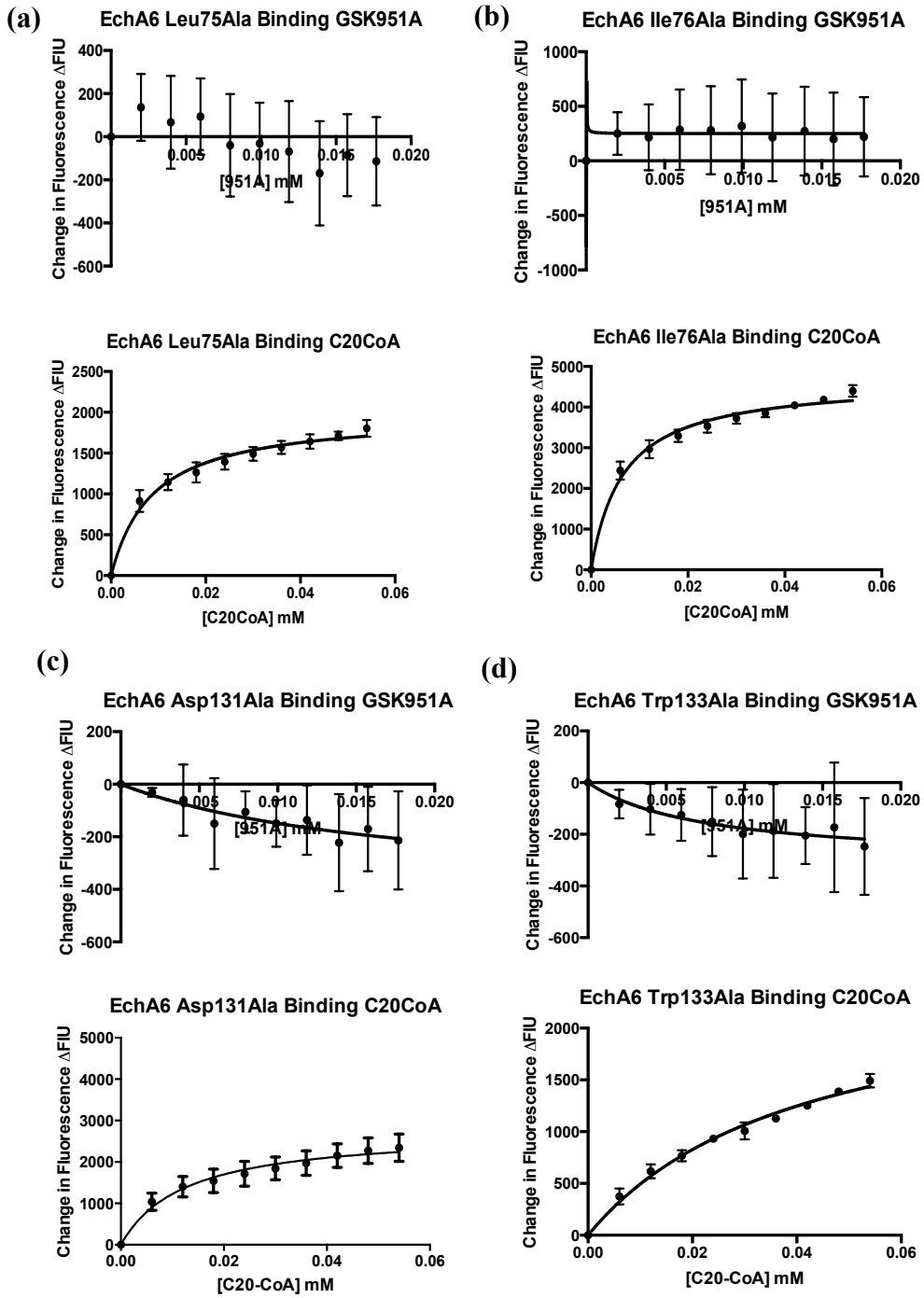


Figure 4.13: SDM of *M. tb* EchA6 amino acids Leu75 (a), Ile76 (b), Asp131 (c) and Trp133 (d) to Ala affects THPP GSK951A binding, but maintains C_{20}-CoA binding with reduced affinity. Mutations of Leu75, Ile 76, Asp 131 and Trp133 to Ala resulted in a complete loss of THPP GSK951A binding but maintained C_{20}-CoA binding with K_ds of 8.7, 6.5, 12.5 and 141.7 μM, respectively, with reduced affinity compared to wildtype EchA6 (K_d = 3.5 μM).

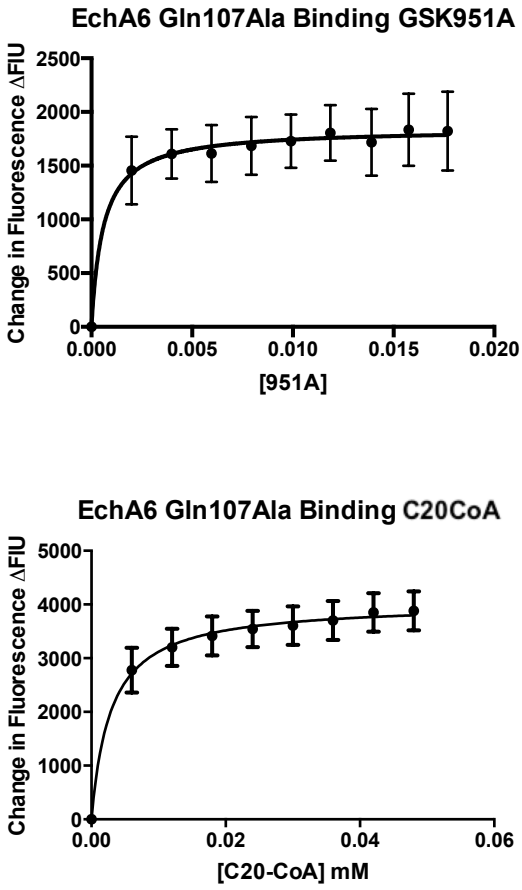


Figure 4.14: SDM of *M. tb* EchA6 amino acid Gln107 to Ala increases affinity for THPP GSK951A and maintains C_{20}-CoA binding. The binding affinity for GSK951A increases with a change in K_d from 2.5 μM (EchA6 wildtype) to 0.6 μM (EchA6 Gln107Ala) and for C_{20}-CoA the affinity increases with a change in K_d from 3.5 μM (EchA6 wildtype) to 2.9 μM (EchA6 Gln107Ala).

4.3.7 *In vivo* validation of EchA6 interaction with GSK951A

The *M. tb* strain transformed with a multi-copy plasmid-borne *echA6* Trp133Ala was tested in an *in vivo* mouse model of acute TB infection, and resulted in a significant shift in the ED_{99} of GSK951A when compared to strains transformed with empty vector or vector containing unmutated *echA6.* The *echA6* Trp133Ala strain resulted in a significant increase in the ED_{99} of GSK951A, from 85 to 77 $mg.kg^{-1}$ for the empty vector and unmutated *echA6* strains to > 250 $mg.kg^{-1}$ for the *echA6* Trp133Ala strain.

This increase of ED_{99} was well outside the 95% confidence interval (CI) for the empty vector and *echA6* strains (41-182 $mg.kg^{-1}$). As a control, INH was also used and all strains possessed similar ED_{99} values and were within calculated 95% CI range (0.2-3 $mg.kg^{-1}$) (Figure 4.15). While the empty vector and unmutated *echA6* strains were able to grow at the same rate when inoculated into C57BL/6 mice in the acute TB infection model, the *echA6* Trp133Ala strain was relatively attenuated for growth, suggesting that the viability of *M. tb in vivo* is compromised by EchA6 point mutations that weaken acyl-CoA binding. In addition, *M. bovis* BCG transformed with *echA6* Trp133Ala in the same vector showed a further increase in resistance to GSK951A, possessing an MIC of 3.20 μM. This is in comparison to a *M. bovis* BCG strain transformed with unmutated *echA6* in the same vector possessing an MIC of 1.60 μM.

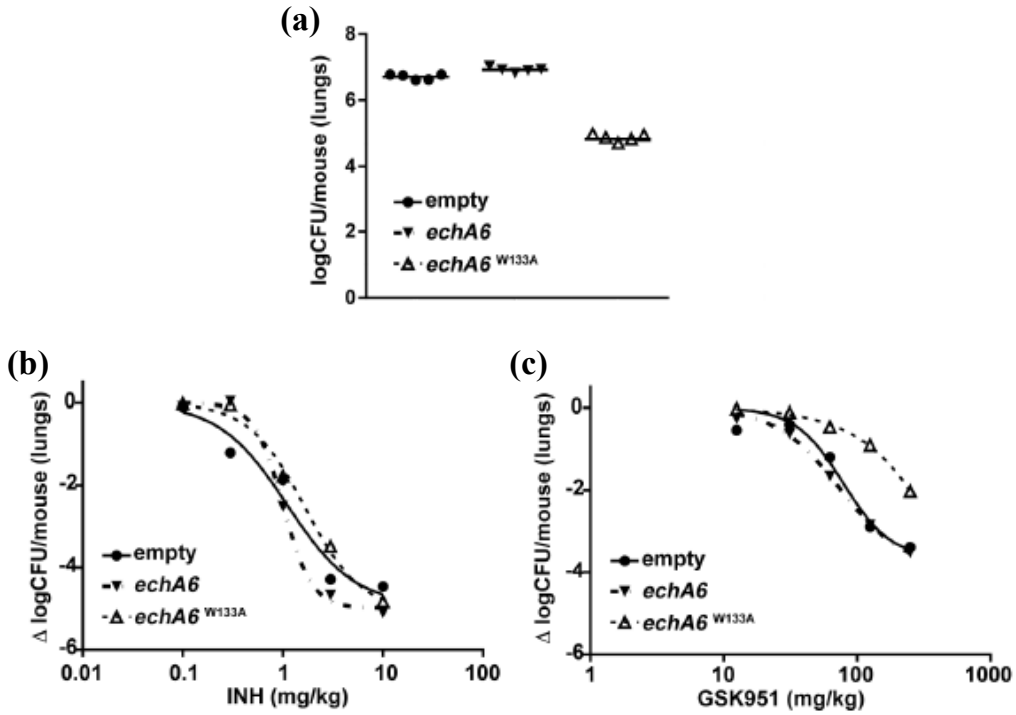


Figure 4.15: The ED_{99} of GSK951A and INH was calculated in a murine model of *M. tb* acute infection. This was performed using *M. tb* transformed with either a multi-copy plasmid-borne empty vector control, *echA6* or *echA6* Trp133Ala. (a) The relative growth of each strain used, where each datapoint represents an individual mouse. (b) and (c) Log.cfu counts are shown as the difference with respect to the untreated control group infected with each strain (Δlog.cfu/mouse).

4.3.8 Crystallography of EchA6

The crystallography of EchA6 commenced following purification and concentration of the protein to >30 $mg.ml^{-1}$. Commercially available sparse matrix screens were used to generate the *apo*-, C_{20}-CoA and THPP bound structures, and crystals generally appeared after 3-4 weeks (Figure 4.16a). Crystals were cryoprotected (if required) with glycerol or ethylene glycol before being flash frozen in liquid nitrogen and stored. Data was collected both in house (School of Biosciences, University of Birmingham) and at Diamond Light Source. All structures were solved by molecular replacement using the structurally similar rat liver enoyl CoA hydratase (RnECH)

(RCSB Protein Data Bank). In all cases, trimeric crystallisation was observed where each asymmetric unit consisted of 1, 3 or 6 EchA6 monomers. Like RnECH, EchA6 contains the β-β-α superhelix of four turns, the N-terminal of which forms a twisted parallel β-sheet (β2, β3, β5 and β7 strands), around which the α-helices of the monomer wrap. Trimerisation occurs in the region of α-helices α9, α10 and α11 (Figure 4.16b). Upon C_{20}-CoA binding, a conformational change occurs in the β3-α3 loop resulting in a change of the substrate-binding groove causing it to close into a tunnel running through each monomer in which resides the acyl-chain of the C_{20}-CoA moiety, termed the 'tense' conformation. By contrast, THPP binding occurs in the 'relaxed' conformation with the substrate-binding groove in the open conformation (Figure 4.16c and d). No covalent contacts have been identified, and potential polar interactions, Van der Waals' contacts and hydrophobic interactions were computed to a 4Å radius of the ligand (Figure 4.16e and f).

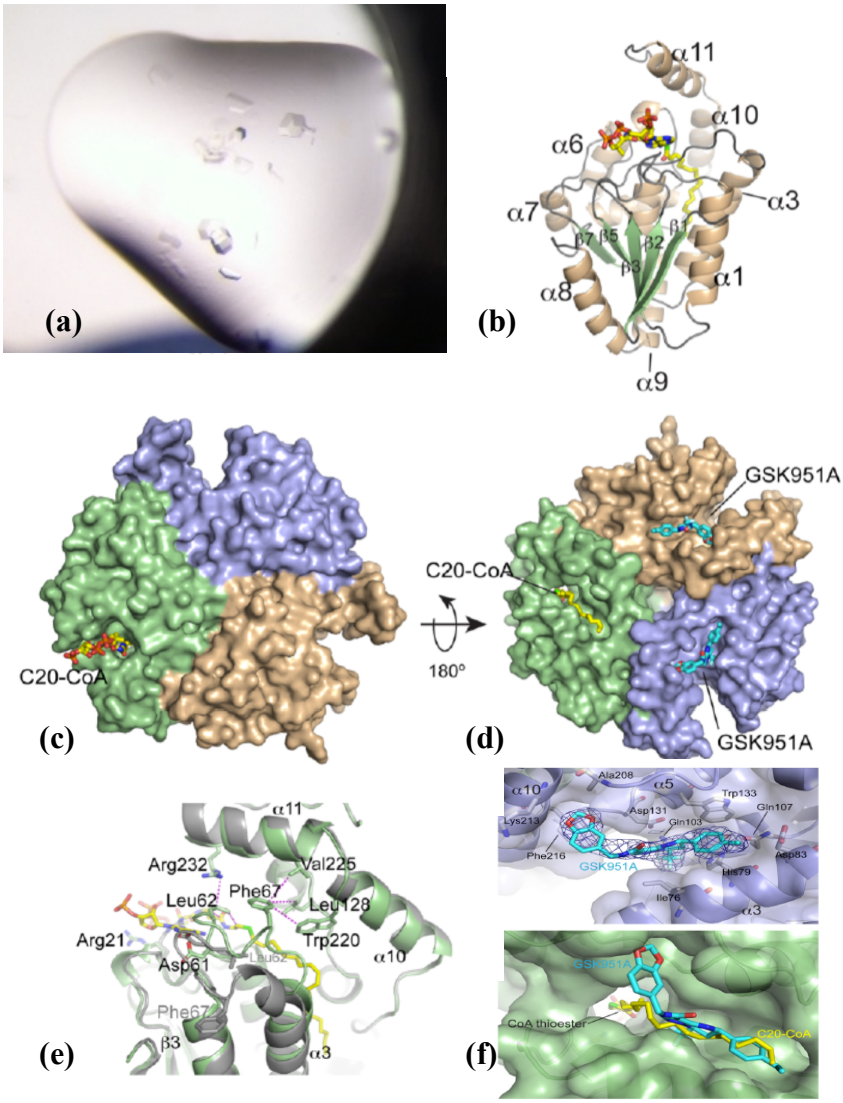


Figure 4.16: (a) EchA6 crystals that gave the *apo*-EchA6 crystal structure (0.1M Tris pH 8.5, 60% v/v polypropylene glycol 400). (b) A ribbon diagram of EchA6 in complex with C_{20}-CoA ligand and (c) the computed molecular surface diagram of the EchA6 trimer bound to C_{20}-CoA in the binding site of one of the monomers (green) and (d) the 180^{o} rotation of the EchA6 trimer shows the acyl-chain of the C_{20}-CoA in the same (green) monomer and two GSK951A inhibitors in the remaining two binding sites. The conformational change of the binding site upon complexation with C_{20}-CoA. (e) The relaxed (*apo*) and the tensed (C_{20}-CoA bound) conformations are shown in grey and green respectively. Predicted contacts between GSK951A and EchA6 are shown (purple). (f) The amino acid side chains within a 4 Å radius of the GSK951A density with the molecular model fitted and below the GSK951A (blue) and C_{20}-CoA acyl-chain (yellow) bound structures superimposed.

Each of the THPPs were complexed with EchA6 in a variety of different crystal conditions already discussed. All THPPs were found to occupy the same ligand-binding site with the same orientation of the core of the THPP compounds. However the *R*-group of the compounds appeared to have considerable variation in the geometry of binding (Figure 4.17). It may be speculated that this may indicate a greater dependence on the THPP core for functional activity.

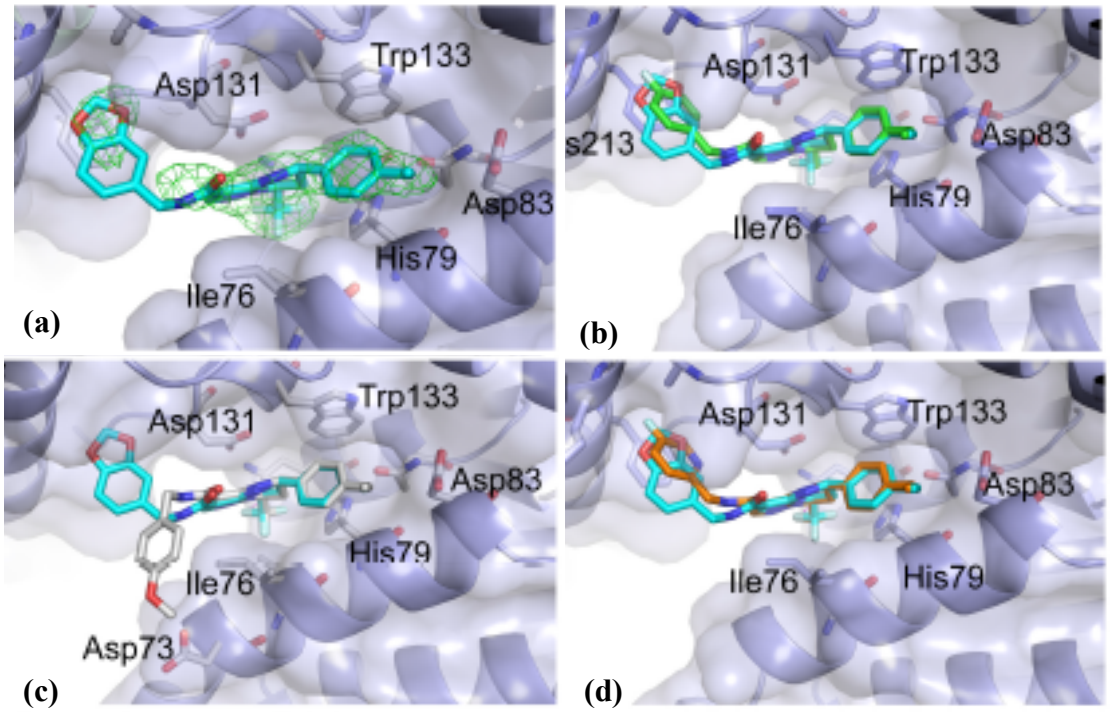


Figure 4.17: Comparison of the mode of THPP compound binding EchA6. The crystal structure of EchA6 bound to GSK951A (blue) (a) has been superimposed onto the complexes of GSK366A (green) (b), GSK059A (grey) (c) and GSK572A (orange) (d). Although the THPP core of the compounds binds consistently in the same orientation and geometry, the *R*-groups show considerable variability between the compounds.

4.4 Discussion

It has been previously reported that the attractive *in vitro* and *in vivo* anti-TB profile of THPP compounds GSK366A and GSK951A, which showed bactericidal activity *in vitro* against both drug-susceptible and MDR/XDR strains of *M. tb*, with MICs close to those of the reference moxifloxacin, a drug currently in late stage clinical development for TB therapy (Remuinan *et al.* 2013; Zvada *et al.* 2013).

Target identification by stereoselective quantitative pull-down points to EchA6 as the target of THPP inhibitors. This result is corroborated by a string of orthogonal evidence: crystallographic structures of THPPs bound to EchA6, *in vitro* ligand binding data, and the observation that THPPs reduce overall mycolic acid levels in a dose-dependent fashion. Importantly, it was demonstrated that the *echA6* gene is essential in mycobacteria. Finally, we demonstrated whole cell target engagement, both *in vitro* and in the mouse acute TB infection model, through resistance *via* overexpression of EchA6 and EchA6 Trp133Ala, respectively. Our evidence is in contrast to the recent target assignment of the essential mycolic acid exporter MmpL3 (Remuinan *et al.* 2013), which was based on spontaneous resistance under selective pressure of THPP, whereas the *echA6* gene (so far) has not been observed to acquire resistance-conferring mutations against THPP. This is not totally unexpected, as INH-resistance, for instance, is caused by mutations in the target-encoding gene *inhA* in only 2 % of clinical isolates (Hazbon *et al.* 2006). The evidence to support EchA6 as a target is consistent across a wide range of experiments, and resistance induced by the Trp133Ala SDM argues strongly that this compound family acts through EchA6, even though complete abrogation of THPP binding by the Trp133Ala mutant would

suggest a more pronounced effect on the ED_{99} value. The continued presence of the wildtype copy in the overexpressing strain could plausibly account for the relatively modest scale of the increase.

The exact nature of the function of EchA6 remains to be established. However, EchA6 has a distinct preference for long-chain acyl-CoAs and shows interactions with selective components of FAS-II in preliminary bacterial two-hybrid system-BACTH experiments. These included the β-ketoacyl-ACP synthase KasA, and the enoyl-ACP reductase InhA. These findings indicate that EchA6 interacts primarily with specific components of the core multi-enzyme FAS-II complex, termed E1-FAS-II (Rullas *et al.* 2010).

The profile of THPP-induced suppression of mycolic acid synthesis, the bacterial 2-hybrid data, and essentiality of the *echA6* gene together argue that EchA6 is a crucial element of this metabolic route to FAS-II. We postulate that EchA6 acts as a shuttle for fatty acid transfer, a role that would be compatible with its catalytically silent state and the moderate affinity it displays for long-chain acyl-CoA ligands. Emerging from these considerations is a model (Figure 4.18) that places EchA6 at a critical junction between FAS-I, β-oxidation and FAS-II pathways. The channelling of acyl-CoA primers from FAS-I or the β-oxidation pathway would undergo an iterative FAS-II cycle initiated by KasA, an interaction partner of EchA6 in the 2-hybrid screen, which, as we have previously shown, utilises long-chain acyl-CoAs as substrates (Kremer *et al.* 2002).

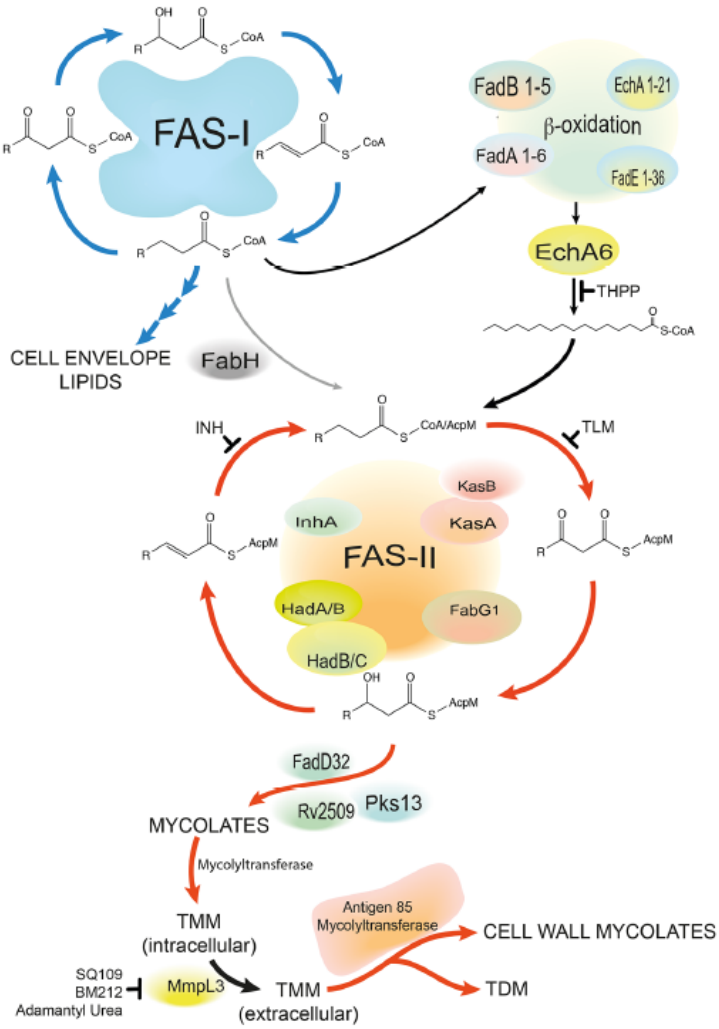


Figure 4.18: Model of the physiological role of EchA6 in mycobacterial fatty acid metabolism. The proposed function of EchA6 is as a fatty acyl-CoA delivery mechanism, feeding fatty acids from β-oxidation into FAS-II for subsequent mycolic acid biosynthesis.

It is also worth noting that of the 21 EchA-like proteins in the *M. tuberculosis* genome, only four (EchA1, EchA8, EchA19 and EchA21) possess the conserved carboxylate side chains residues that would support enoyl-CoA hydratases activity. Despite closely resembling this class of enzymes from the crotonase superfamily in terms of tertiary structure and self-assembly into trimmers (Hamed *et al.* 2008), EchA6 appears to be evolutionary inactive. Nevertheless, it has retained the ability to bind acyl-CoA ligands, with a pronounced preference of longer-acyl chains,

consistent with the extended hydrophobic ligand-binding groove. However, the diversity of crotonase family members in terms of enzymatic activity and substrates (albeit all CoA-linked) leave the door open to an alternative, as yet unidentified catalytic activity.

Using the route of stereoselective quantitative pull-down to identify the target of THPP inhibitors has exposed an inherent weakness of target identification by WGS of resistant mutants following phenotypic screening. Based on resistance, MmpL3 has been proposed to mediate the inhibitory activity of a host of compounds of different chemical scaffolds (Tahlan *et al.* 2012; Grzegorzewicz *et al.* 2012; Remuinan *et al.* 2013; La Rosa *et al.* 2012; Stanley *et al.* 2012; Lun *et al.* 2013). Indeed, the variety of inhibitors yielding spontaneous resistance-conferring SNPs in a single membrane-spanning region of MmpL3 is astonishing (Goldman 2013) (Figure 3.1). The frequency of the MmpL3 resistance phenotype and the increased sensitivity to THPPs upon overexpression of *mmpL3* gives credence to the possibility of MmpL3 moonlighting as a drug importer.

In conclusion, we have shown that THPP compounds mediate bactericidal activity in a mouse infection model of TB and that these compounds act on the catalytically silent enoyl-CoA hydratase-like EchA6 protein. This surprising result of an alternative target deconvolution approach suggests that spontaneous resistance-conferring mutations can potentially obscure the actual or alternative targets of inhibitors emerging from phenotypic screening campaigns.

CHAPTER 5

Identification of novel inhibitors of *M. tuberculosis* drug targets by target-specific high throughput phenotypic screens

5.1 Introduction

HTSs are a recent innovation in the long history of antibiotic discovery, however the advent of such technology has rapidly accelerated the identification of novel compounds with antibiotic properties. It is now possible to test millions of compounds for antibiotic properties in weeks rather than years, thanks to the implementation of robotics and nanoliter technology. As a result many new molecules have been discovered by whole cell phenotypic screening campaigns and published due to their potent inhibitory activity and MoA. The first new TB drug to receive FDA approval since 1971 was first recognised as a potential anti-TB compound in a whole cell phenotypic HTS campaign. Bedaquiline (Sirturo^{TM}, formerly TMC207), from the compound family diarylquinolines (DARQs) has been identified as an inhibitor of both drug sensitive and drug resistant *M. tb* (Andries *et al.* 2005; Matteelli *et al.* 2010). Despite the novelty of phenotypic 'hits', the majority of compounds are unlikely to make it to clinical trials due to the undesirable nature of their molecular structure, their promiscuous MoA and/or their frequent appearance in screening campaigns. These molecules, now considered artefacts of HTS, have recently received the designation of PAINS (pan-assay interference compounds) and new filters are being employed to prevent time and money being invested on molecules of this classification (Baell *et al.* 2014). A pre-requisite to the medicinal chemistry required to improve the drug-like properties of a 'hit' molecule is identification of the MoA of that compound. Here we have circumvented this lengthy process by conducting a number of target specific HTSs against a set of 10,000 known inhibitors of *M. tb*, using the model organism *M. bovis* BCG overexpressing different proteins of interest. These range from proteins involved in cell wall biogenesis and specific

metabolite-synthesising enzymes, to rate-limiting steps in nucleotide biosynthesis. All hits identified in single shot have been progressed to dose response in duplicate assays for further validation, and a PAINS filter has been applied. A brief introduction to each target is provided in the following sections.

5.1.1 GuaB2

The inosine monophosphate dehydrogenase (IMPDH) GuaB2 has already been identified as a drugable target in *M. tb*, however previously identified compounds lack the desired characteristics necessary for further development of a compound into a clinically relevant antibiotic. Inosine monophosphate (IMP) is a metabolic precursor in the biosynthesis of the purine nucleotides adenine and guanine. Guanosine monophosphate (GMP) requires the synthesis of xanthosine monophosphate (XMP) from IMP by the inosine monophosphate dehydrogenases (IMPDH), of which there are three in *M. tb* GuaB1 (Rv1843c), GuaB2 (Rv3411c) and GuaB3 (Rv3410c) (Jackson *et al.* 1975; Cole *et al.* 1998). The rate limiting two-step catalysis of IMP to XMP conversion by IMPDH requires nicotinamide adenine dinucleotide (NAD^+) as a cofactor, which is first reduced to NADH by a dehydrogenation reaction, forming an intermediate covalent bond between IMPDH and XMP, followed by a hydrolysis reaction that breaks the covalent attachment and releases XMP (Hedstrom 2009). GuaB2 is the only catalytically active and essential IMPDH shown by transposon site hybridisation (TraSH) to be required for viability of *M. tb* (Usha *et al.* 2011; Sassetti *et al.* 2001, 2003). Inhibition of GuaB2, results in depletion in guanine nucleotides for DNA and RNA synthesis (Shu *et al.* 2008; Pimkin *et al.* 2009). Biochemical characterisation of GuaB2 has been previously conducted and a series of three potent

diphenyl-urea based inhibitors of *M. tb* and *M. smegmatis* have been shown to inhibit *M. tb* GuaB2. An overexpresser based MIC shift analysis was conducted to validate the target in *M. smegmatis* and a 16-fold increase in MIC (0.5 – 8 μg.ml^{-1}) was observed (Usha *et al.* 2011). There are three distinct classes of IMPDH inhibitors: Type I inhibitors are IMP or XMP analogues, Type II inhibitors are NAD^+/NADH analogues, whereas Type III are muti-substrate inhibitors (Gilbert *et al.* 1979). The aforementioned diphenyl-urea compounds are designated as Type III, along with a series of compounds identified in a screen of commercially available molecules which target mycobacterial GuaB2. In this instance, the lead molecule, 7759844, demonstrated high potency with an inhibitory constant (K_i) of 0.603 μM and MIC of 0.633 μg.ml-1, however displayed toxicity in a chronic mouse model (Usha *et al.* 2012).

5.1.2 MurC

ATP-dependent Mur ligases are essential for the biosynthesis of the key cell wall component PG. They couple the hydrolysis of ATP to ADP and inorganic phosphate (Pi) to the ligation of critical amino acid residues to the stem peptide, produced by the non-ATP dependent Mur ligases. Firstly, the non-ATP dependent Mur ligase MurA (Rv1315), an enoylpyruvyl transferase, catalyses the addition of phosphor-enol-pyruvate to UDP-GlcNAc, producing a UDP-enoylpyruvyl-GlcNAc, of which the enoylpyruvate moiety is converted to a lactoyl ether moiety by the NADPH dependent MurB (Rv0482), resulting in UDP-MurNAc (Kim *et al.* 1996; Benson *et al.* 1996). UDP-MurNAc is then hydroxylated by NamH (Rv3808) to produce a second UDP-Muramyl substrate, UDP-MurNGlyc (Raymond *et al.* 2005). It is at this

point the ATP dependent Mur ligases begin the addition of amino acid residues to the UDP-Muramyl substrates, beginning with the essential MurC (Rv2151c), producing UDP-*N*-acetylmuramoyl:L-alanine. MurD (Rv2155c) then ligates D-isoglutamate, MurE (Rv2158c) adds *m*-DAP and finally a terminal D-alaninyl-D-alanine is added by MurF (Rv2157c). This results in a muramyl-pentapeptide UDP-MurNAc/Glyc-L-ala-D-isoglu-*m*-DAP-D-ala-D-ala that forms the precursor of mature PG (Kurosu *et al.* 2007). Only *M. tb* MurC and MurE have biochemical assays developed (Mahapatra *et al.* 2000; Basavannacharya *et al.* 2010).

5.1.3 Antigen 85A

The antigen 85 complex is composed of three fibronectin-binding proteins, antigen 85A (FbpA, Rv3804c), antigen 85B (FbpB, Rv1886c) and antigen 85C (FbpC2, Rv0129c) which function as mycolyltransferases, catalysing the transfer of mycolates to form the major cell wall components TMM and TDM (Belisle *et al.* 1997). These three proteins are the most abundantly secreted proteins by mycobacteria, contributing as much as 41% to culture supernatant proteins (Fukui *et al.* 1965). FbpA has been shown to play a central role in infection as its disruption prevents replicative infection of human and mouse macrophages (Armitage *et al.* 2000). The crystal structures of FbpB and FbpC2 have led to the identification of the catalytic residues (Ser124, Glu228 and His260), however the structure of FbpA has yet to be elucidated (Ronning *et al.* 2000). A protein similar to those forming the antigen 85 complex, FbpC1, has been found to lack mycolyltransferase activity, and therefore cannot be considered part of the complex (Kremer *et al.* 2002). FbpA has been shown to have substrate selectivity for the mycolation of TMM to form TDM, whereas the other two

orthologues favor the addition of mycolate to free trehalose, producing TMM (Backus *et al.* 2014). This thesis has reviewed the wide variety of anti-TB compounds that target cell wall biosynthesis, and therefore this essential protein involved in end-stage mycolic acid processing shows considerable potential as a future drug target, hence its use in this HTS (Griffin *et al.* 2011). Previously identified inhibitors of the antigen 85 complex have poor MICs; 6-azido-trehalose and ebselen have MICs of 200 and 20 $\mu g.ml^{-1}$, respectively (Belisle *et al.* 1997; Favrot *et al.* 2013).

5.1.4 DHFR (DfrA)

M. tb dihydrofolate reductase (DHFR, DfrA or Rv2763c) is an essential protein that catalyses the reduction of dihydrofolate (DHF) to tetrahydrofolate (THF), a fundamental precursor to the synthesis of thymidylate, purine bases and several amino acids (Figure 5.1) (Dias *et al.* 2014).

The reductive activity of DHFR is dependent on an NADPH co-factor. Inhibition of DHFR leads to cessation of DNA production and cell death, and as a result, it has been extensively explored as a drug target for anti-fungal (Trimetrexate), anti-protozoal (WR99210), anti-cancer (Methotrexate) and anti-bacterial agents (Trimethoprim). The crystal structure of *M. tb* DHFR has been solved (Li *et al.* 2000), and has paved the way for computational drug discovery efforts with DHFR. Recently two *M. tb* inhibitors belonging to the tetrahydro-1,3,5-triazin-2-amine (THT) family were identified from a set of 776 known *M. tb* inhibitors (MIC > 10 μM) to target DHFR by *in silico* drug discovery.

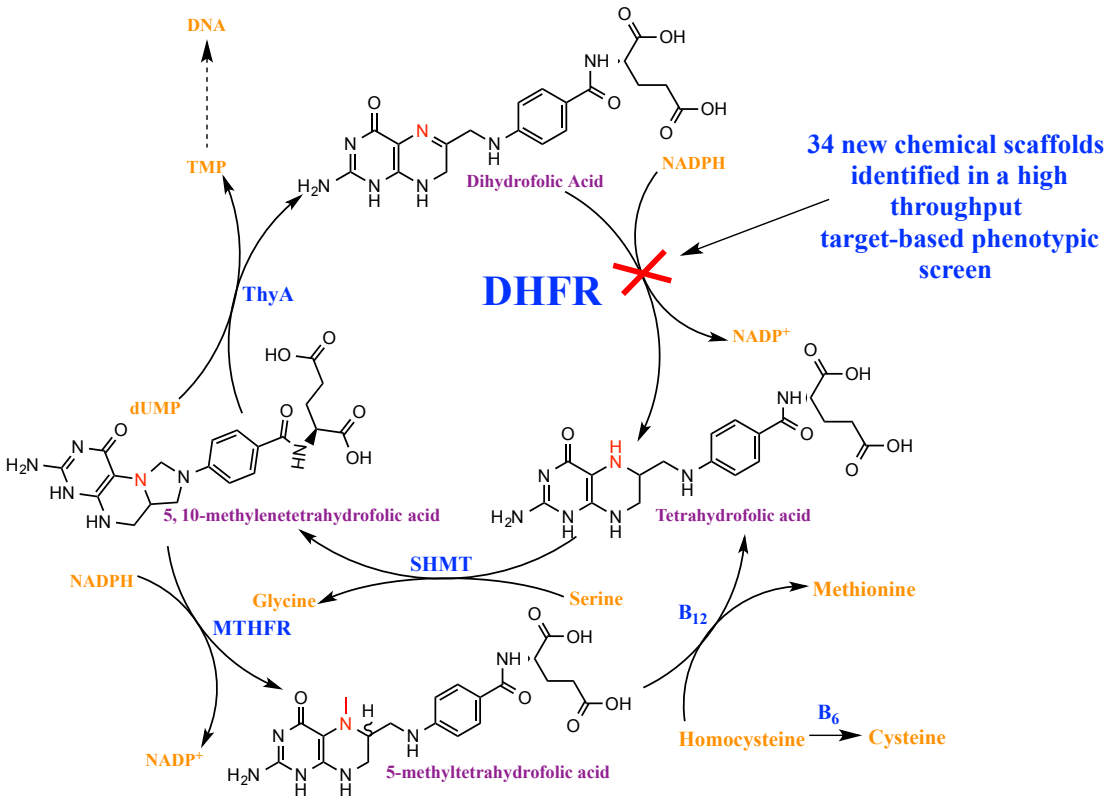
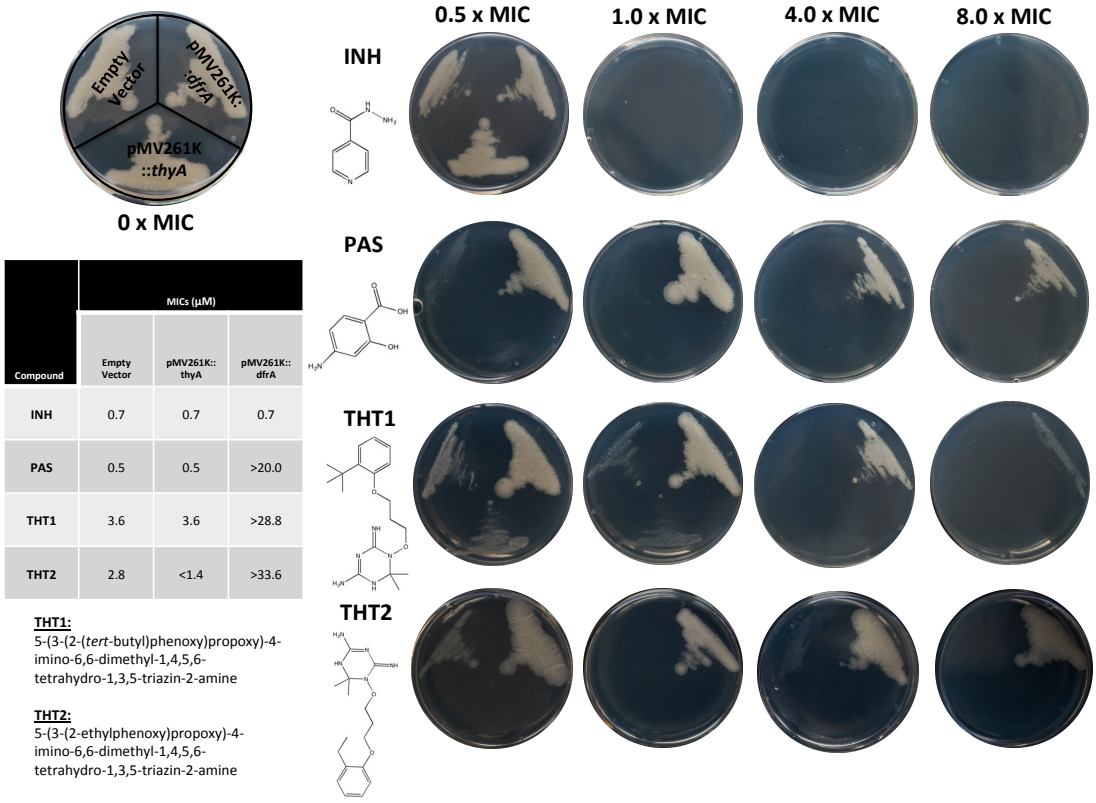


Figure 5.1: The folate pathway around dihydrofolate reductase (DHFR) that reduces dihydrofolate (DHF) to tetrahydrofolate (THF), a precursor to the pyrimidine nucleotide threonine monophosphate (TMP). (Figure adapted from Mugumbate *et al.* 2015).

We subsequently validated the MoA of these compounds using the same DHFR overexpressing strain as was used to conduct this HTS. This phenotypic validation was achieved by plating the DHFR overexpresser on solid media containing a dose response of each THT compound, along side a dose response of INH and *para*-amino salicylic acid (PAS) as respective negative and positive controls for phenotypic resistance of the overexpresser. In this instance, we observed THT resistance at > 28.8 µM for THT1 and > 33.6 µM for THT2 with the DHFR overexpresser, compared with 3.6 µM and 2.8 µM for the empty vector strain, respectively (Figure 5.2) (Mugumbate *et al.* 2015). This serves as a proof of concept for DHFR inhibitor identification by virtue of this overexpresser strain.



Compound	MICs (µM)		
	Empty Vector	pMV261K::thyA	pMV261K::dfrA
INH	0.7	0.7	0.7
PAS	0.5	0.5	>20.0
THT1	3.6	3.6	>28.8
THT2	2.8	<1.4	>33.6

THT1:
5-(3-(2-(*tert*-butyl)phenoxy)propoxy)-4-imino-6,6-dimethyl-1,4,5,6-tetrahydro-1,3,5-triazin-2-amine

THT2:
5-(3-(2-ethylphenoxy)propoxy)-4-imino-6,6-dimethyl-1,4,5,6-tetrahydro-1,3,5-triazin-2-amine

Figure 5.2: Phenotypic validation of the MoA of the THT compounds as inhibitors of *M. tb* DHFR, following their identification by *in silico* drug discovery. Impact on the MIC of THT1 and THT2 upon the overexpression of ThyA and DHFR with INH and *para*-aminosalicylic acid (PAS) as negative and positive controls. The MICs of THT1 and THT2 were determined in *M. bovis* BCG containing pMV261, pMV261-*thyA* and pMV261-*dfrA*. Plates are shown at 0.5, 1.0, 4.0 and 8.0 x MIC of each compound (with respect to the empty vector), the structures of which are given along with the IUPAC nomenclature for THT1 and THT2 and tabulated MIC data. (Figure and legend adapted from Mugumbate *et al.* 2015).

Despite this progress, there remain no TB drugs under current clinical use that exploits this mechanism of inhibition. This may in part be due to the conservation of DHFR across taxonomic phyla (including animals), necessitating high specificity for mycobacterial DHFR for TB drug development.

5.1.5 DapF

PG is one of the fundamental building blocks of the key virulence factor of *M. tb,* the mycobacterial cell wall. PG is composed of linear glycan chains that are cross-linked by pentapeptide linkers (Nanninga 1998; Heijenoort 2001). Mycobacteria produce two different types of pentapeptide cross-linkages, D-Ala to diaminopimelic acid (L,L-DAP or D,L-(*meso*)-DAP) and *meso*-DAP to *meso*-DAP linkages depending on growth phase, the former produced during exponential growth phase and the latter in stationary phase (Wietzerbin *et al.* 1974). The *meso*-DAP to *meso*-DAP linkages are thought to contribute to the resistance to β–lactams observed in mycobacteria (Goffin *et al.* 2002). The essential enzyme diaminopimelic acid epimerase (DapF or Rv2726c) catalyses the reversible conversion of L,L-DAP to *meso*-DAP (Sassetti *et al.* 2001, 2003), and this mechanism of interconversion has been identified to be the result of two conserved cysteine residues at positions 73 and 216, which deprotonate and reprotonate the α-carbon (Figure 5.3) (Pillai *et al.* 2006). A biochemical assay for DapF has been developed and the crystal structure of ligand-free mycobacterial DapF has been determined (Usha *et al.* 2006, 2008, 2009).

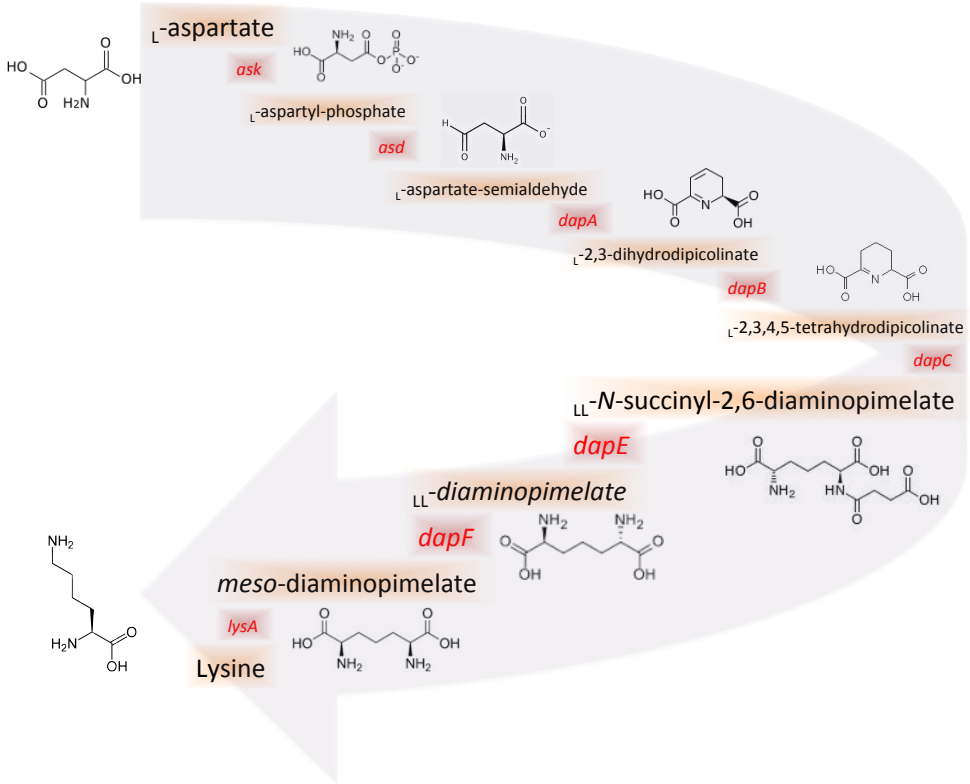


Figure 5.3: Lysine/*meso*-diaminopimelate (mDAP) synthesis pathway from L-aspartate incorporating the DapA-F enzymes. This diagram highlights the roles of two essential steps in lysine biosynthesis.

5.1.6 DapE

Similarly to DapF (5.1.5), DapE (Rv1202) is also involved in the synthesis of *meso*-diaminopimelate (mDAP) for cross-linking peptidoglycan in the cell wall and also lysine for peptide synthesis. DapE functions as a *N*-succinyl-L,L-diaminopimelic acid desuccinylase, catalysing the hydrolysis of L,L-*N*-succinyl-2,6-diaminopimelate to form L,L-diaminopimelate and succinate, with strict specificity for the L,L-isomer of the substrate and is essential for *M. tb* viability and growth (Figure 5.3) (David *et al.* 2006; Sassetti *et al.* 2001, 2003). DapE is metal dependent, requiring two divalent metal ions for each mole of protein and can be activated with Zn^{2+}, Co^{2+}, Cd^{2+} or

Mn^{2+}, however DapE exhibits the highest affinity for Zn^{2+} (Born *et al.* 1998; Bienvenue *et al.* 2003). The crystal structure of DapE from *H. influenzae* has been solved with two Zn^{2+} ions *in situ*, giving clear detail of the catalytic mechanism of this enzyme (Nocek *et al.* 2010). A number of inhibitors have been found to interfere with the divalent metal ions, including 5-mercaptopentanoic acid (MSPA), where inhibition is the result of an interaction with the thiol group and at least one of the Zn^{2+} ions (Cosper *et al.* 2003). Subsequently a screen involving zinc-binding group containing compounds (namely, thiols, carboxylic acids, boronic acids, phosphonates and hydroxamates) identified several competitive inhibitors of DapE, the most potent of which, L-captopril, exhibited a K_i of 1.8 μM (Gillner *et al.* 2009). The structure-function relationship of each of the Dap enzymes has been reviewed in the context of their relative drug target characteristics, which gives the conclusion that the mDAP biosynthetic pathway is a favorable target for anti-TB drug development (Usha *et al.* 2012).

5.1.7 KasA

The outer most fundamental layer of the mycobacterial cell wall is the mycolic acid layer, composed of mycolates that are covalently bound to the arabinosyl motif of arabinogalactan, and free mycolates in the form of TMM and TDM. Mycolic acids are α-alkyl, β-hydroxy fatty acids ranging from 70 to 90 carbons. Due to the length of these fatty acids, their biosynthesis beyond 20-26 carbons long, takes place *via* FAS-II, a series of enzymes that elongate the acyl-chain by successive rounds of reduction, dehydration, reduction and condensation until the required acyl-chain length is reached (54-64 carbons). KasA (Rv2245), in complex with KasB form the β-ketoacyl-

ACP synthases, catalysing the elongation by condensation of the growing acyl chain with malonyl-AcpM, producing β-ketoacyl-AcpM. The role of KasA in mycolic acid biosynthesis has already been discussed in detail in Chapter 4.1 of this thesis (Figure 4.3). KasA has been demonstrated to be essential for the survival of *M. tb*, and inhibition of β-ketoacyl-ACP synthase activity in *M. tb* by TLM and its analogues have been observed and characterised (Sassetti *et al.* 2003; Griffin *et al.* 2011; Kremer *et al.* 2000).

5.1.8 HadAB

Mycolic acid synthesis in *M. tb* FAS-II is dependent upon sequential reduction, dehydration, reduction and condensation of the elongating fatty acid chain. Dehydration of the acylated-AcpM is catalysed by the HadB moiety of the HadAB (Rv0635-6) and HadBC complexes, which function as 3-hydroxyacyl dehydratases (Had) in FAS-II along side InhA, KasA/B and MabA (Chapter 4.1 of this thesis), (Figure 4.3) (Sacco *et al.* 2007). HadAB/BC has been proposed as the target of isoxyl (thiocarlide,4,4'-diisoamythio-carbanilide) and thiacetazone (TAC). Isoxyl and TAC are pro-drugs, activated by EthA, a monooxygenase that has been shown to activate other thiocarbamide containing compounds, such as ETH (Dover *et al.* 2007) (Table 1.1). Following evidence that a concentration range of isoxyl led to a dose-dependent reduction in mycolic acid methyl esters (MAMEs), a full operon *hadABC* overexpresser was generated and demonstrated resistance to 5-10x MIC against the empty vector control strain, confirming HadAB/BC as the target (Gannoun-Zaki *et al.* 2012). Subsequently, HadA was specifically identified as the target of isoxyl and TAC, which were shown to inhibit by formation of a disulfide bond between their

sulfhydryl groups and cysteine 61 of HadA, thus specifically inhibiting the HadAB heterodimer (Grzegorzewicz *et al.* 2015).

5.1.9 MabA

Mycobacterial MabA (FabG1 or Rv1483) functions as the β-ketoacyl-ACP reductase in FAS-II, catalysing the NADP dependent conversion of β-ketoacyl-AcpM to β-hydroxyacyl-AcpM (Chapter 4.1), (Figure 4.3). MabA has been demonstrated to be essential for *M. tb in vitro* growth and for survival in murine macrophages (Griffin *et al.* 2011), (Parish *et al.* 2007). MabA was previously thought to be the secondary target for isoniazid (INH) due to the apparent resistant mutations identified in clinical isolates that located to the ribosomal binding site of the *mabA* gene (Musser 1995; Musser 1996). It was later determined that *mabA* and *inhA* genes exist on a single operon in *M. tb*, and that the mutations previously observed in the *mabA* ribosomal binding site resulted in increased InhA expression (Mdluli *et al.* 1996). In addition, overexpression of *M. tb* MabA did not result in an INH resistant phenotype as observed with InhA (Banerjee *et al.* 1998). The crystal structure of MabA has been solved, providing a potential starting point for fragment-based drug design, however to date no inhibitors of mycobacterial MabA have been published (Cohen-Gonsaud *et al.* 2002).

The above discussed targets were cloned into pMV261 and electroporated into *M. bovis* BCG. These strains were screened against the GSK library of 10,000 compounds (TB box) using the HTS facility at GSK Tres Cantos, Madrid. A plate reader was used to observe viability of BacTiter-Glo™ (Microbial Cell Viability

Assay, Promega) treated cells. Initial hits from the single shot experiment were subsequently validated in a dose response experiment, performed in duplicate. These validated hits provide a platform for further development and elucidation by biochemical and biophysical methods.

5.2 Materials and methods

5.2.1 Strains, transformation and culture

All experiments were performed in *M. bovis* BCG which has been transformed by a standard electroporation protocol (Parish *et al.* 1998) with pMV261k, a kanamycin-resistant mycobacterial overexpresser plasmid, which had been modified by addition of genes expressing each of the overexpresser targets; MurC, GuaB2, FbpA, DfrA, DapF, DapE, KasA, HadAB and MabA (Besra Lab strain database). An empty vector strain (pMV261(k) only) was also prepared. Transformants were selected on Middlebrook 7H11 mycobacterial media (Difco) supplemented with 10% (v/v) OADC (oleic acid ($1.25x10^{-2}$ % v/v), albumin (1.25 % w/v), dextrose (0.5 % w/v) and catalase ($1x10^{-3}$ % w/v) (Sigma-Aldrich)), containing kanamycin at 25 $\mu g.ml^{-1}$. Successful transformants were transferred into Middlebrook 7H9 liquid media (Difco) containing kanamycin at 25 $\mu g.ml^{-1}$, 0.05 % (v/v) Tween-80, 0.25 % (v/v) glycerol and supplemented with 10 % (v/v) ADC (albumin (1.25 % w/v), dextrose (0.5 % w/v) and catalase ($7.5 x10^{-4}$ % w/v) (Sigma-Aldrich)). Growth rate was monitored by measuring optical density (OD) at 600nm and cells were passaged to maintain a mid-log OD_{600} of 0.4-0.8. To prevent mutagenesis, no more than 4 passages were conducted before cultures were reinitiated from a glycerol stock.

5.2.2 High throughput screening of overexpresser strains in single shot

The initial HTS was conducted in single shot, with 1536 well plates (32 rows x 48 columns) prepared with compounds at 1 and 0.1 mM (50 nl total compound volume). A liquid dispensing robot [Multidrop^{TM} Combi (Thermo Scientific)] was used to dispense 5 µl of a diluted mid-log culture (diluted to OD_{600} 0.125 corresponding to $1x10^7$ cfu.ml^{-1}) into each well, so compounds were tested at 1uM and 10uM final assay concentration. A negative (DMSO only) control (control 1, column 11 and 12) and INH treated positive control (control 2, column 35 and 36) were also prepared on each plate. Plates were hermetically wrapped in aluminum foil with dummy plates at the top and bottom of each stack and incubated for 7 days at 37ºC in 5% CO_2 with humidity. Following incubation, 5 µl of reconstituted BacTiter-Glo™ was added to each well and the luminescence was measured using a Viewlux Reader (Perkin Elmer). The BacTiter-Glo™ assay causes cell lysis and allows the fluorimetric quantification of the amount of ATP present in the reaction mix by an ATP-dependent thermostable luciferase luminescent signal, which is directly proportional to the number of viable cells in the culture. This method was favored over conventional Resazurin treatment as there is a lesser propensity for false positives. The effect of a given inhibitor was calculated as:

$$\% \text{ inhibition} = 100 \times \frac{(\text{data} - \text{control 1})}{(\text{control 2} - \text{control 1})}$$

(control 1 = maximum activity (DMSO only; uninhibited growth), and control 2 = bacterial growth completely inhibited (by treatment with 10 µM isoniazid)

Assay performance statistics (signal to background ratio and Z′) were calculated using templates in ActivityBase XE (ID Bussines Solutions Ltd, Surrey, UK).

[The 256 compounds with the higher shift (calculated as % inhibition in the empty vector strain - % inhibition in the overexpresser strain) from each strain tested were selected to be tested in dose response.]

5.2.3 Dose response validation of hits

Hits identified in the single shot HTS were investigated further by conducting a dose response experiment following the same 1536 well format and experimental conditions as in section 5.2.2 of this thesis. The only difference in method is that hit compounds were plated in serial dilution of 11 steps from 10 mM to 0.17 nM using a 1/3 dilution factor all in a 50 nl total volume. The controls as described above were repeated for each plate and data was obtained in duplicate.

5.2.4 Data analysis

The percentage inhibition for each compound concentration tested were calculated as described in section 5.2.2. Dose response curves for each of the compounds were analysed using the ActivityBase XE template (ID Business Solutions Ltd, Surrey, UK). pIC_{50} values were obtained using the ActivityBase XE nonlinear regression function in the full curve analysis bundle.

5.3 Results

5.3.1 Z-factor

Z-factor (Z') is a statistical measure of success of a high throughput screen. It is calculated using four parameters: the means (μ) and standard deviations (σ) of the positive (p) and negative (n) controls in the following way:

$$Z' = 1 - \frac{3(\sigma p + \sigma n)}{(\mu p - \mu n)}$$

The Z' output can be interpreted as:

Z' = 1, the ideal value

Z' = < 1 > 0.5, an assay of high value

Z' = < 0.5 > 0, an assay of low value

Z' = < 0, an irrelevant assay

(Zhang *et al.* 1999)

The Z' values for each assay here described have been tabulated and are presented in table 5.1. From these data, it can be concluded that this HTS is of high value and therefore proves itself as a valid method of high throughput drug discovery.

Table 5.1: The Z' values for each overexpresser HTS

	Z' Value			
Target	Plate 1	Plate 2	Plate 3	Plate 4
KasA	0.75	0.79	0.75	0.79
KasA EV	0.7	0.78	0.81	0.8
DapE	0.76	0.65	0.72	0.61
DapE EV	0.67	0.59	0.74	0.68
DapF	0.76	0.78	0.78	0.68
DapF EV	0.61	0.51	0.39	0.65
FbpA	0.81	0.77	0.76	0.72
FbpA EV	0.6	0.64	0.6	0.6
HadAB	0.73	0.73	0.73	0.68
HadAB EV	0.57	0.64	0.61	0.54
MabA	0.71	0.73	0.75	0.36
MabA EV	0.71	0.67	0.66	0.68
DfrA	0.85	0.83	0.89	0.83
DfrA EV	0.76	0.69	0.56	0.72
GuaB2	0.74	0.75	0.75	0.74
GuaB2 EV	0.43	0.67	0.73	0.74
MurC	0.52	0.07	0.57	0.65
MurC EV	0.8	0.77	0.78	0.79

5.3.2 GuaB2

The results of dose response validated hits with a significant shift in resistance (measured in terms of shift in 50 % inhibitory concentration, shift IC_{50} and expressed in terms of pIC_{50} (= $-\log_{10}(IC_{50})$) upon GuaB2 overexpression are presented in Table 5.2. They equate to a total of 66 hit compounds, with mean shift pIC_{50} values ranging from 2.13 to 0.31. This indicates that 0.66 % of the 10,000 compounds screened target GuaB2.

Table 5.2: Results of GuaB2 overexpresser HTS

Compound ID	pIC_{50} Mean for Empty Vector	pIC_{50} Mean for GuaB2	Shift pIC_{50}	MIC (µM) H37Rv
GuaB2_1	6.64	4.51	2.13	
GuaB2_2	6.05	4	2.05	
GuaB2_3	5.7	4.04	1.66	> 80
GuaB2_4	5.48	4	1.48	> 80
GuaB2_5	6.14	4.71	1.43	
GuaB2_6	5.42	4	1.42	> 80
GuaB2_7	5.32	4	1.32	
GuaB2_8	5.1	4	1.1	
GuaB2_9	5.1	4	1.1	> 80
GuaB2_10	5.06	4	1.06	
GuaB2_11	5.05	4	1.05	> 80
GuaB2_12	5.23	4.19	1.04	
GuaB2_13	5.46	4.44	1.02	> 80
GuaB2_14	5.02	4	1.02	> 80
GuaB2_15	4.99	4	0.99	10
GuaB2_16	4.99	4	0.99	> 80
GuaB2_17	5.37	4.4	0.97	> 80
GuaB2_18	5.36	4.42	0.94	> 100
GuaB2_19	5.1	4.16	0.94	
GuaB2_20	5.34	4.43	0.91	> 80
GuaB2_21	4.9	4	0.9	
GuaB2_22	5.03	4.15	0.88	> 100
GuaB2_23	5.13	4.26	0.87	
GuaB2_24	5.2	4.34	0.86	
GuaB2_25	5.06	4.2	0.86	
GuaB2_26	4.85	4	0.85	
GuaB2_27	5.08	4.23	0.85	
GuaB2_28	5.08	4.24	0.84	> 80
GuaB2_29	4.84	4	0.84	
GuaB2_30	4.99	4.18	0.81	
GuaB2_31	5.49	4.69	0.8	> 80
GuaB2_32	4.89	4.1	0.79	
GuaB2_33	5.3	4.53	0.77	
GuaB2_34	4.87	4.12	0.75	
GuaB2_35	5.03	4.3	0.73	
GuaB2_36	4.7	4	0.7	
GuaB2_37	5.22	4.53	0.69	
GuaB2_38	5.08	4.41	0.67	
GuaB2_39	4.99	4.35	0.64	> 80
GuaB2_40	4.9	4.26	0.64	

GuaB2_41	5.21	4.58	0.63	
GuaB2_42	4.92	4.32	0.6	
GuaB2_43	5.17	4.57	0.6	
GuaB2_44	5	4.41	0.59	
GuaB2_45	4.87	4.3	0.57	
GuaB2_46	4.61	4.06	0.55	
GuaB2_47	4.95	4.4	0.55	> 80
GuaB2_48	4.54	4	0.54	
GuaB2_49	4.93	4.39	0.54	
GuaB2_50	4.97	4.46	0.51	
GuaB2_51	4.96	4.46	0.5	
GuaB2_52	4.87	4.37	0.5	
GuaB2_53	4.89	4.42	0.47	
GuaB2_54	4.73	4.27	0.46	
GuaB2_55	4.9	4.46	0.44	
GuaB2_56	4.94	4.5	0.44	
GuaB2_57	4.62	4.21	0.41	
GuaB2_58	4.8	4.4	0.4	
GuaB2_59	5	4.61	0.39	
GuaB2_60	4.62	4.23	0.39	> 80
GuaB2_61	4.65	4.28	0.37	
GuaB2_62	5.36	5.01	0.35	50
GuaB2_63	4.78	4.45	0.33	
GuaB2_64	4.78	4.45	0.33	
GuaB2_65	4.87	4.56	0.31	
GuaB2_66	4.68	4.37	0.31	

5.3.3 MurC

The results of dose response validated hits with a significant shift in resistance (measured in terms of shift in 50 % inhibitory concentration, shift IC_{50} and expressed in terms of pIC_{50} (= $-\log_{10}(IC_{50})$) upon MurC overexpression are presented in Table 5.3. They equate to a total of 80 hit compounds, with mean shift pIC_{50} values ranging from 2.47 to 0.32. This indicates that 0.8 % of the 10,000 compounds screened target MurC.

Table 5.3: Results of MurC overexpresser HTS

Compound ID	pIC_{50} Mean for MurC	pIC_{50} Mean for Empty Vector	Shift pIC_{50}	MIC (µM) H37Rv
MurC_1	4	6.47	2.47	11
MurC_2	4	6.34	2.34	
MurC_3	4	5.82	1.82	
MurC_4	4	5.73	1.73	0.012
MurC_5	4.14	5.81	1.67	
MurC_6	4	5.66	1.66	
MurC_7	4	5.61	1.61	
MurC_8	4	5.56	1.56	>80
MurC_9	4	5.54	1.54	
MurC_10	4.13	5.65	1.52	
MurC_11	4	5.48	1.48	
MurC_12	4	5.44	1.44	
MurC_13	4	5.36	1.36	0.45-1.9
MurC_14	4	5.32	1.32	1.25
MurC_15	5.4	6.68	1.28	
MurC_16	4.51	5.74	1.23	
MurC_17	4	5.17	1.17	
MurC_18	4	5.07	1.07	>80
MurC_19	4	5.06	1.06	
MurC_20	5.14	6.19	1.05	
MurC_21	4	5.01	1.01	8
MurC_22	4	5.01	1.01	
MurC_23	4	5	1	
MurC_24	4	5	1	
MurC_25	4	4.98	0.98	
MurC_26	4	4.98	0.98	
MurC_27	4.33	5.3	0.97	
MurC_28	4	4.96	0.96	
MurC_29	4	4.95	0.95	
MurC_30	4	4.93	0.93	
MurC_31	4	4.87	0.87	>80
MurC_32	4.43	5.28	0.85	
MurC_33	4.27	5.12	0.85	
MurC_34	4	4.81	0.81	
MurC_35	4.45	5.26	0.81	
MurC_36	4.73	5.54	0.81	
MurC_37	4.77	5.57	0.8	40
MurC_38	4	4.77	0.77	
MurC_39	4	4.77	0.77	
MurC_40	5.21	5.97	0.76	
MurC_41	4	4.73	0.73	

MurC_42	4.41	5.14	0.73	
MurC_43	5.36	6.07	0.71	10->80
MurC_44	4.16	4.87	0.71	27
MurC_45	4	4.71	0.71	>80
MurC_46	4	4.7	0.7	>80
MurC_47	4	4.68	0.68	
MurC_48	4.49	5.14	0.65	
MurC_49	4.24	4.89	0.65	
MurC_50	4	4.64	0.64	
MurC_51	4.54	5.18	0.64	
MurC_52	4	4.62	0.62	40
MurC_53	4	4.61	0.61	
MurC_54	4.9	5.49	0.59	
MurC_55	4	4.58	0.58	
MurC_56	4.38	4.96	0.58	
MurC_57	4	4.56	0.56	
MurC_58	4	4.55	0.55	
MurC_59	4.13	4.67	0.54	
MurC_60	4	4.54	0.54	>80
MurC_61	4.24	4.77	0.53	10-50
MurC_62	4.02	4.54	0.52	
MurC_63	5.45	5.97	0.52	
MurC_64	4.61	5.12	0.51	4
MurC_65	4.48	4.99	0.51	35
MurC_66	4.65	5.14	0.49	
MurC_67	4	4.48	0.48	
MurC_68	4	4.48	0.48	
MurC_69	4.58	5.06	0.48	5
MurC_70	5.28	5.76	0.48	>80
MurC_71	4.69	5.15	0.46	
MurC_72	4	4.43	0.43	>80
MurC_73	4.81	5.2	0.39	
MurC_74	5.34	5.73	0.39	
MurC_75	4.6	4.97	0.37	
MurC_76	4.89	5.24	0.35	
MurC_77	4.94	5.28	0.34	
MurC_78	4.65	4.99	0.34	
MurC_79	5.31	5.64	0.33	
MurC_80	4.47	4.79	0.32	>80

5.3.4 Antigen 85A (FbpA)

The results of dose response validated hits with a significant shift in resistance (measured in terms of shift in 50 % inhibitory concentration, shift IC_{50} and expressed in terms of pIC_{50} (= $-\log_{10}(IC_{50})$) upon FbpA overexpression are presented in Table 5.4. They equate to a total of 43 hit compounds, with mean shift pIC_{50} values ranging from 1.49 to 0.3. This indicates that 0.43 % of the 10,000 compounds screened target Antigen 85A.

Table 5.4: Results of FbpA overexpresser HTS

Compound ID	pIC_{50} Mean for Empty Vector	pIC_{50} Mean for FbpA	Shift pIC_{50}	MIC (µM) H37Rv
FbpA_1	5.49	4	1.49	
FbpA_2	5.47	4	1.47	
FbpA_3	5.42	4.21	1.21	
FbpA_4	5.31	4.23	1.08	
FbpA_5	5.05	4	1.05	
FbpA_6	5.01	4	1.01	20-80
FbpA_7	4.98	4	0.98	
FbpA_8	5.11	4.14	0.97	
FbpA_9	4.92	4	0.92	>80
FbpA_10	4.88	4	0.88	
FbpA_11	5.1	4.27	0.83	
FbpA_12	5.06	4.3	0.76	
FbpA_13	4.75	4	0.75	
FbpA_14	5.01	4.34	0.67	
FbpA_15	5.57	4.93	0.64	
FbpA_16	4.9	4.27	0.63	
FbpA_17	4.76	4.15	0.61	
FbpA_18	4.77	4.17	0.6	
FbpA_19	4.84	4.26	0.58	35
FbpA_20	5.02	4.45	0.57	
FbpA_21	4.81	4.25	0.56	
FbpA_22	5.13	4.62	0.51	
FbpA_23	4.67	4.18	0.49	
FbpA_24	4.82	4.34	0.48	
FbpA_25	4.88	4.4	0.48	

FbpA_26	4.65	4.17	0.48	
FbpA_27	5.05	4.61	0.44	>80
FbpA_28	4.95	4.52	0.43	
FbpA_29	5.22	4.79	0.43	
FbpA_30	5.04	4.61	0.43	
FbpA_31	5.1	4.68	0.42	
FbpA_32	4.62	4.21	0.41	
FbpA_33	4.89	4.48	0.41	
FbpA_34	4.65	4.26	0.39	
FbpA_35	4.69	4.31	0.38	
FbpA_36	5.34	4.96	0.38	
FbpA_37	4.97	4.61	0.36	>80
FbpA_38	4.47	4.11	0.36	
FbpA_39	4.72	4.38	0.34	
FbpA_40	4.59	4.25	0.34	
FbpA_41	4.96	4.64	0.32	
FbpA_42	5.11	4.81	0.3	60
FbpA_43	4.9	4.6	0.3	

5.3.5 DHFR (DfrA)

The results of dose response validated hits with a significant shift in resistance (measured in terms of shift in 50 % inhibitory concentration, shift IC_{50} and expressed in terms of pIC_{50} (= $-\log_{10}(IC_{50})$) upon DfrA overexpression are presented in Table 5.5. They equate to a total of 34 hit compounds, with mean shift pIC_{50} values ranging from 2.06 to 0.32. This indicates that 0.34 % of the 10,000 compounds screened target DHFR.

Table 5.5: Results of DfrA overexpresser HTS

Compound ID	pIC_{50} Mean for Empty Vector	pIC_{50} Mean for DfrA	Shift pIC_{50}	MIC (µM) H37Rv
DfrA_1	6.06	4	2.06	
DfrA_2	6.51	5.28	1.23	>80
DfrA_3	5.44	4.22	1.22	
DfrA_4	5.2	4	1.2	
DfrA_5	5.88	4.72	1.16	
DfrA_6	4.81	4	0.81	
DfrA_7	6.13	5.34	0.79	> 100
DfrA_8	4.91	4.15	0.76	
DfrA_9	5.92	5.22	0.7	100
DfrA_10	4.85	4.21	0.64	50->80
DfrA_11	5.48	4.88	0.6	100
DfrA_12	5.03	4.43	0.6	
DfrA_13	5.44	4.85	0.59	> 80
DfrA_14	4.59	4	0.59	
DfrA_15	5.76	5.19	0.57	40
DfrA_16	4.52	4	0.52	
DfrA_17	4.64	4.15	0.49	
DfrA_18	5.99	5.51	0.48	
DfrA_19	4.62	4.14	0.48	
DfrA_20	5.31	4.84	0.47	80
DfrA_21	4.67	4.21	0.46	
DfrA_22	4.69	4.24	0.45	>80
DfrA_23	5.39	4.95	0.44	100
DfrA_24	5.09	4.66	0.43	80
DfrA_25	5.18	4.75	0.43	
DfrA_26	5.14	4.73	0.41	>80
DfrA_27	4.47	4.07	0.4	
DfrA_28	4.78	4.4	0.38	
DfrA_29	4.64	4.26	0.38	
DfrA_30	4.66	4.29	0.37	
DfrA_31	4.67	4.31	0.36	
DfrA_32	5.08	4.72	0.36	
DfrA_33	5.2	4.88	0.32	
DfrA_34	5.17	4.85	0.32	

5.3.6 DapF

The results of dose response validated hits with a significant shift in resistance (measured in terms of shift in 50 % inhibitory concentration, shift IC_{50} and expressed in terms of pIC_{50} (= $-\log_{10}(IC_{50})$) upon DapF overexpression are presented in Table 5.6. They equate to a total of 18 hit compounds, with mean shift pIC_{50} values ranging from 1.43 to 0.31. This indicates that 0.18 % of the 10,000 compounds screened target DapF.

Table 5.6: Results of DapF overexpresser HTS

Compound ID	pIC_{50} Mean for Empty Vector	pIC_{50} Mean for DapF	Shift pIC_{50}	MIC (µM) H37Rv
DapF_1	6.07	4.64	1.43	80
DapF_2	5.07	4	1.07	
DapF_3	5.37	4.47	0.9	
DapF_4	5.32	4.59	0.73	> 10
DapF_5	5.21	4.48	0.73	
DapF_6	4.6	4	0.6	
DapF_7	6.33	5.78	0.55	
DapF_8	5.43	4.88	0.55	
DapF_9	5.53	5.01	0.52	
DapF_10	5.47	4.95	0.52	
DapF_11	5.11	4.67	0.44	
DapF_12	5.03	4.6	0.43	
DapF_13	4.6	4.17	0.43	> 50
DapF_14	4.44	4.05	0.39	>80
DapF_15	5.24	4.85	0.39	
DapF_16	4.71	4.34	0.37	
DapF_17	5.45	5.1	0.35	
DapF_18	4.56	4.25	0.31	

5.3.7 DapE

The results of dose response validated hits with a significant shift in resistance (measured in terms of shift in 50 % inhibitory concentration, shift IC_{50} and expressed in terms of pIC_{50} (= $-\log_{10}(IC_{50})$) upon DapE overexpression are presented in Table 5.7. They equate to a total of 16 hit compounds, with mean shift pIC_{50} values ranging from 1.6 to 0.32. This indicates that 0.16 % of the 10,000 compounds screened target DapE.

Table 5.7: Results of DapE overexpresser HTS

Compound ID	pIC_{50} Mean for Empty Vector	pIC_{50} Mean for DapE	Shift pIC_{50}	MIC (µM) H37Rv
DapE_1	5.68	4.08	1.6	
DapE_2	4.92	4	0.92	
DapE_3	6.67	5.82	0.85	
DapE_4	5.21	4.56	0.65	
DapE_5	4.81	4.18	0.63	
DapE_6	6.06	5.49	0.57	>80
DapE_7	4.61	4.07	0.54	
DapE_8	4.61	4.1	0.51	125
DapE_9	5.52	5.05	0.47	
DapE_10	5.65	5.2	0.45	140
DapE_11	5.15	4.7	0.45	
DapE_12	5.97	5.54	0.43	>80
DapE_13	5.4	4.98	0.42	
DapE_14	5.52	5.1	0.42	>80
DapE_15	5.25	4.88	0.37	>80
DapE_16	5.96	5.64	0.32	

5.3.8 KasA

The results of dose response validated hits with a significant shift in resistance (measured in terms of shift in 50 % inhibitory concentration, shift IC_{50} and expressed in terms of pIC_{50} (= $-\log_{10}(IC_{50})$) upon KasA overexpression are presented in Table 5.8. They equate to a total of 13 hit compounds, with mean shift pIC_{50} values ranging from 1.87 to 0.41. This indicates that 0.13 % of the 10,000 compounds screened target KasA.

Table 5.8: Results of KasA overexpresser HTS

Compound ID	pIC_{50} Mean for Empty Vector	pIC_{50} Mean for KasA	Shift pIC_{50}	MIC (µM) H37Rv
KasA_1	5.87	4	1.87	
KasA_2	5.1	4	1.1	
KasA_3	5.18	4.13	1.05	
KasA_4	4.52	3.5	1.02	
KasA_5	4.89	3.9	0.99	
KasA_6	4.98	4	0.98	
KasA_7	4.94	4	0.94	
KasA_8	5.28	4.39	0.89	
KasA_9	4.8	4	0.8	
KasA_10	5.02	4.34	0.68	
KasA_11	5	4.44	0.56	
KasA_12	4.65	4.11	0.54	
KasA_13	4.86	4.45	0.41	

5.3.9 HadAB

The results of dose response validated hits with a significant shift in resistance (measured in terms of shift in 50 % inhibitory concentration, shift IC_{50} and expressed in terms of pIC_{50} (= $-\log_{10}(IC_{50})$) upon HadAB overexpression are presented in Table 5.9. They equate to a total of 12 hit compounds, with mean shift pIC_{50} values ranging from 1.07 to 0.3. This indicates that 0.12 % of the 10,000 compounds screened target HadAB.

Table 5.9: Results of HadAB overexpresser HTS

Compound ID	pIC_{50} Mean for HadAB	pIC_{50} Mean for Empty Vector	pIC_{50} Shift EV-HadAB	MIC (µM) H37Rv
HadAB_1	4	5.07	1.07	
HadAB_2	5.09	5.69	0.6	
HadAB_3	4.92	5.32	0.4	
HadAB_4	4.85	5.25	0.4	
HadAB_5	5.14	5.53	0.39	
HadAB_6	5.1	5.48	0.38	
HadAB_7	4.34	4.67	0.33	> 10
HadAB_8	5.55	5.88	0.33	>80
HadAB_9	5.6	5.93	0.33	40
HadAB_10	4.36	4.68	0.32	
HadAB_11	4.56	4.86	0.3	
HadAB_12	4.54	4.84	0.3	

5.3.10 MabA

The results of dose response validated hits with a significant shift in resistance (measured in terms of shift in 50 % inhibitory concentration, shift IC_{50} and expressed in terms of pIC_{50} (= $-\log_{10}(IC_{50})$) upon MabA overexpression are presented in Table 5.10. They equate to a total of 2 hit compounds, with mean shift pIC_{50} values of 0.52 and 0.39. This indicates that 0.02 % of the 10,000 compounds screened target MabA.

Table 5.10: Results of MabA overexpresser HTS

Compound ID	pIC_{50} Mean for Empty Vector	pIC_{50} Mean for MabA	Shift pIC_{50}	MIC (µM) H37Rv
MabA_1	4.52	4	0.52	>80
MabA_2	4.68	4.29	0.39	

5.4 Discussion

The engineering of nine strains of *M. bovis* BCG which express ≥ 5 times the normal wildtype levels of known drug targets or proteins for which functional activity has been deemed essential for viability, has facilitated the screening of 10,000 known inhibitors of *M. tb.* The targets and essential proteins tested here have been selected to be overexpressed because they have promise as a potential MoA for new anti-TB drugs. Some of the proteins form essential enzymatic stepping-stones in the biosynthesis of fundamental building blocks of the mycobacterial cell wall, thereby playing an integral role in the virulence and viability of *M. tb.* Mycolic acid biosynthesis has been well characterised as an Achilles heel of *M. tb* with the

activated moiety of the most successful TB drug, INH, shown to target InhA of FAS-II biosynthesis. We have therefore conducted this HTS with KasA, HadAB, MabA and Antigen 85A (FbpA) due to their similarly fundamental role in the biosynthesis of mycolic acids. We have similarly screened overexpressers of essential proteins in PG biosynthesis, namely DapE, DapF and MurC. The already widely recognised, but to date unyielding drug target DHFR (DfrA) has also been included in this HTS, along with the drug target GuaB2. In both of these cases, clinically relevant molecules for use as antimicrobials have yet to be identified with these proteins as targets.

The HTS was conducted in two phases, the first involved a single shot screen of each overexpresser and the empty vector control strain against 10,000 compounds at 1 and 0.1 mM in order to identify a resitant phenotype with the overexpresser strain. Subsequent hits were validated in duplicate by a dose response screen in order to obtain accurate information regarding the change in 50% inhibitory concentration (measured as pIC50). Here we have identified a total of 284 new chemical series that gave a significant pIC50 shift and therefore appear to target these nine overexpressers tested. The highest frequency of validated hits was identified against MurC and over half of the total hits were against MurC and GuaB2 (28% and 23% of the total hits, respectively). The lowest hit rate was against MabA, representing only 2% of the overall hits. A summary of all the hits identified is presented in Figure 5.3.

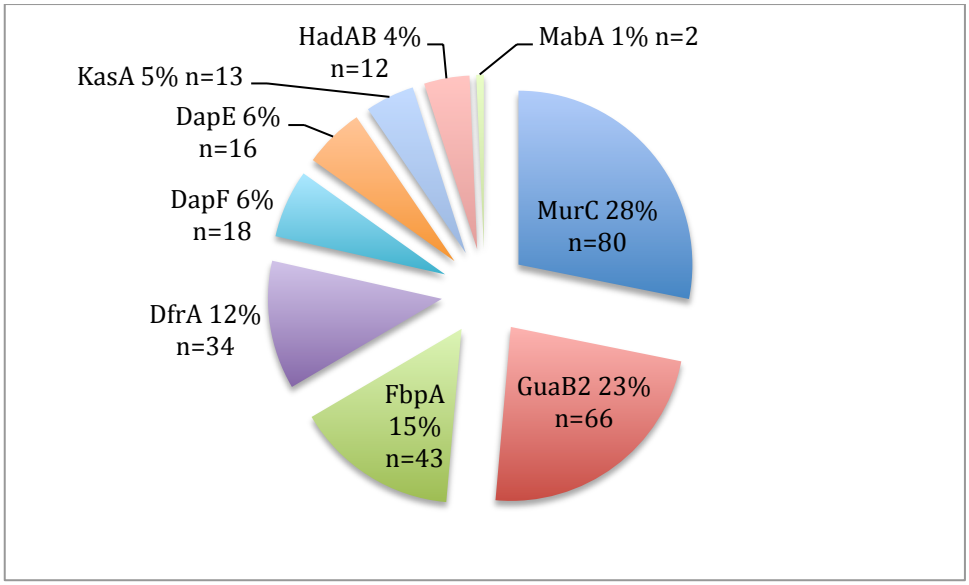


Figure 5.3: A summary of the distribution of 284 hits identified in a target-specific phenotypic HTS of 10,000 known inhibitors of *M. tb.* The highest frequency of hits was observed with MurC, accounting for 28% of the total, which along with GuaB2 make up 51% of the total hits observed. The lowest frequency of hits was observed with MabA where only 2 compounds were identified. The considerable success of this HTS in delivering new anti-TB compounds with known novel targets represents a change in primary strategy for antimicrobial drug discovery by phenotypic screening. This work serves as a proof of concept for future screening campaigns as well as a strong platform for hit-to-lead medicinal chemistry that may deliver a clinically relevant drug to treat TB in the future.

CHAPTER 6

General Discussion

The work presented in this thesis has been conducted with the practical and intellectual input of many people as detailed in the Acknowledgements section. The author takes credit for the molecular biology and microbiology presented in Chapters 2 and Chapter 3, while recognising the contribution of the overexpresser constructs from Dr. Katherine Abrahams (University of Birmingham). In both of these chapters, whole genome sequencing and the analysis of sequencing data was conducted by the Genomics facility at the University of Birmingham. The multidisciplinary approach presented in Chapter 4 required the contribution of a number of collaborating scientists. The author takes full credit for the cloning of EchA6 and site-directed mutant EchA6 constructs along with the protein expression, purification and analysis by intrinsic tryptophan fluorescence binding assays and X-ray crystallography (the latter, conducted under the supervision and with the assistance of Dr. Klaus Fütterer (University of Birmingham)). The author takes partial credit for the overexpression-based resistance of EchA6 on solid and in liquid medium, and the FAMEs and MAMEs analysis, conducted with the assistance of Dr. Katherine Abrahams and Dr. Sudagar Gurcha (University of Birmingham). The author takes full credit for the HTS conducted in Chapter 5, whilst acknowledging various members of the Besra Lab for their contribution of the overexpresser constructs through the Besra Lab strain database (University of Birmingham) and Dr. Laura Vela-Glez Del Peral (GSK) for her assistance with the data analysis. The work presented in this thesis has delivered a significant contribution to knowledge in the field of TB drug discovery research.

The identification of the MoA of the IP compounds as targeting *M. tb* QcrB was published in *PLoS ONE* in 2012. This drug-to-target approach to novel 'hit' compound identification produced a previously undiscovered drug target in

mycobacteria, giving credence to the top-down drug discovery strategy over conventional target-driven approaches. The group of Dr. Kevin Pethe of Institute Pasteur Korea (IPK) picked up this first crucial step in the discovery of a new anti-mycobacterial compound series and set about the hit-to-lead medicinal chemistry, resulting in the production of a library of imidazopyridine amide (IPA) derivatives of the original IP hit compounds. From this library, they subsequently identified Q203; a compound with significantly improved potency over the original IPs in a chronic model of TB infection, as well as improved pharmacokinetics and drug-drug interaction profile, whilst the FoR and locus of resistance-conferring SNPs in *qcrB* remained the same (Pethe *et al.* 2013). This compound has been entered into Phase I EBA clinical trials, the results of which are due to be made publically available shortly.

Despite the lack of success presently in the MoA determination for the BM compounds, as reported in Chapter 3, the primary evidence supporting the hypothesis of MmpL3 functioning as a drug-import mechanism in terms of the overexpresser growth curves and comparative FAMEs and MAMEs analysis have led to a continuation of this research program. The future work that will be conducted based on Chapter 3 is to investigate MmpL3 against the backdrop of MmpL5, a recently discovered mycobacterial drug-efflux pump (Hartkoorn *et al.* 2014). Utilising azole as a marker for drug-efflux and a selective RND pump inhibitor, I intend to probe the functional variations of these two proteins, exploiting the phenotypic strategies already discussed in this thesis. This work will serve as a major contribution to the field as apparent 'target' promiscuity derived from an MmpL3-based phenotypic resistance mechanism could lead to the discontinuation of research programs

surrounding novel anti-mycobacterial compounds based on a lack of novelty of their MoA.

This was very much the case with the THPP compounds, which were publically released by GSK after the publication of their [apparent] MoA in inhibiting mycobacterial MmpL3 (Ballell *et al.* 2013; Remuinan *et al.* 2013). Fortuitously however, this chemical series had by that time already been entered into a new chemoproteomics program conducted by Cellzome (now a GSK company), who identified high selectivity of the THPP chemical series for EchA6, with no such selectivity for MmpL3. I was given this project due to the high probability that this previously unexplored mycobacterial protein was likely to be a 'red herring'. The work that followed established EchA6 as an essential, acatalytic [as an enoyl-CoA hydratase], FAS-II interacting, CoA-binding target of the THPP compounds both *in vitro* and *in vivo*. This work has led to a hypothesised, previously undiscovered, acyl-CoA shunt pathway between fatty acid catabolism and anabolism; a sensible evolutionary trait in bacteria for whom fatty acids are the cornerstone of their survival, pathogenicity and success as an organism. This is also the first compelling evidence that MmpL3 may not represent the MoA, as previously thought, but more accurately should may be defined as the MoR (mode of resistance) of the numerous published, and probably even greater number of unpublished compounds designated "MmpL3 inhibitors." The acronym "MoR" could be extended further to MoRUPT (mode of resistance until proven target) and applied to all targets that have been assigned based upon the locus of resistance-conferring mutations without further biochemical, phenotypic or other method of validation. This work has now been accepted for publication in *Nature Microbiology* and is likely to be published in

January 2016. Investigations into the function of the apparently catalytically silent EchAs and their value as drug targets are continuing with EchA12, where resistance-conferring SNPs have been identified against a novel inhibitor of *M. tb*, which is structurally distinct from the THPPs.

The overlap between the stories of MmpL3 and EchA6 (Chapter 3 and 4 respectively), as well as the literature surrounding the development and fundamental limitations of Bedaquiline (Chapter 1) serve to highlight an inherent weakness in the drug-to-target approach to TB drug discovery, whereby the target outcome is uncontrollable. Without prior selection for a compound that inhibits by a MoA that is not essential for humans, but is essential for bacteria, many millions of dollars can be spent chasing antibacterial agents that, despite their efficacy *in vitro*, will never make it into the clinic. Overcoming this problem led to the conception of a drug-to-target:target-to-drug combined strategy for anti-tubercular drug discovery, detailed in Chapter 5 of this thesis. By conducting a phenotypic resistance-based HTS using *M. bovis* BCG strains overexpressing proteins of specific interest to mycobacteria, using a pool of 10,000 known inhibitors of *M. tb*, I was able to obtain preliminary evidence for the MoA of 284 anti-mycobacterial compounds, targeting 9 promising *M. tb* drug targets. This work represents an unprecedented success in the space of a year, as between 1995 and 2001, GSK conducted 67 HTS campaigns on TB targets which only resulted in 5 lead compounds (Payne *et al.* 2007). I am continuing this research by working to validate the MoRUPT of these inhibitors by various biochemical, microbiological and metabolomics-based strategies with a view to publishing each validated collection of compounds along with their respective MoAs.

At the start of this thesis I set out to identify the MoA of novel anti-tubercular drugs, with the end result of having potentially identified the target of a total of 291 anti-mycobacterial compounds over 3.5 years. However, the most significant long-term contribution to scientific knowledge of this work is likely to be the greater understanding of the inherent strengths and weaknesses of different approaches at the coalface of drug discovery. This leads me to the overriding conclusion that interdisciplinary strategies will pave the way to the discovery of tomorrow's antibiotics.

CHAPTER 7

References

Abrahams K, Cox J, Spivey V, Loman N, Pallen M, Constantinidou C, Fernandez R, Alemparte C, Remuinan M, Barros D, Ballell L and Besra G (2012). Identification of novel imidazo[1,2-a]pyridine inhibitors targeting *M. tuberculosis* QcrB. PLoS One 7(12):e52951

Adams P, Grosse-Kunstleve R, Hung L, Ioerger T, McCoy A, Moriarty N, Read R, Sacchettini J, Sauter N and Terwilliger T (2002). PHENIX: building new software for automated crystallographic structure determination. Acta. Crystallogr. D. Biol. Crystallogr. 58, 1948-1954

Agrawal D, Udwadia F, Rodriguez C and Mehta A (2009). Increasing incidence of fluoroquinolone-resistant *Mycobacterium tuberculosis* in Mumbai, India. Int. J. Tuberc. Lung Dis. 13, 79–83

Alvin A, Miller K and Neilan B (2014). Exploring the potential of Endophytes from Medicinal Plants as Sources of Antimycobacterial Compounds. Microbiological Research, http://dx.doi.org/10.1016/j.micres.2013.12.009

Anaflous A, Benchat N, Mimouni S, Abouricha S, Ban-Hadda T, El-Bali B, Hakkou A and Hacht B (2004). Armed Imidazo[1,2-a]Pyrimidines (Pyridines): Evaluation of Antibacterial Activity. Lett. Drug Des. & Disc. 1:224-229

Andries K, Gevers T and Lounis N (2010). Bactericidal potencies of new regimens are not predictive for their sterilizing potencies in a murine model of tuberculosis. Antimicrob. Agents Chemother. 54:4540–4544

Andries K, Verhasselt P, Guillemont J, Göhlmann W, Neefs J, Winkler H, Gestel J, Timmerman P, Zhu M, Lee E, Williams P, de Chaffoy D, Huitric E, Hoffner S, Cambau E, Truffot-Pernot C, Lounis N and Jarlier V (2005). A diarylquinoline drug active on the ATP synthase of *Mycobacterium tuberculosis*. Science 307: 223-227

Armitige L, Jagannath C, Wanger A and Norris S (2000). Disruption of the genes encoding antigen 85A and antigen 85B of *Mycobacterium tuberculosis* H37Rv: effect on growth in culture and in macrophages. Infection and Immunity 68: 767–778

Asselineau J, Lederer E (1950). Structure of the mycolic acids of Mycobacteria. Nature 166(4227):782-3

Backus K, Dolan M, Barry C, Joe M, McPhie P, Bochoff H, Lowary T, Davis B and Barry III C (2014). The three *Mycobacterium tuberculosis* antigen 85 isoforms have unique substrates and activities determined by non-active site regions. J Biol Chem 289(36): 25041-25053

Baell J and Walters M (2014). Chemical con artists foil drug discovery. Nature 513:481-483

Bahnson B, Anderson V and Petsko G (2002). Structural Mechanism of Enoyl-CoA Hydratase: Three ATms from a Single Water Are Added in either an E1cb Stepwise or Concerted Fashion. ACS Biochemistry 41(8):2621-2629

Bakasubramanian V, Solapure S, Iyer H, Ghosh A, Sharma S, Kaur P, Deepthi R, Subbulakshmi V, Ramya V, Ramachandran V, Balganesh M, Wright L, Melnick D, Butler S and Sambandamurthy V (2014). Bactericidal activity and mechanism of action of AZD5847, a novel oxazolidinone for treatment of tuberculosis. Antimicrob. Agents. Chemother. 58(1):495-502

Balani S, Devishree V, Miwa G, Gan L, Wu J and Lee F (2005). Strategy of utilizing in vitro and in vivo ADME tools for lead optimization and drug candidate selection. Curr Top Med Chem. 5 (11):1033–8.

Ballell L, Bates R, Young R, Alvarez-Gomez D, Alverez-Ruiz E, Barroso V, Blanco D, Crespo B, Escribano J, Gonzalez R, Lozano S, Huss S, Santos-Villarejo A, Martin-Plaza J, Mendoza A, Rebollo-Lopez M, Remuinan M, Lavandera J, Perez-Herran E, Gamo-Benito F, Garcia Bustos J, Barros D, Castro J and Cammack N (2013). Fuelling Open-Source Drug Discovery: 177 Small-Molecule Leads against Tuberculosis. Chem. Med. Chem. 8(2):313-321

Banerjee A, Dubnau E, Quemard A, Balasubramanion V, Um K, Wilson T, Collins D, de Lisle G and Jacobs W. (1994) inhA, a gene encod- ing a target for isoniazid and ethionamide in *M. tuberculosis*. Science 263: 227–230.

Banerjee A, Sugantino M, Sacchettini J and Jacobs W (1998). The mabA gene from the inhA operon of *Mycobacterium tuberculosis* encodes a 3-ketoacyl reductase that fails to confer isoniazid resistance. *Microbiology* 114(10): 2697-2704

Bantscheff M, Hopf C, Savitski M, Dittman A, Grandi P, Michon A, Schlegl J, Abraham Y, Becher I, Bergamini G, Boesche M, Delling M, Dumpelfeld B, Eberhard D, Huthmacher C, Mathieson T, Poeckel D, Reader V, Strunk K, Sweetman G, Kruse U, Neubauer G, Ramsden N and Drewes G (2011). Chemoproteomics profiling of HDAC inhibitors reveals selective targeting of HDAC complexes. Nat. Biotechnol. 29, 255-265

Barnard M, Albert H, Coetzee G, O'Brien R and Bosman M (2008). Rapid Molecular Screening for Multidrug-Resistant Tuberculosis in a High-Volume Public Health Laboratory in South Africa. American Journal of Respiratory and Critical Care Medicine 177(7):787-792

Barry, C. E. III, Boshoff H, Dartois V, Dick T, Ehrt S, Flynn J, Schnappinger D, Wilkinson R and Young D (2009). The spectrum of latent tuberculosis: rethinking the biology and intervention strategies. Nature Rev. Microbiol. 7:845–855

Basavannacharya C, Robertson G, Munshi T, Keep N and Bhakta S (2010). ATP-dependent MurE ligase in *Mycobacterium tuberculosis*: biochemical and structural characterisation. Tuberculosis (Edinb) 90: 16-24

Batt S, Jabeen T, Bhowruth V, Quill L, Lund P, Eggeling L, Alderwick L, Futterer K and Besra G (2012). Structural basis of inhibition of *Mycobacterium tuberculosis* DprE1 by benzothiazinone inhibitors. Proc. Natl. Acad. Sci. USA 109(28):11354-9

Baulard A, Betts J, Engohang-Ndong J, Quan S, Brennan P, Locht C and Besra G (2000). Activation of the pro-drug ethionamide is regulated in mycobacteria. J. Biol. Chem. 275(36): 28326-31

Belisle J, Vissa V, Sievert T, Takayama K, Brennan P and Besra G (1997). Role of the major antigen of *Mycobacterium tuberculosis* in cell wall biogenesis. Science 276:1420-1422

Benson T, Walsh C and Hogle J (1996). The structure of the substrate-free form of MurB, an essential enzyme for the synthesis of bacterial cell walls. Structure 4: 47-54

Besra G, Sievert T, Lee R, Slayden R, Brennan P and Takayama K (1994). Identification of the apparent carrier in mycolic acid synthesis. Proc Natl Acad Sci U S A 91, 12735-12739

Bhatt A, Molle V, Besra G, Jacobs W, and Kremer L (2007). The *Mycobacterium tuberculosis* FAS-II condensing enzymes: their role in mycolic acid biosynthesis, acid-fastness, pathogenesis and in future drug development. Molecular microbiology 64, 1442-1454, doi:10.1111/j.1365-2958.2007.05761.x

Biava M, Porretta G and Manetti F (2007). New Derivatives of BM212: A Class of Antimycobacterial Compounds Based on the Pyrrole Ring as a Scaffold. Mini Rev. Med. Chem. 7(1):65-78

Bienvenue D, Gilner D, Davis R, Bennett B and Holz R (2003). Substrate specificity, metal binding properties, and spectroscopic characterization of the DapE-encoded N-succinyl-L,L-diaminopimelic acid desuccinylase from Haemophilus influenzae. Biochemistry 42: 10756–10763.

Born T, Zheng R and Blanchard J (1998). Hydrolysis of N-succinyl-L,L-diaminopimelic acid by the Haemophilus influenzae dapE-encoded desuccinylase: metal activation, solvent isotope effects, and kinetic mechanism. Biochemistry 37:10478–10487.

Bowman J, Merino E, Brooks C, Striepen B, Carlier P and Cassera M (2014). Antiapicoplast and Gametocytocidal Screening To Identify the Mechanisms of Action of Compounds within the Malaria Box. Antimicrob. Agents. Chemother. 58(2):811-819

Brennan P (2003). Structure, function and biogenesis of the cell wall of *Mycobacterium tuberculosis*. Tuberculosis 83: 91-97

Brown A, Taylor R, Bhatt A, Futterer K and Besra G (2009). Platensimycin activity against mycobacterial beta-ketoacyl-ACP synthases. PLoS One 4(7):e6306

Brown A, Bhatt A, Singh A, Saparia E, Evans A and Besra G (2007). Identification of the dehydratase component of the mycobacterial mycolic acid-synthesizing fatty acid synthase-II complex. Microbiology 153, 4166-4173

Butler S (2013). AZD5847: oxazolidinone for the treatment of tuberculosis. Infection Innovative Medicines Group, AstraZeneca R&D, Boston http://cptrinitiative.org/wp-content/uploads/2013

Cantaloube S, Veyron-Churlet R, Haddache N, Daffe M and Zerbib D (2011). The *Mycobacterium tuberculosis* FAS-II dehydratases and methyltransferases define the specificity of the mycolic acid elongation complexes. PLoS One 6, e29564

CCP4 (1994). The CCP4 suite: programs for protein crystallography. Acta Crystallogr D Biol Crystallogr 50, 760-763

Centers for Disease Control and Prevention (2013). Provisional CDC guidelines for the use and safety monitoring of bedaquiline fumarate (Sirturo) for the treatment of multidrug-resistant tuberculosis. MMWR Recomm. Rep. 62(RR-09):1-12

Chadhuri R, Loman N, Snyder L, Bailey C, Stekel D and Pallen M (2008). xBase2: a comprehensive resource for comparative bacterial genomics. Nucleic Acids Res 36:543-546

Choi K, Kremer L, Besra G and Rock C (2000). Identification and substrate specificity of beta -ketoacyl (acyl carrier protein) synthase III (mtFabH) from

Mycobacterium tuberculosis. The Journal of biological chemistry 275, 28201-28207, doi:10.1074/jbc.M003241200

Cole S, Brosch R, Parkhill J, Garnier T, Churcher C, Harris D, Gordon S, Eiglmeier K, Gas S and other authors (1998). Deciphering the biology of *Mycobacterium tuberculosis* from the complete genome sequence. Nature 393, 537–544

Cox, H and Ford N (2012). Linezolid for the treatment of complicated drig-resistant tuberculosis: a systematic review and meta-analysis. Int. J. Tuberc. Lung. Dis. http://dx.doi.org/10.5588/ijtld.11.0451

Crofton J and Mitchison D (1948). Streptomycin resistance in pulmonary tuberculosis. Br. Med. J. 2(4588): 1009-1015

Curtis S (1987). Genes encoding the beta and epsilon subunits of the proton-translocating ATPase from Anabaena sp. Strain PCC7120. J. Bacteriol. 169(1): 80-86

Davis R, Bienvenue D, Swierczek S, Gilner D, Rajagopal L, Bennett B and Holz R (2006). Kinetic and spectroscopic characterization of the E134A- and E134D-altered dapE- encoded N-succinyl-L,L-diaminopimelic acid desuccinylase from Haemophilus influenzae. J Biol Inorg Chem 11: 206– 216.

Diacon A, Dawson R, Groote-Bidlingmaier F, Symons G, Venter A, Donald P, Niekerk C, Everitt D, Winter H, Becker P, Mendel C and Spigelman M (2012). 14-

day bactericidal activity of PA-824, bedaquiline, pyrazinamide and moxifloxacin combinations: a randomized trial. The Lancet 380(9846):986-993

Diacon A, Pym A, Grobusch M, Patientia R, Rustomjee R, Page-Shipp L, Pistorius C, Krause R, Bogoshi M, Churchyard G, Venter A, Allen J, Palomino J, Marez T, van Heeswijk R, Lounis N, Meyvisch P, Verbeeck J, Parys W, de Beule K, Andries K, and Mc Neeley D (2009). The diarylquinoline TMC207 for multidrug-resistant tuberculosis. New England Journal Medicine 360(23):2397-2405

Dias M, Tyrakis P, Domingues R, Leme A and Blundell T (2014). *Mycobacterium tuberculosis* Dihydrofolate Reductase Reveals Two Conformational States and a Possible Low Affinity Mechanism to Antifolate Drugs. Structure 22(1):94-103

Dinnes J, Deeks J, Kunst H, Gibson A, Cummins E, Waugh N, Drobinewski F and Lalvani A (2007). A systematic review of rapid diagnostic tests for the detection of tuberculosis infection. Health Technol. Assess. 11(3)

Donald P and Diacon H (2008). The early bactericidal activity of anti-tuberculosis drugs: a literature review. Tuberculosis 88:75–83

Dover L, Alahari A, Gratraud P, Gomes J, Bhowruth V, Reynolds R, Besra G and Kremer L (2007). EthA, a common activator of thiocarb- amide-containing drugs acting on different mycobacterial targets. Antimicrob. Agents Chemother. 51:1055–1063.

"Drug Approval Package: Zyvox". FDA Center for Drug Evaluation and Research. November 20, 2001. Comprehensive review of the FDA approval process.

Emsley P, Lohkamp B, Scott W and Cowtan K (2010). Features and development of Coot. Acta Crystallogr D Biol Crystallogr 66, 486-501

Escombe R, Moore D, Gilman R, Navincopa M, Ticona E, Mitchell B, Noakes C, Martinez C, Sheen P, Ramirez R, Quino W, Gonzalez A, Friedland J and Evans C (2009). Upper-Room Ultraviolet Light and Negative Air Ionization to Prevent Tuberculosis Transmission. PLoS Medicine 6(3): e1000043

Falzon D, Jaramillo E, Schunemann H, Arentz M, Bauer M, Bayona J, Blanc L, Caminero J, Daley C, Duncombe C, Fitzpatrick A, Gebhard H, Getahun M, Henkens T, Holtz J, Keravec S, Keshavjee A, Khan R, Kulier V, Leimane C, Lienhardt C, Lu A, Mariandyshev G, Migliori F, Mirzayev C, Mitnick P, Nunn G, Nwagboniwe O, Oxlade D, Palmero P, Pavlinac M, Quelapio M, Raviglione M, Rich S, Royce S, Rüsch-Gerdes A, Salakaia R, Sarin D, Sculier F, Varaine M, Vitoria J, Walson F, Wares K, Weyer R and White M (2011) WHO guidelines for the programmatic management of drug-resistant tuberculosis: 2011 update. Eur. Resp. J. 38:516-528

Fattorini L, Iona E, Ricci M, Thoresen O, Orru G, Oggioni M, Tortoli E, Piersimoni, C, Chiaradonna P, Tronci M, Pozzi G, and Orefici G (1999). Activity of 16

antimicrobial agents against drug-resistant strains of *Mycobacterium tuberculosis*. Microb. Drug Resist. 5, 265-70

Favrot, L, Grzegorzewicz A, Lajiness D, Marvin R, Boucau J, Isailovic D, Jackson M, and Ronning D (2013) Mechanism of inhibition of *Mycobacterium tuberculosis* antigen 85 by ebselen. Nat. Commun. 4, 2748

Fischbach M and Walsh C (2009) Antibiotics for emerging pathogens. Science 325:1089–1093

Ford C, Hamel J, Stapert D, Moerman J, Hutchin- son D, Barbachyn M and Zurenko G (1997). Oxazolidinones: new antibacterial agents. Trends in Microbiology 5:196–200.

Fortun J, Davila P, Navas E, Perez-Elias M, Cobo J, Toto M, Pedrosa E, Gomez-Mampaso E and Moreno S (2005). Linezolid for the treatment of multidrug-resistant tuberculosis. Antimicrob. Chemother. 56(1):180-185

Fukui Y, Hirai T, Uchida T, and Yoneda M (1965). Extracellular proteins of tubercle bacilli. IV. α and β antigens as major extracellular protein products and as cellular components of a strain (H37Rv) of *Mycobacterium tuberculosis*. Biken J. 8, 189 –199

Gandhi N, Nunn P, Dheda K, Schaff S, Zignol M, Soolingen D, Jensen P and Bayona J (2010). Multidrug-resistant and extensively drug-resistant tuberculosis: a threat to global control of tuberculosis. Lancet 375:1830–1843

Gannoun-Zaki L, Alibaud L and Kremer L (2012). Point mutations within the fatty acid synthase type II dehydratase components HadA or HadC contribute to Isoxyl resistance in *Mycobacterium tuberculosis*. Antimicrob. Agents Chemother. 57(1): 629-632

Gavalda S, Léger M, van der Rest B, Stella A, Bardou F, Montrozier H, Chalut C, Burlet-Schiltz O, Marrakchi H, Daffé M and Quémard A (2009). The Pks13/FadD32 crosstalk for the biosynthesis of mycolic acids in *Mycobacterium tuberculosis*. Journal of Biological Chemistry. 284: 19255–19264

George K, Yuan Y, Sherman D and Barry C (1995). The biosynthesis of cyclopropanated mycolic acids in *Mycobacterium tuberculosis*. Identification and functional analysis of CMAS-2. J. Biol. Chem. 270(45):27292-8

Getahun H, Gunneberg C, Granich R and Nunn P (2010). HIV Infection – Associated Tuberculosis: The Epidemiology and the Response. Clin. Infect. Dis. 50(3):201-207

Gilbert H, Lowe C and Drabble W (1979). Inosine 59-monophosphate dehydrogenase of Escherichia coli. Purification by affinity chromatography, subunit structure and inhibition by guanosine 59-monophosphate. Biochem. J. 183: 481–94

Gillner D, Armoush N, Holz R and Becker D (2009). Inhibitors of bacterial N-succinyl-L,L-diaminopimelic acid desuccinylase (DapE) and demonstration of in vitro antimicrobial activity. Bioorg. Med. Chem. Lett. 19: 6350–6352.

Gler M, Skripconoka V, Sanchez-Garavito E, Xiao H, Cabrera-Rivero J, Vargas-Vasquez D, Gao M, Awad M, Park S, Shim T, Suh G, Danilovits M, Ogata H, Kurve A, Chang J, Suzuki K, Tupasi T, Koh W, Seaworth S, Geiter L and Wells C (2012) Delamanid for multidrug-resistant pulmonary tuberculosis. N. Engl. J. Med. 366:2151–2160

Goble M, Iseman M, Madsen L, Waite D, Ackerson L and Horsburgh R (1993). Treatment of 171 patients with pulmonary tuberculosis resistant to isoniazid and rifampin. New England Journal of Medicine 328(8): 527-532

Goffin C and Ghuysen J (2002). Biochemistry and Comparative Genomics of SxxK Superfamily Acyltransferases Offer a Clue to the Mycobacterial Paradox: Presence of Penicillin-Susceptible Target Proteins versus Lack of Efficiency of Penicillin as Therapeutic Agent. Microbiol. Mol. Biol. Rev. 66: 702-738

Griffin J, Gawronski J, DeJesus M, Ioerger T, Akerley B and Sassetti C (2011). High resolution phenotypic profiling defines genes essential for mycobacterial growth and cholesterol catabolism. PLoS Pathogens 7(9):e1002251 .doi:10.1371/journal.ppat.1002251

Grover S, Alderwick L, Mishra A, Krumback K, Marienhagen J, Eggeling L, Bhatt A and Besra G (2014). Benzothiazinones mediate killing of Corynebacterianeae by blocking decaprenyl phosphate recycling involved in cell wall biosynthesis. J. Biol. Chem. [Epub ahead of print]

Grzegorzewicz A, Eynard N, Quemard A, North J, Margolis A, Lindenberger J, Jones V, Kordulakova J, Brennan P, Lee R, Ronning D, McNeil M, and Jackson M (2015). Covalent modification of the *Mycobacterium tuberculosis* FAS-II dehydratase by Isoxyl and Thiacetazone. ACS Infect. Dis. 1(2): 91-97

Grzegorzewicz A, Pham H, Gundi V, Scherman M, North E, Hess T, Jones V, Gruppo V, Born S, Kordulakova J, Chavadi S, Morisseau C, Lenaerts A, Lee R, McNeil M and Jackson M (2012). Inhibition of mycolic acid transport across the *Mycobacterium tuberculosis* plasma membrane. Nat. Chem. Biol. 8:334-341

Hartkoorn R, Uplekar S and Cole S (2014). Cross-resistance between clofazimine and bedaquiline through upregulation of MmpL5 in *Mycobacterium tuberculosis*. Antimicrobial Agents Chemotherapy 58(5):2979-2981

Hazbon M, Brimacombe M, Valle B, Cavatore M, Guerrero M, Varma-Basil M, Billman-Jacobe H, Lavender C, Fyfe J, Garcia-Garcia L, Leon C, Bose M, Chaves F, Murray M, Eisenach K, Sifuentes-Osornio J, Cave M, Ponce A and Alland D (2006). Population genetics study of isoniazid resistance mutations and evolution of multidrug-resistant *Mycobacterium tuberculosis*. Antimicrob. Agents Chemother. 50: 2640-2649

Hedstrom L (2009). IMP dehydrogenase: structure, mechanism, and inhibition. Chem. Rev. 109, 2903–2928.

Heep M, Brandstatter B, Rieger U, Lehn N, Richter E, Rusch-Gerdes S and Niemann S (2001). Frequency of rpoB mutations inside and outside the cluster 1 region in rifampin-resistant clinical *Mycobacterium tuberculosis* isolates. J. Clin. Microbiol. 39(1): 107-110

Heijenoort (2001). Formation of the glycan chains in the synthesis of bacterial peptidoglycan. Glycobiology 11: 25R-36R

Hershkovitz I, Donoghue H, Minnikin D, Besra G, Lee O, Gernaey A, Galili E, Eshed V, Greenblatt C, Lemma E, Bar-Gal G and Spigelman M (2008). Detection and Molecular Characterization of 9000-Year-Old *Mycobacterium tuberculosis* from a Neolithic Settlement in the Eastern Mediterranean. PLoS One 3(10): e3426

Hu Y, Geize R, Besra G, Gurcha S, Liu A, Rohde M, Singh M and Coates A (2010). 3-Ketosteroid 9alpha-hydroxylase is an essential factor in the pathogenesis of *Mycobacterium tuberculosis*. Mol Microbiol 75, 107-121

Jackson M, Raynaud C, Lanéelle MA, Guilhot C, Laurent-Winter C, Ensergueix D, Gicquel B and Daffé M (1999). Inactivation of the antigen 85C gene profoundly affects the mycolate content and alters the permeability of the *Mycobacterium tuberculosis* cell envelope. Molecular Microbiology. 31: 1573– 1587

Jackson R, Weber G and Morris H (1975). IMP dehydrogenase, an enzyme linked with proliferation and malignancy. Nature 256, 331–333.

Jankute M, Cox J, Harrison J and Besra G (2015). Assembly of the mycobacterial wall. Annual Review Microbiology 69 In Press

Jones D, Taylor W, and Thornton J (1994). A Model Recognition Approach to the Prediction of All-Helical Membrane Protein Structure and Topology. Biochemistry, 33:3038-3049

Kabsch W (2010). XDS. Acta Crystallogr D Biol Crystallogr 66, 125-132

Karimova G, Pidoux J, Ullmann A and Ladant D (1998). A bacterial two-hybrid system based on a reconstituted signal transduction pathway. Proc Natl Acad Sci U S A 95, 5752-5756

Kasimogullari B and Cesur Z (2004). Fused heterocycles: synthesis of some new imidazo[1,2-a]-pyridine derivatives. Molecules. 9:894-901

Kim D, Lees W, Kempsell K, Lane W, Duncan K and Walsh C (1996). Characterization of a Cys115 to Asp substitution in the Escherichia coli cell wall biosynthetic enzyme UDP-GlcNAc enolpyruvyl transferase (MurA) that confers resistance to inactivation by the antibiotic fosfomycin. Biochemistry 35: 4923-8

Kloss P, Xiong L, Shinabarger D and Mankin A (1999). Resistance mutations in 23S rRNA identify the site of action of the protein synthesis inhibitor linezolid in the ribosomal peptidyl trans- ferase center. Journal of Molecular Biology 294:93–101

Koseki Y and Aoki S (2014). Computational Medicinal Chemistry for Rational Drug Design: Identification of Novel Chemical Structures with Potential Anti-Tuberculosis Activity. Curr. Top. Med. Chem. 14(1):176-188

Koul A, Arnoult E, Lounis N, Guillemont J and Andries K (2011). The challenge of new drug discovery for tuberculosis. Nature 469:483-490

Koul A, Vranckx L, Dendouga N, Balemans W, Wyngaert I, Vergauwen K, Göhlmann W, Willebrords R, Poncelet A, Guillemont J, Bald D and Andries K (2008). Diarylquinolines are bactericidal for dormant mycobacteria as a result of disturbed ATP homeostasis. J. Biol. Chem. 283:25273-25280

Kremer L, Dover L, Carrere S, Nampoothiri K, Lesjean S, Brown A, Brennan P, Minnikin D, Locht C and Besra G (2002). Mycolic acid biosynthesis and enzymic characterization of the beta-ketoacyl-ACP synthase A-condensing enzyme from *Mycobacterium tuberculosis*. Biochem. J. 364, 423-430

Kremer L, Douglas J, Baulard A, Morehouse C, Guy M, Alland D, Dover L, Lakey J, Jacobs W, Brennan P, Minnikin D and Besra G (2000). Thiolactomycin and related analogues as novel anti-mycobacterial agents targeting KasA and KasB condensing enzymes in *Mycobacterium tuberculosis*. J. Biol. Chem. 275(22): 16857-16864

Kremer L, Maughan W, Wilson R, Dover L and Besra G (2002). The *M. tuberculosis* antigen 85 complex and mycolyltransferase activity. Letters in Applied Microbiology 34: 233-237

Kurosu M, Mahapatra S, Narayanasamy P and Crick D (2007). Chemoenzymatic synthesis of Park's nucleotide: toward the development of high throughput screening for MraY inhibitors. Tetrahedron Letters 48: 799-803

La Rosa V, Poce G, Caneseco J, Buroni S, Pasca M, Biava M, Raju R, Porretta G, Alfonso S, Battilocchio C, Javid B, Sorrentino F, Ioerger T, Sacchettini J, Manetti F, Botta M, De Logu A, Rubin E and De Rossi E (2012). MmpL3 is the cellular target of the antitubercular pyrrole derivative BM212. Antimicrob. Agents Chemother. 56:324-331

Lechartier B, Rybniker J, Zumla A and Cole S (2014). Tuberculosis drug discovery in the post-post-genomic era. EMBO MolMed 6(1): e201201772

Lee M, Lee J, Carroll M, Choi H, Min S, Song T, Via L, Goldfeder L, Kang E, Jin B, Park H, Kwak H, Kim H, Jeon H, Jeong I, Joh J, Chen R, Olivier K, Shaw P, Follmann D, Song S, Lee J, Lee D, Kim C, Dartois V, Park S, Cho S, and. Barry C (2012). Linezolid for treatment of chronic extensively drug-resistant tuberculosis. N. Engl. J. Med. 367:1508-18.

Li R, Sirawaraporn R, Chitnumsub P, Sirawaraporn W, Wooden J, Athappilly F, Turley S and Hol W (2000). Three-dimensional structure of *M. tuberculosis* dihydrofolate reductase reveals opportunities for the design of novel tuberculosis drugs. J. Mol. Biol. 295: 307-323

Li W, Upadhyay A, Fontes F, North J, Wang Y, Crans D, Grzegorzewicz A, Jones V, Franzblau S, Lee R, Crick D and Jackson M (2014). Novel insights into the mechanism of inhibition of MmpL3, a target of multiple pharmacophores in *Mycobacterium tuberculosis*. Antimicrob. Agents Chemother. 58(11): 6413-6423

Lin P, Dartois V, Johnston P, Janssen C, Via L, Goodwin M, Klein E, Barry C and Flynn J (2012). Metronidazole prevents reactivation of latent *Mycobacterium tuberculosis* infection in macaques. PNAS 109(35):14188–14193

Lipinski C, Lombardo F, Dominy B and Feeney P (1997). Experimental and computational approaches to estimate solubility and permeability in drug discovery and development settings. Advanced Drug Delivery Reviews 23:3–25

Lounis N, Gevers T, Berg J and Andries K (2008). Impact of the interaction of R207910 with Rifampin on the treatment of tuberculosis studied in the mouse model. Antimicrob. Agents Chemother. 52(10):3568-3572

Lun S, Guo H, Onajole O, Pieroni M, Gunosewoyo H, Chen G, Tipparaju S, Ammerman N, Kozikowski A and Bishai W (2013). Indoleamides are active against drug-resistant *Mycobacterium tuberculosis*. Nat. Commun. 19(4):2907

Mahapatra S, Crick D and Brennan P (2000). Comparison of the UDP-N-acetylmuramate:L-alanine ligase enzymes from *Mycobacterium tuberculosis* and Mycobacterium leprae. J. Bacteriol. 182: 6827-30

Makarov V, Maniana G, Mikusova K, Mollmann U, Ryabova O, Saint-Joanis B, Dhar N, Pasca M, Buroni S, Lucarelli A, Milano A, De Rossi E, Belanova M, Bobovoska A, Dianiskova P, Kordulakova J, Sala C, Fullam E, Schneider P, McKinney J, Brodin P, Cristophe T, Waddell S, Butcher P, Albrethsen J, Rosenkrands I, Brosch R, Nandi V, Bharath S, Gaonkar S, Shandil R, Balasubramanian V, Balganesh T, Tyagi S, Grosset J, Riccardi G and Cole S (2009). Benzothiazinones kill *Mycobacterium tuberculosis* by blocking arabinan synthesis. Science 324(5928):801-4

Makarov V, Riabova O, Yuschenko A, Urlyapova N, Daudova A, Zipfel P and Mollmann U (2006). Synthesis and antileprosy activity of some dialkyldithiocarbamates. J. Antimicrob. Chemother. 57(6): 1134-8

Manjunatha U, Boshoff H and Barry C (2009). The mechanism of action of PA-824. Communicative & Integrative Biology 2(3):215-218

Marrakchi H, Ducasse S, Labesse G, Montrozier H, Margeat E, Emorine L, Charpentier X, Daffe M and Quemard A (2002). MabA (FabG1), a *Mycobacterium tuberculosis* protein involved in the long-chain fatty acid elongation system FAS-II. Microbiology 148, 951-960

Marrakchi H, Laneelle G, and Quemard A (2000). InhA, a target of the antituberculous drug isoniazid, is involved in a mycobacterial fatty acid elongation system, FAS-II. Microbiology 146 (Pt 2), 289-296

Matsumoto M, Hashizume H, Tomishige T, Kawasaki M, Tsubouchi H, Sasaki H, Shimokawa Y and Komatsu M (2006). OPC-67683, a nitro-dihydro- imidazooxazole derivative with promising action against tuberculosis in vitro and in mice. PLoS Med. 3:e466

Matteelli A, Carvalho A, Dooley K and Kritski A (2010). TMC207: the first compound of a new class of potent anti-tuberculosis drugs. Future Microbiol. 5(6):849-858

Matteelli A, Carvalho A, Dooley K and Kritski A (2010). TMC207: the first compound of a new class of potent anti-tuberculosis drugs. Future Microbiol. 5(6):849-858

McCoy A, Grosse-Kunstleve R, Adams P, Winn M, Stroni L and Read R (2007). Phaser crystallographic software. J. Appl. Crystallogr. 40, 658-674

Mdluli K, Sherman D, Hickey M, Kreiswirth B, Morris S, Stover C and Barry C (1996). Biochemical and genetic data suggest that lnhA is not the primary target for activated isoniazid in *Mycobacterium tuberculosis*. J. lnfect. Dis. 174: 1085-1090.

Mdluli K, Slayden R, Zhu Y, Ramaswamy S, Pan X, Mead D, Crane D, Musser J and Barry C (1998). Inhibition of a *Mycobacterium tuberculosis* β-Ketoacyl ACP Synthase by Isoniazid. Science 280(5369):1607-1610

Mikusova K, Slayden R, Besra G and Brennan P (1995). Biogenesis of the mycobacterial cell wall and the site of action of Ethambutol. Antimicrob. Agents. Chemother. 39(11): 2484-9

Mitchell P (1976). Possible molecular mechanisms of the proton motive function of cytochrome systems. J. Theor. Biol. 62:327–367

Mitnick C, Bayona J, Palacois E, Shin S, Furin J, Alcantara F, Sanchez E, Sarria M, Becerra M, Fawzi M, Kapiga S, Neuberg D, Maguire J, Kim J and Farmer P (2003).

Community-based therapy for multidrug-resistant tuberculosis in Lima, Peru. N. Engl. J. Med. 348:119–128

Moraski G, Markley L, Hipskind P, Boshoff H, Cho S, Franzblau S and Miller M (2011). Advent of Imidazo[1,2-a]pyridine-3-carboxamides with Potent Multi- and Extended Drug Resistant Antituberculosis Activity. ACS Med. Chem. Lett. 2(6):466-470

Mugumbate G, Abrahams K, Cox J, Papadatos G, van Westen G, Lelievre J, Calus S, Loman N, Ballell L, Barros D, Overington J and Besra G (2015). Mycobacterial dihydrofolate reductase inhibitors identified using chemogenomic methods and in vitro validation. PLoS ONE 10(3): e0121492. doi:10.1371/journal.pone.0121492

Murshudov G, Vagin A and Dodson E (1997). Refinement of macromolecular structures by the maximum-likelihood method. Acta. Crystallogr. D. Biol. Crystallogr. 53, 240-255

Musser J (1995). Antimicrobial agent resistance in myco- bacteria - molecular genetic insights. Clin. Microbiol. Rev. 8, 496-514.

Musser J, Kapur V, Williams D, Kreiswirth B and Vansoolingen D (1996). Characterization of the catalase-peroxidase gene (katc) and inhA locus in isoniazid-resistant and -susceptible strains of *Mycobacterium tuberculosis* by automated DNA

sequencing - restricted array of mutations associated with drug resistance. J. lnfect. Dis. 173, 196-202.

Nanninga (1998). Morphogenesis of Escherichia coli. Microbiol. Mol. Biol. Rev. 62: 110-129

Newman D and Cragg G (2012). Natural products as sources of new drugs over the 30 years from 1981 to 2010. J. Nat. Prod. 75(3):311-335

Nocek B, Gillner D, Fan Y, Holz R and Joachimiak A (2010). Structural basis for catalysis by the mono- and dimetalated forms of the dapE-encoded N-succinyl-L,L-diaminopimelic acid desuccinylase. J. Mol. Biol. 397: 617–626.

Odell L, Nilsson M, Gising J, Lagerlund O, Muthas D, Nordgvist A, Karien A and Larhed M (2009). Functionalized 3-amino-imidazo[1,2-a]pyridines: a novel class of drug-like *Mycobacterium tuberculosis* glutamine synthetase inhibitors. Bioorg. Med. Chem. Lett. 19(16):4790-4793

Parish T, Roberts G, Laval F, Schaeffer M, Daffe M, and Duncan K (2007). Functional complementation of the essential gene fabG1 of *Mycobacterium tuberculosis* by Mycobacterium smegmatis fabG but not Escherichia coli fabG. J. Bacteriol. 189: 3721–3728

Parish T and Stoker N (1998) Electroporation of mycobacteria. Methods in molecular biology: Mycobacteria protocols. New Jersey: Humana Press. 129–144.

Payne D, Gwynn M, Holmes D and Pompliano D (2007). Drugs for bad bugs: confronting the challenges of antibacterial discovery. Nature Reviews Drug Discovery 6(1):29-40

Pethe K, Bifani P, Jang J, Kang S, Park S, Ahn S, Jiricek J, Junj J, Jeon H and authors (2013). Discovery of Q203, a potent clinical candidate for the treatment of tuberculosis. Nature Medicine 19(9): 1157-1160

Pethe K, Sequiera P, Agarwalla S, Rhee K, Kuhen K, Phong W, Patel V, Beer D, Walker J, Duraiswamy J and authors (2010). A chemical genetic screen in *Mycobacterium tuberculosis* identifies carbon-source-dependent growth inhibitors devoid of in vivo efficacy. Nature Commun. 1:57

Pillai B, Cherney M, Diaper C, Sutherland A, Blanchard J, Vederas J and James M (2006). Structural insights into stereochemical inversion by diaminopimelate epimerase: An antibacterial drug target Proc. Natl. Acad. Sci. USA 103:8668-8673

Pimkin M, Pimkina J and Markham G (2009). A regulatory role of the Bateman domain of IMP dehydrogenase in adenylate nucleotide biosynthesis. J. Biol. Chem. 284, 7960–7969.

Poce G, Bates R, Alfonso S, Cocozza M, Porretta G, Ballell L, Rullas J, Ortega F, De Logu A, Agus E, La Rosa V, Pasca M, De Rossi E, Wae B, Franzblau S, Manetti F, Botta M and Biava M (2013). Improved BM212 MmpL3 Inhibitor Analogue Shows Efficacy in Acute Murine Model of Tuberculosis Infection. PloS One 8(2):e56980

Protopopova M, Hanrahan C, Nikonenko B, Samala R, Chen P, Gearhart J, Einck L and Nacy C (2005). Identification of a new antitubercular drug candidate, SQ109, from a combinatorial library of 1,2-ethylenediamines. J. Antimicrob. Chemother. 56(5):968-974

Qureshi N, Sathyamoorthy N and Takayama K (1984). Biosynthesis of C30 to C56 fatty acids by an extract of *Mycobacterium tuberculosis* H37Ra. J. Bacteriol. 157(1):46-52

Ramakrishnan L (2013). Looking within the zebrafirsh to understand the tuberculosis granuloma. Adv. Exp. Med. Biol. 783: 251-266

Rana A, Singh A, Gurcha S, Cox L, Bhatt A and Besra G (2012). Ppm1-encoded polyprenyl monophosphomannose synthase activity is essential for lipoglycan synthesis and survival in mycobacteria. PLoS One 7, e48211

Rao S, Lakshminarayana S, Kondreddi R, Herve M, Camacho L, Bifani P, Kalapala S and authors (2013). Indolecarboxamide is a preclinical candidate for treating multidrug-resistant tuberculosis. Sci. Transl. Med. 5: 214 (ra168)

Rayasam G (2013). MmpL3 a potential new target for development of novel anti-TB drugs. Expert Opin. Ther. Targets 18(3)

Raymond J, Mahapatra S, Crick D and Pavelka M (2005). Identification of the namH gene, encoding the hydroxylase responsible for the N-glycolylation of the mycobacterial peptidoglycan. J. Biol. Chem. 280: 326-33

Reddy V, Einck L, Andries K and Nacy C (2010). In vitro interactions between new antitubercular drug candidates SQ109 and TMC207. Antimicrob. Agents Chemother. 54:2840–2846

Remuinan M, Perez-Herran E, Rullas J, Alemoarte C, Martinez-Hoyos M, Dow D, Afari J, Mehta N, Esquivias J, Jimenez E, Ortega-Muro F, Fraile-Gabaldon M, Spivey V, Loman N, Pallen M, Constantinidou C, Minick D, Cacho M, Rebollo-Lopez M, Gonzales C, Sousa V, Barturen I, Mendoza A, Barros D, Besra G, Ballell L and Cammack N (2013). Tetrahydropyrazolo[1,5-a]pyrimidine-3-carboxamide and N-benzyl-6',7'-dihydrospiro[piperidine-4,4'-thieno[3,2-c]pyran] analogues with bactericidal efficacy against *Mycobacterium tuberculosis* targeting MmpL3. PLoS One 8:e60933

Riley R (1957). Aerial dissemination of pulmonary tuberculosis. Am. Rev. Tuberc. 76, 931–941

Ronning D, Klabunde T, Besra G, Vissa V, Belisle J and Sacchettini J (2000) Crystal structure of the secreted form of antigen 85C reveals potential targets for

mycobacterial drugs and vaccines. Nature Structural Biology 7: 141–146.

Rouse D, Li Z, Bai G and Morris S (1995). Characterization of the katG and inhA genes of isoniazid-resistant clinical isolates of *Mycobacterium tuberculosis*. Antimicrob. Agents. Chemother. 39(11):2472-7

Rullás J, Garcia J, Beltran M, Cardona P, Caceres N, Garcia-Bustos J and Barturen I (2010). Fast standardized therapeutic-efficacy assay for drug discovery against tuberculosis. Antimicrob Agents Chemother 54, 2262-2264

Sacco E, Covarrubias AS, O'Hare HM, Carroll P, Eynard N, Jones TA, Parish T, Daffé M, Bäckbro K and Quémard A (2007). The missing piece of the type II fatty acid synthase system from *Mycobacterium tuberculosis*. Proceedings of the National Academy of Sciences of the United States of America 104: 14628–14633

Saint-Joanis B, Souchon H, Wilming M, Johnsson K, Alzari P, and Cole S (1999). Use of site-directed mutagenesis to probe the structure, function and isoniazid activation of the catalase-peroxidase, KatG, from *Mycobacterium tuberculosis*. Biochem. J. 338:753-760.

Salian S, Matt T, Akbergenov R, Harish S, Meyer M, Duscha S, Shcherbakov D, Bernet B, Vasella A, Westhof E and Bottger E (2012). Structure-activity relationships among the kanamycin aminoglycosides: role of ring I hydroxyl and amino groups. Antimicrob. Agents Chemother. 56(12):6104-6108

Sambrook J and Fritsch E (1989). Molecular Cloning: A laboratory manual 2nd Edition. New York: Cold Spring Harbor Laboratory

Sassetti C, Boyd D and Rubin E (2003). Genes required for mycobacterial growth defined by high density mutagenesis. Mol. Microbiol. 48(1):77-84

Sassetti C, Boyd D and Rubin E (2001). Comprehensive identification of conditionally essential genes in mycobacteria. Proc. Natl. Acad. Sci. U S A 98, 12712-12717.

Sassetti C, Boyd D and Rubin E (2003). Genes required for mycobacterial growth defined by high density mutagenesis. Mol. Microbiol. 48, 77–84.

Schaeffer M, Agnihotri G, Volker C, Kallender H, Brennan P and Lonsdale J (2001). Purification and biochemical characterization of the *Mycobacterium tuberculosis* beta-ketoacyl-acyl carrier protein synthases KasA and KasB. The Journal of biological chemistry 276, 47029-47037, doi:10.1074/jbc.M108903200

Schluger N, Karunakara U, Lienhardt C, Nyirenda T and Chaisson R (2007). Building clinical trials capacity for tuberculosis drugs in high-burden countries. PLoS Medicine 4(11):e302

Schroeder E, de Souza O, Santos D, Blanchard J and Basso L (2002). Drugs that Inhibit Mycolic Acid Biosynthesis in *Mycobacterium tuberculosis*. Current Pharmaceutical Biotechnology 3:197-225

Shi C, Shi J and Xu Z (2011). A review of murine models of latent tuberculosis infection. Scand. J. Infect. Dis. 43(11-12): 848-856

Shu Q and Nair V (2008) Inosine monophosphate dehydrogenase (IMPDH) as a target in drug discovery. Med. Res. Rev. 28: 219–32

Skripconoka V, Danilovits M, Pehme L, Tomson T, Skenders G, Hummik T, Cirule A, Leimane V, Kurve A, Levina K, Geiter L, Manissero D and Wells C (2012). Delamanid improves outcomes and reduces mortality for multidrug-resistant tuberculosis. Eur. Respir. J. 41(6):1393-1400

Slee A, Wuonola M, McRipley R, Zajac I, Zawada M, Bartholomew P, Gregory W and Forbes M (1987). Oxazolidinones, a new class of synthetic antibacterial agents: in vitro and in vivo activities of DuP 105 and DuP 721. Antimicrobial Agents and Chemotherapy 31:1791–7.

Stanley S, Grant S, Kawate T, Iwase N, Shimizu M, Wivagg C, Silvis M, Kazyanskaya E, Aquardro J, Golas A, Fitzgerald M, Dai H, Zhang L and Hung D (2012). Identification of novel inhibitors of *M. tuberculosis* growth using whole cell based high throughput screening. ACS Chem. Biol. 7:1377-1384

Suzuki Y, Katsukawa C, Tamaru A, Abe C, Makino M, Mizuguchi Y and Taniguchi H (1998). Detection of kanamycin-resistant *Mycobacterium tuberculosis* by identifying mutations in the 16S rRNA gene. J. Clin. Microbiol. 36(5): 1120-1125

Tahlan K, Wilson R, Kastrinsky D, Arora K, Nair V, Fischer E, Barnes S, Walker J, Alland D, Barry C and Boshoff H (2012) SQ109 targets MmpL3, a membrane transporter of trehalose monomycolate involved in mycolic acid donation to the cell wall core of *Mycobacterium tuberculosis*. Antimicrob. Agents Chemother. 56:1797-1809

Takayama K and Qureshi N (1984). The Mycobacteria: a Sourcebook. (Kubica and Wayne: Editors), Marcel Dekker, New York pp. 315-344

Takayama K, Wang C and Besra G (2005). Pathway to synthesis and processing of mycolic acids in *Mycobacterium tuberculosis*. Clinical Microbiology Reviews 18: 81-101

Trivedi OA, Arora P, Sridharan V, Tickoo R, Mohanty D and Gokhale RS (2004). Enzymic activation and transfer of fatty acids as acyl-adenylates in mycobacteria. Nature. 428: 441–445

Udwadia Z, Amale R, Ajbani K and Rodrigues C (2012). Totally drug-resistant tuberculosis in India. Clin. Infect. Dis. 54(4): 579-581

Usha V, Dover L, Roper D and Besra G (2008). Characterization of *Mycobacterium tuberculosis* diaminopimelic acid epimerase: paired cysteine residues are crucial for racemization FEMS Microbiol. Lett. 280: 57–63.

Usha V, Dover L, Roper D, Futterer K and Besra G (2009). Structure of the diaminopimelate epimerase DapF from *Mycobacterium tuberculosis*. Acta. Cryst. D65: 383-387

Usha V, Dover L, Roper D, Lloyd A and Besra G (2006). Use of a codon alteration strategy in a novel approach to cloning the *Mycobacterium tuberculosis* diaminopimelic acid epimerase. FEMS Microbiol. Lett. 262: 39–47

Usha V, Gurcha s, Lovering A, Lloyd A, Papaemmanouil A, Reynolds R and Besra G (2011). Identification of novel diphenyl urea inhibitors of Mt-GuaB2 active against *Mycobacterium tuberculosis*. Microbiology 157:290-299

Usha V, Hobrath J, Gurcha S, Reynolds R and Besra G (2012). Identification of novel Mt-Guab2 inhibitor series active against *M. tuberculosis*. PLoS ONE 7(3): e33886. doi:10.1371/journal.pone.0033886

Usha V, Lloyd A, Lovering A and Besra G (2012). Structure and function of *Mycobacterium tuberculosis* meso-diaminopimelic acid (mDAP) biosynthetic enzymes. FEMS Microbiol. Lett. 330: 10-16

Varela C, Rittmann D, Singh A, Krumbach K, Bhatt K, Eggeling L, Besra G and Bhatt A (2012). MmpL genes are associated with mycolic acid metabolism in mycobacteria and corynebacteria. Chem. Biol. 19(4):498-506

Velayati A, Masjedi M, Farnia P, Tabarsi P, Ghanavi J, Ziazarifi A and Hoffner S (2009). Emergence of new forms of totally drug-resistant tuberculosis bacilli: super extensively drug-resistant tuberculosis or totally drug-resistant strains in Iran. Chest. 136:420–5.

Von Jagow G, Gribble G and Trumpower B (1986). Mucidin and strobilurin A are identical and inhibit electron transfer in the cytochrome bc_1 complex of the mitochondrial respiratory chain at the same site as myxothiazol. Biochemistry 25: 775–780

Von Jagow G, Ljungdahl P, Graf P, Ohnishi T and Trumpower B (1984). An inhibitor of mitochondrial respiration which binds to cytochrome b and displaces quinone from the iron-sulfur protein of the cytochrome bc_1 complex. J. Biol. Chem. 259: 6318–6326

Wallis R, Jakubiec W, Kumar V, Silvia A, Paige D, Dimitrova D, Li X, Ladutko L, Campbell S, Friedland G, Mitton-Fry M and Miller P (2010). Pharmacokinetics and whole-blood bactericidal activity against *Mycobacterium tuberculosis* of single doses of PNU-100480 in healthy volunteers. J. Infect. Dis. 202 (5):745-751

Wietzerbin J, Das B, Petit J, Lederer E, Leyh-Bouille M and Ghuysen J (1974). Occurrence of D-alanyl-(D)-meso-diaminopimelic acid and meso-diaminopimelyl-mesodiaminopimelic acid interpeptide linkages in the peptidoglycan of Mycobacteria. Biochemistry 13: 3471-3476

Williams K, Stover C, Zhu T, Tasneen R, Tyagi S, Grosset J and Nuermberger E (2009). Promising antituberculosis activity of the oxazolidinone PNU-100480 relative to that of linezolid in a murine model. Antimicrob. Agents. Chemother. 53(4):1314-1319

World Health Organization. Global Tuberculosis Report 2012 (WHO, 2012).

World Health Organization. Treatment of Tuberculosis Guidelines 4th edn (WHO, 2010)

Xia D, Yu C, Kim H, Xia J, Kachurin A, Zhang L, Yu L and Deisenhofer J (1997). Crystal structure of the cytochrome bc_1 complex from bovine heart mitochondria. Science 277: 60–66

Yuan Y and Barry C (1996). A common mechanism for the biosynthesis of methoxy and cyclopropyl mycolic acids in *Mycobacterium tuberculosis*. Proc. Natl. Acad. Sci. U S A. 93(23):12828-33.

Yuan Y, Lee R, Besra G, Belisle J and Barry C (1995). Identification of a gene involved in the biosynthesis of cyclopropanated mycolic acids in *Mycobacterium tuberculosis*. Proc. Natl. Acad. Sci. U S A. 92(14):6630-4.

Zvada S, Denti P, Sirgel F, Chugutsa E, Hatherill M, Charalambous S, Mungofa S, Weisner L, Simonsson U, Jindani A, Harrison T and McIlleron H (2013). Moxifloxacin population pharmacokinetics and model-based comparison of efficacy between moxifloxacin and ofloxacin in African patients. Antimicrob Agents Chemother

Zhang J, Chung T and Oldenburg K (1999). A simple statistical parameter for use in evaluation and validation of high throughput screening assays. Journal of Biomolecular Screening. 4(2):67-73

Zhang Y, Vilcheze C and Jacobs W (2005). In: Tuberculosis and the Tubercle Bacillus. American Society for Microbiology Press; 115–140.

Zhang Y and Young D (1994). Molecular genetics of drug resistance in *Mycobacterium tuberculosis*. J. Antimicrob. Chemother. 34(3): 313-319

Zumla A, Nahid P and Cole S (2013). Advances in the development of new tuberculosis drugs and treatment regimens. Nature Reviews Drug Discovery. 12:5, 388-404

Zwarenstein M, Schoeman J, Vundule C, Lombard C and Tatley M (1998). Randomised controlled trial of self-supervised and directly observed therapy for tuberculosis. Lancet 352:1340–1343